NTNU – Trondheim
Norwegian University of
Science and Technology

Investigation of Adsorption of Surfactants onto Illite and Relations to Enhanced Oil Recovery Methods

Ingrid Karlsen Hov

Chemical Engineering and Biotechnology
Submission date: June 2014
Supervisor: Gisle Øye, IKP
Co-supervisor: Meysam Nourani, IKP

Norwegian University of Science and Technology
Department of Chemical Engineering

Preface

This report is my master thesis for the conclusion of my Master programme within the Colloid and Polymer chemistry division at the Department of Chemical engineering, NTNU, spring 2014. The experimental part of the project has been carried out in the Ugelstad Laboratory at NTNU from January 2014 to June 2014.

The project is a continuation of my specialization project from last semester and a part of a research program carried out in collaboration with Department of Petroleum Engineering and SINTEF Petroleum, and is sponsored by Det Norske Oljeselskap, GDF SUEZ, Lundin, Statoil and Unger Surfactants.

I would like to express my appreciation to my supervisors Professor Gisle Øye and Post. Doc Meysam Nourani for sharing their theoretical knowledge and for the valuable advice and support given to me both in the experimental part of the project, as well as in the writing of the report. I have learned a lot during the last two semesters and gained both theoretical and practical experience during my work at the laboratory. In addition, I would like to express my gratitude to Thomas Tichelkamp for proofreading the first draft of the report.

I declare that this is an independent work according to the exam regulations of the Norwegian University of Science and Technology (NTNU).

_____

Ingrid K. Hov

Trondheim, 17.06.2014

Abstract

Surfactants have many applications in enhanced oil recovery (EOR) and for each of these applications, care must be taken in selecting the right surfactant. Surfactants tend to be a major portion of the costs associated with EOR, and losing surfactants to adsorption leads to substantial economic losses. In this report, surfactant flooding and low salinity water injection are the two EOR methods of interest, and the effect of combining these two has been studied. Surfactant adsorption depends on many parameters, and the parameters investigated in this reports are salinity and the effect of divalent cations. In this experiment, the adsorption of the anionic surfactant SDBS onto Illite clay has been studied using UV-vis spectroscopy. Initially, the indirect method of surface tension was supposed to be used as well. However, because of an alteration in the execution of the experimental method regarding the UV-vis, the experiment became more time consuming than first expected.

The adsorption studies were carried out using five different salinity conditions. The ionic strengths were 0.2, 0.08 and 0.02 for high salinity, medium salinity and low salinity, respectively. In addition, each of the salinity concentrations was conducted both with and without $CaCl_2$, except the high salinity condition, which was only conducted without $CaCl_2$ due to precipitation when adding calcium. Originally, the high salinity concentration was supposed to be that of sea water, above 35 000 ppm, but this did not work, again due to precipitation.

The adsorption isotherms obtained for the various salinities indicate that a combination of the two methods low salinity water injection and surfactant flooding indeed leads to a reduced surfactant adsorption onto Illite clay, and that the adsorption decreases with a decrease in the concentration of multivalent cations.

Sammendrag

Surfaktanter har mange bruksområder i økt oljeutvinning (EOR), og for hvert av disse bruksområdene er det viktig å velge riktig surfaktant. Surfaktanter pleier å inngå som en stor del av kostnadene forbundet med EOR, og tap av surfaktanter grunnet adsorpsjon fører til betydelige økonomiske tap. I denne rapporten er det de to EOR-metodene surfaktantfløming og vanninjeksjon med lav saltholdighet som er av interesse, og effekten av å kombinere disse to har blitt studert. Adsorpsjon av surfaktanter er avhengig av mange parametere, og parameterne som er undersøkt i dette rapporter er saltholdighet og effekten av divalente kationer. I dette forsøket har adsorpsjon av den anionske surfaktanten SDBS på Illitt-leire blitt undersøkt ved hjelp av UV-vis spektroskopi. Opprinnelig skulle også den indirekte metoden for overflatespenning benyttes i tillegg, men på grunn av en endring i den eksperimentelle utførelsen av UV-vis eksperimentene, ble forsøket mer tidkrevende enn det forventet.

Adsorpsjonsstudiet ble utført med fem forskjellige saltinnhold. Ionestyrken var på henholdsvis 0,2, 0,08 og 0,02 for høyt saltinnhold, middels saltinnhold og lavt saltinnhold. I tillegg ble hver saltkonsentrasjon utført både med og uten $CaCl_2$, bortsett fra den med høyt saltinnhold, som bare ble gjennomført uten $CaCl_2$ grunnet utfelling ved tilsats av kalsium. Opprinnelig skulle det høye saltinnholdet ha samme konsentrasjon som sjøvann, over 35 000 ppm, men dette var ikke gjennomførbart, igjen på grunn av utfelling.

De oppnådde adsorpsjonsisotermene for de forskjellige saltinnholdene indikerer at en kombinasjon av de to metodene vanninjeksjon med lav saltholdighet og surfaktantfløming fører til en mindre adsorpsjon av surfaktanter på Illitt leire, og at adsorpsjonen minker med minkende konsentrasjon av flervalente kationer.

Table of contents

1. Introduction

As the oil prices and the cost of exploration and production have increased along with the discoveries moving farther offshore, there is a much greater focus within the oil and gas industry on increasing the production from existing reservoirs. The goals are to minimize operating costs and maximize energy efficiency, while maintaining production and increasing oil recovery. Enhanced oil recovery (EOR) is a generic term for methods that increase the extracted amount of crude oil from an oil reservoir and is typically the final stage in the recovery of crude oil. In recent years, various innovative EOR techniques that seek to maximize total reservoir recovery have gained renewed interest and attention. At the 2011 EORC held in Kuala Lumpur, leading industry experts emphasized on the potential for EOR techniques that promise to be more time efficient and cost effective, increase recovery process, and are environmentally sustainable. [1]

In the Norwegian Continental Shelf, several oil fields are entering the tail production phase. At this point, it is desired to extract as much crude oil as possible from the reservoir, which is the reason that EOR methods are utilized. There are many different EOR methods, but in this project the main focus will be on surfactant flooding and low salinity water injection and the combination of these two techniques. Surfactant flooding is a well-known EOR method and has been commercially utilized for decades, while low salinity water injection is a relatively new method which has only been carried out in laboratory tests and in single well field tests. While these two methods earlier have been viewed as stand-alone techniques, the industry is now interested in combining them in order to achieve higher and more efficient crude oil production.

There is however one problem that restrains the method of surfactant flooding; the loss of surfactants due to adsorption. On the Norwegian Continental Shelf, the crude oil reservoirs are sandstones, which contains huge amounts of fine-grained clay

minerals such as Illite and Kaolinite. These clay minerals can lead to adsorption of surfactants during the EOR process, which is a very undesirable side effect since low retention of surfactants in the reservoir is important for the method to be efficient and economically feasible. Thus, it is crucial to understand which parameters that influence the surfactant adsorption onto these minerals.

The aim of this project is to investigate the adsorption of surfactants onto clay at various conditions. The parameters to be investigated are salinity and the effect of divalent cations. The experimental part will be carried out using the anionic surfactant SDBS and Illite clay, which is found in sandstone reservoirs. The loss of adsorption will be measured by UV-visible spectroscopy.

2. Theory

2.1 Oil Recovery

The oil extraction process can be divided into three parts. The primary oil recovery takes advantage of the natural pressure present in the oil reservoir. The production is often limited to about 10-20% of original oil in place (OOIP). The secondary oil recovery uses methods such as water flooding and immiscible gas injection to extract the oil. This method increases the oil recovery to 20-30% of OOIP, which means a huge part of the original oil is still trapped in pores in the reservoir due to high capillary pressure from water. The final method is the tertiary oil recovery, which changes the rock and/or fluid properties by addition of chemicals. This method is also known as enhanced or improved oil recovery (EOR/IOR), and uses steam injection, in-situ combustion, surfactant flooding and polymer flooding. This method extracts an additional 5-30% of OOIP. [2] The various phases of oil recovery in a reservoir are shown in Figure 2.1.1.

Primary Recovery	Natural Reservoir Pressure	10-20% of OOIP
Secondary Recovery	Waterflooding, Gas Cycling	20-30% OOIP
Enhanced Recovery	Polymer Flooding	5-15% OOIP (additional)
	Gas Flooding	5-15% OOIP (additional)
	Surfactant Flooding	15-30% OOIP (additional)
Heavy Oil Primary Recovery		0-10% OOIP
Heavy Oil Enhanced Recovery	Thermal EOR	> 50% OOIP

Figure 2.1.1: A chart showing the different phases occurring in EOR, including the methods used for recovery along with the amount of oil extracted. [3].

2.2 Interfacial Tension

The interfacial free energy per unit area represents the amount of work required to expand an interface, and is often known as interfacial tension. Interfacial tension has the dimension force per unit of length, mN/m. When interfacial tension occurs between a gas and a liquid it can also be denoted as the surface tension. This means

that the surface tension of for example water is equivalent to the interfacial free energy per unit area of the phase boundary between water and air. The surface tension between air and water at 25°C and atmospheric pressure is 72.8 mN/m. The interfacial tension is defined by Equation 1 [3]:

$$\left(\frac{dG}{dF}\right)_{p,F} = \gamma \tag{1}$$

where G is the free enthalpy, F the surface area, and γ the interfacial tension. Surface tension occurs as a result from the attractive forces between the molecules in each phase. As shown in Figure 2.2.1, the molecules in the bulk phase will be symmetrical surrounded by other molecules, causing the net sum of the attractive forces to be equal to zero. On the interface however, the molecules will only experience attractive forces in two dimensions. The molecules on the surface is thereby exposed to a net force directed into the liquid phase. The surface will try to reduce its own area, and as a result, it will be under constant tension. This is the origin of the force known as the surface tension. [4]

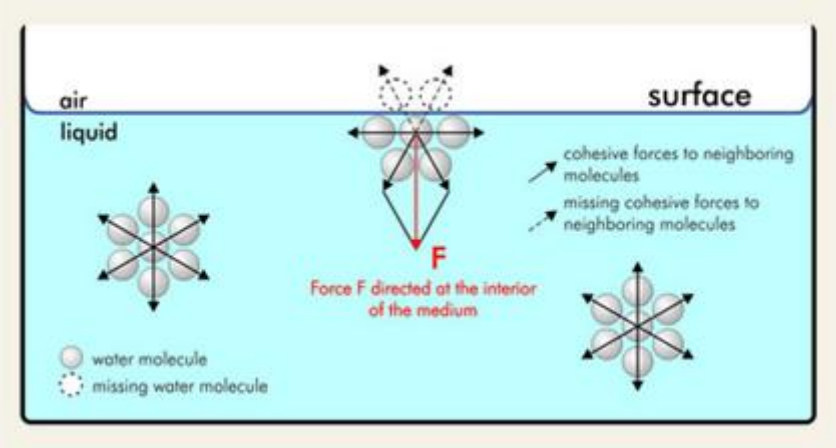

Figure 2.2.1: Schematic illustration of how interfacial tension occurs [5]

The surface tension between air and various fluids will differ due to changes in the intermolecular forces in each of the different fluids. For a system composed of two

immiscible fluids, the interfacial tension is dependent on the attractive forces between the molecules in each of the two phases. Two immiscible phases can become miscible by reducing the interfacial tension between them.

2.2.1 The Effect of Solutes on Interfacial Tension

The interfacial tension of an aqueous solution can be affected by addition of co-solutes. Addition of electrolytes will usually lead to an increase of the surface tension due to negative adsorption of ions at the liquid-air interface. Addition of surfactants and water-soluble organic compounds, such as ethanol, will on the other hand decrease the surface tension. These three effects are illustrated in Figure 2.2.1.1. A breakpoint can be observed from this figure, where further addition of surfactants will not effect the surface tension. This point is called the CMC, and is more thoroughly described in Chapter 2.4.

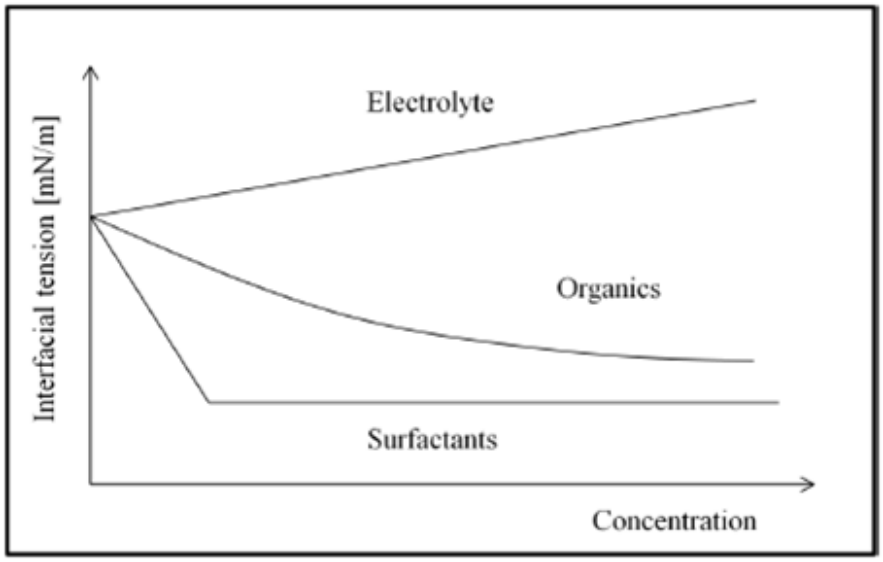

Figure 2.2.1.1: Schematic illustration of the effects of added co-solutes to an aqueous solution [6]

2.2.2 Changes in Interfacial Tension Due to Diffusion

The interfacial tension between an aqueous solution and air may change over time due to rearrangements of the molecules in the bulk solution. This phenomenon is illustrated in figure 2.2.2.1. These kinds of systems will always arrange themselves in order to lower the interfacial tension. Molecules and compounds that are able to lower the interfacial tension will adsorb at the interface. At first, a quite rapid decrease will be observed, but after a while, the interfacial tension stabilizes at a constant level.

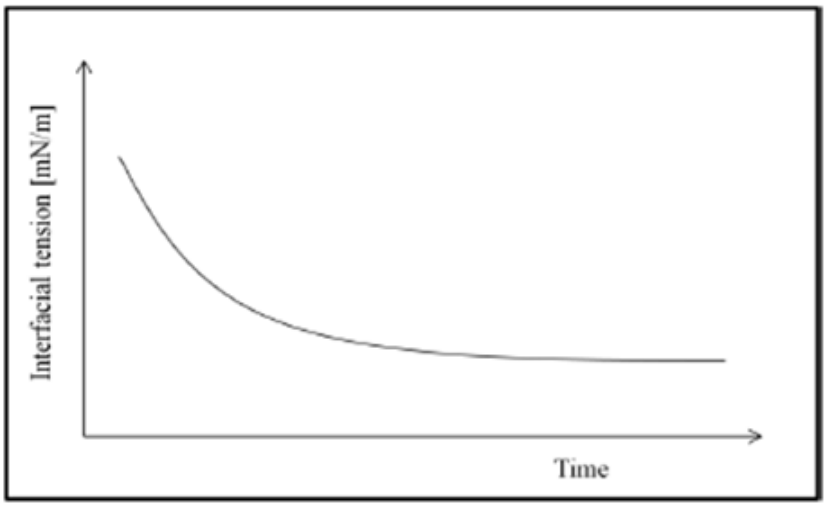

Figure 2.2.2.1: Schematic illustration of how the interfacial tension of an aqueous solution changes over time due to diffusion [6]

2.3 Surfactants

2.3.1 Basic Concepts of Surfactants

The word surfactant is an abbreviation for surface active agent. In other words, surfactants are compounds which tend to adsorb at interfaces. The stronger the tendency, the better the surfactant. The driving force of surfactant adsorption onto an interface is to reduce the free energy of the specific phase boundary, also known as

the interfacial tension. Thus, a dense packing of surfactants at an interface will lead to a great reduction in the surface tension.

There is no surfactant suitable for all kinds of systems. This is because the surfactant concentration at a phase boundary depends on the surfactant structure as well as the nature of the two phases in the specific system. Therefore, all systems are analyzed before a suitable surfactant for the specific application can be chosen. A good surfactant should have low solubility in the bulk phase. The limit of surface tension reduction for a surfactant is reached when the so-called critical micelle concentration (CMC) is reached.

Surfactants are amphiphilic compounds. The word amphiphilic is derived from the Greek word for both, amphi, and relates to the fact that surfactants consist of at least two parts. [7] One part is lyophobic and means that it is insoluble in a specific fluid, while another part is lyophilic which means it is soluble. If the specific fluid is water these two parts are usually called hydrophobic and hydrophilic, respectively. As illustrated in Figure 2.3.1.1, the hydrophobic part is referred to as the tail of the surfactant, while the hydrophilic part is known as the head group.

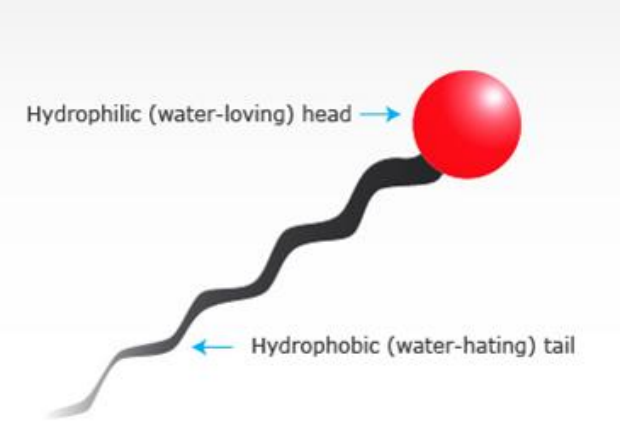

Figure 2.3.1.1: Schematic illustration of a surfactant [8]

It is due to the combination of these two parts that surfactants possess the ability to reduce interfacial tension. When a surfactant adsorbs at a hydrophobic surface in a aqueous solution, it will arrange itself with the hydrophobic tail towards the hydrophobic interface and the hydrophilic head group towards the aqueous solution. This will alter the surface, make it hydrophilic, and thereby reduce the interfacial tension.

Surfactants are primarily classified by the charge of their polar head group; anionics, cationics, non-ionics and zwitterionics. The latter class is related to surfactants, which experience both anionic and cationic charge under normal conditions [9]. The surfactant used in this experiment, SDBS, is classified as an anionic surfactant.

Anionics are the most used out of all the surfactant classes due to their ease and low cost of manufacture. In addition, they possess good surfactant properties; they are relative stable and robust and they experience less adsorption onto sandstone reservoirs than cationics. [10]

2.3.2 Surfactants in the Petroleum Industry

Surfactants have a variety of applications in the petroleum industry. In EOR, surfactants are used in classic micellar/polymer (surfactant) flooding, alkaline/surfactant/polymer (ASP) flooding or in foams for mobility control or blocking and diverting. In all of these applications, surfactant adsorption must be taken into consideration. The surfactants can behave in different ways in order to enhance oil production. They can reduce the interfacial tension between the oil trapped in small capillary pores and the surrounding water, which will lead to mobilization of the oil. They can also solubilize the oil (micellar systems), form emulsions of oil and water (alkaline methods) and change the wettability of the reservoir (alkaline methods). [11]

When choosing the proper surfactant for a specific EOR application, there are many criteria to think about. Primarily, it is important to minimize the loss of surfactant due to adsorption. The factors that has to be taken into account include temperature, pH, salinity, type of surfactant and the solids present in the reservoir. These factor are often determined by the reservoir conditions and can not be manipulated, the reservoir therefore has to be analyzed before selecting a suitable surfactant.

2.4 Micelle Formation

2.4.1 Critical Micelle Concentration

The critical micelle concentration, abbreviated as CMC, is defined as the surfactant concentration at which the surfactant molecules self-aggregate and form spherically shaped micelles. [12]

In dilute concentrations, surfactants in aqueous solutions act similar to electrolytes. This behavior will alter by increasing the surfactant concentration in the bulk solution. The amount of surfactant accumulation at the interface will increase, which will lead to a reduction in interfacial tension. There is however a limit to the amount of surfactants that can accumulate at a specific surface. This limit is reached when the surfactant molecules start to aggregate and form micelles in the bulk solution. The concentration where this phenomenon occurs is known as the CMC. In other words, CMC is the concentration of maximum solubility of a monomer in a particular solvent. Only surfactant unimers contribute to lowering of the interfacial tension. Thus, increasing the surfactant concentration above CMC will have no effect on the interfacial tension. [13] This is illustrated in Figure 2.4.1.1.

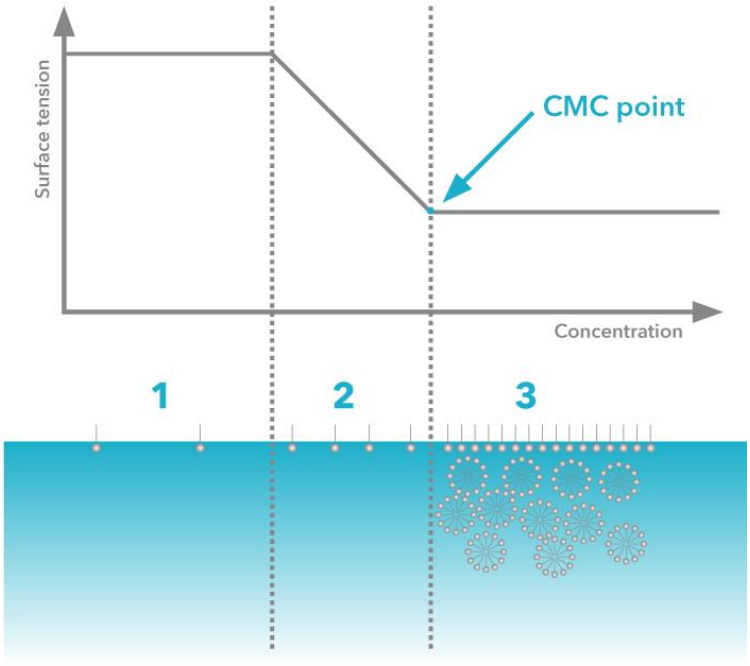

Figure 2.4.1.1: Schematic illustration of the critical micelle concentration [14]

2.4.2 Factors Affecting the CMC

There are several factors that influence the CMC. The chemical structure of the surfactant is one of these factors. The physical properties of the surfactant structure that affect the CMC are listed below [15]

- By increasing the alkyl chain length, the CMC will strongly decrease.
- The CMC for ionics are much higher than for the non-ionics.
- For nonionics, the CMC increases when the head group becomes larger.
- Cationics have a slightly higher CMC than anionics.
- Increasing the valence will lower the CMC. An increase in the valence to 2 gives a CMC reduction by a factor of 4.
- Perfluorination of the alkyl chain results in a lowering of the CMC. However, partial fluorination may lead to an increase of the CMC due to unfavorable interactions between the hydrocarbon and fluorocarbon groups.

Other factors that may affect CMC are temperature and added electrolyte. The influence of temperature is quite moderate, but the addition of an electrolyte can lead to significant changes in CMC for ionic surfactants. These effects are listed below [16]:

- By addition of salt, the CMC will reduce. This effect is much larger for long-chained alkyls.
- The effect of added salt will depend on the valency of the ions and will be more sensitive to the valency of added counterions.
- The effects observed by adding electrolytes to ionic surfactants systems are big compared to the non-ionics.

2.4.3 The Krafft Point

As mentioned earlier, temperature has a small effect on CMC. However, it can have a great impact on the solubility of surfactant systems. The solubility may be very low at low temperature, but when temperature increases, the solubility can increase by orders of magnitude [17]. This observation is known as the Krafft phenomenon, and the temperature at which it occurs is called the Krafft point. At the Krafft point, the solubility increases drastically as a function of increasing temperature, as illustrated in Figure 2.4.3.1.

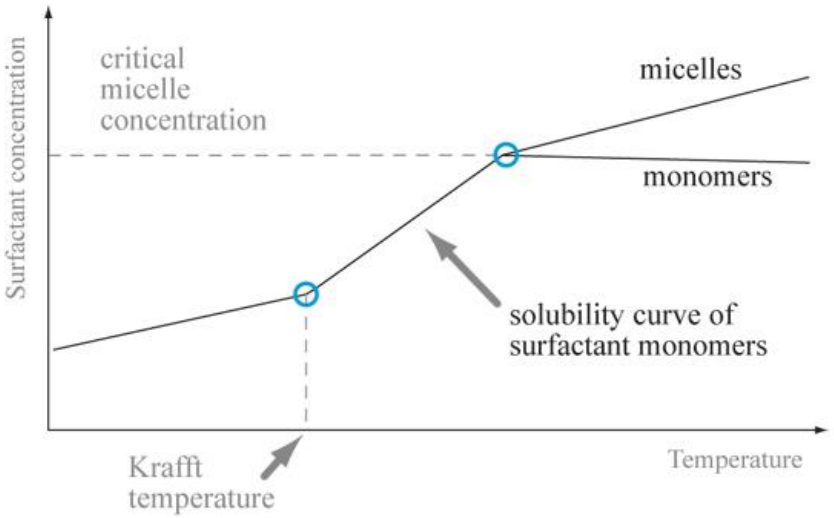

Figure 2.4.3.1: Schematic illustration of the Krafft phenomenon [18]

At concentrations below CMC, the solubility is only limited by the solubility of the unimers and no micelles can be formed. As the solubility curve crosses the CMC, the amount of added surfactants can be increased while the number of free unimers remains almost constant since the excess amount of surfactants from micelles.

2.4.4 Measuring the CMC

There are many various methods of measuring the CMC of a specific surfactant. One method is to measure the interfacial tension of a number of surfactant samples with different concentrations, and then plotting the concentration against the interfacial tension. This plot can then be analyzed, and the CMC is observed at the point where the interfacial tension flattens out. Other methods include measurements of the solubility, measurements of the self-diffusion and nuclear magnetic resonance (NMR).

Measuring the CMC using different methods will lead to several different values. Thus, the CMC can be considered as a range of concentrations rather than just one value.

2.5 Electrically Charged Surfaces

Surfactants usually adsorb onto a solid due to electrostatic interactions between the charged solid surface and the charged head-groups of the ionic surfactants. Most mineral surfaces present in crude oil reservoirs are assumed to be electrically charged. The adsorption of surfactants at the solid-liquid interface is controlled by the properties of both the solid substrates and the solution. The minerals most reservoir rocks are made up of include Quartz, Kaolinite, Illite, Chlorite and Montmotillonite, which all generally display a net negative charge. In order to lower the adsorption, negatively charged surfactants are usually considered as the main surfactant species of the slug. Thus, anionic surfactants are believed to be the most used type of chemicals in the flooding of sandstone oil reservoirs [19].

The charge imbalance on a surface arises from the imperfections in the crystal structure and the preferential adsorption of counter-ions or potential determining ions. Imperfections in the crystal structure include isomorphous replacement of ions within the crystal lattice, broken bonds, dislocations, and lattice defects. A common replacement of ions is the substitution of silicon atoms by aluminum atoms in Kaolinite clay. When the surface of Kaolinite is fractured, the bonds between the alumina-silica layers be broken. This may lead to ions with unsatisfied valence conditions. Depending on the type of bond broken, the resulting charge can be either negative or positive. Unsatisfied valence conditions can also be promoted by dissolution by water of the solid surface. Charge imbalances and broken bonds are induced by chemical adsorption of water by the solid surface. The adsorbed water molecules create an amphoteric site on the surface, and deprotonation of the amphoteric group forms a negative charge on the surface, while protonation of the group leads to a positive charge. As a consequence, the charge of a surface it highly dependent on the pH of the surrounding solution. Defects in the crystal lattice are related to holes in the lattice due to missing ions, which results in unbalanced charges. Dislocations may also be a

reason for charge imbalances in crystal structure. There are typically two types of dislocations; the screw and the edge dislocation. In the screw dislocation a section of a crystal is skewed one atom spacing, and in the edge dislocation an extra plane of atoms is inserted into a section of a crystal. The charge imbalances arise at the sites of the dislocations [20].

At dilute surfactant concentrations, the adsorption is highly determined by the nature of the charged surface. As the surfactant concentration increases, factors like the tendency of self-aggregation of the surfactants become more and more significant.

2.5.1 The Electrical Double Layer

The theory of the electrical double layer was one of the first theories that explained the interactions of charged particles at solid-liquid interfaces. It was originally proposed by Helmholtz in 1879, and later modified by Stern in 1924 [21].

The adsorption of counter ions or potential determining ions in dilute surfactants concentrations can be explained by the concept of the electrical double layer, which is created due to a charge on the mineral surface. An unequal charge distribution on the interface will give the rising of an electrical potential. Since the unequal charge distribution is a phenomenon that occurs on both sides of the interface, there will be a net sum of positive and negative charges.

In the Stern modification from 1924, the counter ions in the solution, which have the opposite charge of the surface, were divided into two different layers; the Stern layer and the Gouy layer. As shown in Figure 2.5.1.1, the Stern layer, δ, is the layer of ions that are adsorbed close to the surface, while the Gouy layer, d, also known as the diffuse layer, is the layer of counter ions. From the same figure, it can also be observed

that the potential decreases rapidly within the Stern layer and more moderately within the diffuse layer, d.

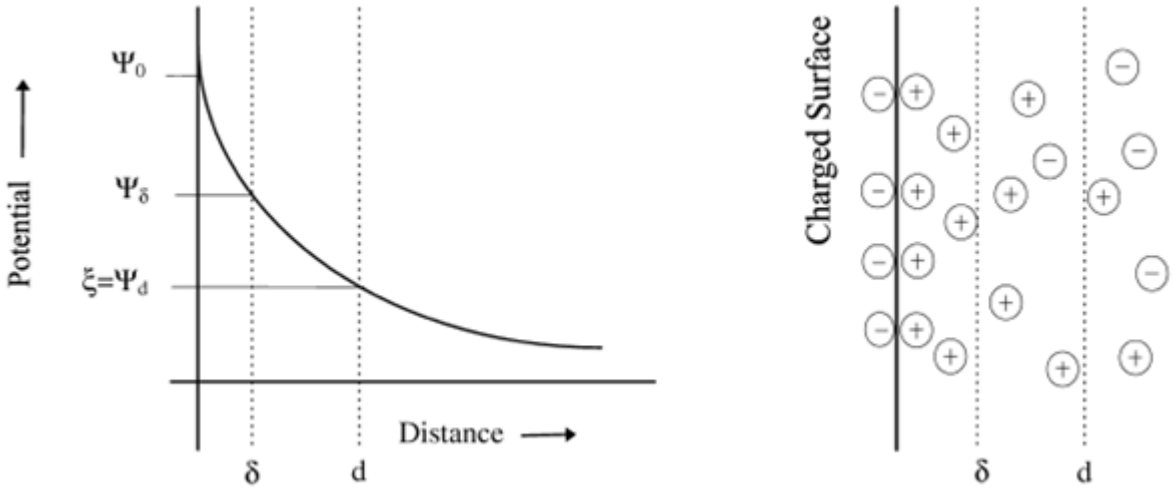

Figure 2.5.1.1: Schematic illustration of the Gouy-Chapman model of the electrical double layer and the corresponding potential distribution where δ is the Stern plane within which counterions are adsorbed close to the surface and d is the diffuse layer of counterions.[21].

The characteristic thickness of the electrical double layer is referred to as the Debye length and is the inverse of the decay length. The Debye length is an important parameter when describing the effects of the electrical double layer. It characterizes the range over which the perturbation due to an electrical double layer extends. In an electrolyte or a colloidal suspension, the Debye length is given by Equation 2 [22]:

$$k_D^{-1} = \sqrt{\frac{\varepsilon_r \cdot \varepsilon_0 \cdot k_B \cdot T}{2 \cdot N_A \cdot e^2 \cdot I}} \qquad (2)$$

Where I is the ionic strength of the electrolyte, ε_0 is the permittivity of free space, ε_r is the dielectric constant, k_B is the Boltzmann's constant, T is the absolute temperature, e is the elementary charge and N_A is the Avogadro number. In aqueous solutions, the Debye length is typically on the scale of a few nanometers and the thickness decreases with increasing concentration of the electrolyte, as seen in Figure 2.5.1.2.

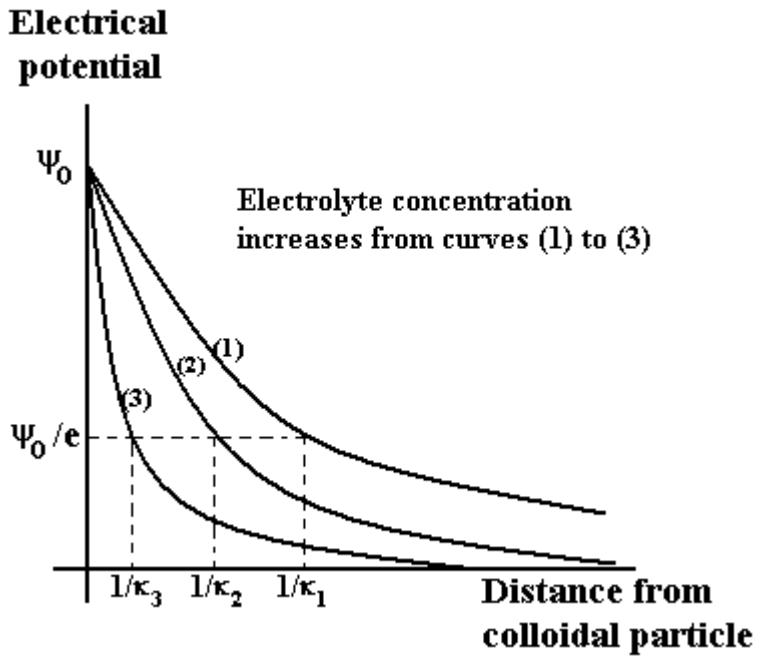

Figure 2.5.1.2: The figure shows how the Debye length decreases with increasing electrolyte concentration [23].

2.5.2 The Site-Binding Model

The electrical double layer is a good theory when describing the behaviour of simple ions like Na^+ or Cl^- or single ions like surfactants when a non-electrostatic term is added to the adsorption potential. When describing potential determining ions such as H^+ and OH^- however, it is more convenient to adopt the so called site-binding model. This model explains how a surface charge changes at a mineral-solution interface. It limits the concentration of the species at the surface to the total number of sites available on the surface in a specific system. For the model to be feasible, the reactions

responsible for the change in surface charge and the potential-charge relationships at the interface has to be known.

The adsorption of H^+ and OH^--ions will influence the charge on a solid surface. The charge can be negative, positive or neutral. The neutral surface condition is referred to as the point of zero charge, abbreviated as PZC. The PZC can be defined as the pH at which the net charge of the surface is zero. At a pH below or above the PZC, the surface is positively or negatively charged, respectively. For Kaolinite, the PZC is approximately 4.5 [21]. For Illite there is a considerable variability of published experimental data regarding the PZC value. The values vary from 2.5 to 7.5-8 [24]. These variations can be caused due to differences in the origin of the samples, data treatment for determining PZC, and to different models used to analyze the experimental data. It is evident that such variability has a direct influence on the determination of PZC value and thereby prevents comparisons and generalizations of published results for Illite samples.

If adsorption is desirable, it is preferred that the surfactant and the surface have opposite charges. On the other hand, if adsorption is undesirable, like it is in EOR treatment, then it is preferred that the surfactants has the same charge as the surface. However, surfactants will adsorb on like charged surfaces, especially at high surfactant concentrations (above the CMC) and in the presence of multivalent counter ions.

2.6 Mechanisms of Surfactant Adsorption in Single Surfactant Systems

2.6.1 Adsorption on Solid Surfaces

There are two main factors that influence the surfactant adsorption on solid surfaces; the interaction of the surfactant with the surface and the hydrophobicity of the surfactant, also known as the hydrophobic effect. The latter driving force is closely

related to the surfactant structure and the solubility properties of the surfactant in water, and is often the most dominating force in surfactant adsorbing systems. The interaction with the surface only plays a minor role on hydrophobic surfaces. This is because the surfactants adsorb with their hydrophobic tail oriented towards the surface and their hydrophilic head facing towards the solution, as illustrated in Figure 2.6.1.1. This arrangement is similar to a micelle configuration in the sense that the hydrophobic group is transferred from the aqueous environment upon adsorption. It is found that the adsorption free energy of surfactants at a hydrophobic surface is very close to the micelliization free energy of the surfactant. At polar surfaces on the other hand, the surfactants will adsorb with their polar head-groups oriented towards the surface, as illustrated in Figure 2.6.1.1. This phenomenon is known as a hemimicelle and are only valid at low surfactant concentrations. At higher concentrations, two different structures are possible. If there are strong attractions between the polar head-groups and the surface, a monolayer is formed, in which the head-groups are facing towards the surface and the tails are oriented towards the solution. This will create a hydrophobic surface that will lead to further adsorption in the same manner as described for hydrophobic surfaces. Hence, at higher concentrations, a surfactant bilayer known as an admicelle is formed, also illustrated in Figure 2.6.1.1. At intermediate attraction forces between the polar head-groups and the surface, micelles or other surfactants aggregates will form at the surface. This is because attractions between tail-groups are stronger than the interaction of the head-groups with the surface [25].

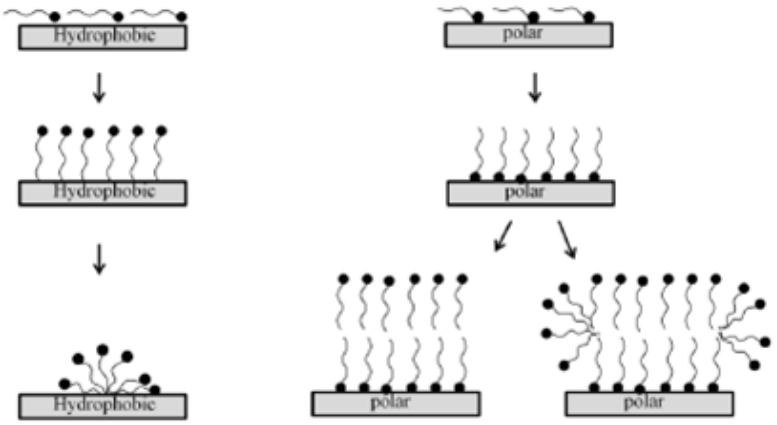

Figure 2.6.1.1: Schematic illustration of surfactant adsorption at hydrophobic and polar surfaces [26]

2.6.2 The Langmuir Adsorption Isotherm

Determination of surfactant adsorption in dispersed systems is obtained by adding a known amount of the surfactant that is to be studied, wait until the system reaches equilibrium, separating the dispersed solids and then finally measure the surfactant concentration.

There are various methods of determining the surfactant concentration, for example ion-selective electrodes, UV-vis spectroscopy, refractive index, titration, chromatography or surface tension.

The analysis of surfactant adsorption is often carried out in terms of the Langmuir equation. It is often desirable to analyze surfactant adsorption with the help of a theoretical model in order to obtain knowledge on a molecular level. The parameters from such an analysis can later be used to compare the adsorption behaviour of different surfactants and to predict the adsorption in new systems. The following assumptions are made when using the Langmuir isotherm:

- The surface is homogeneous
- The surfactants may only adsorb in one monolayer
- There are no surfactant-solvent or surfactant-surfactant interaction
- The surfactant and solvent molecules have equal cross-sectional surface area

The first two assumptions are considered quite reasonable, despite the fact that surfactants may form double layers at the interface, while the last two assumptions on the other hand, are not. However, since these two deviations are opposites, they will cancel each other out. The equation for Langmuir adsorption can be obtained by defining the adsorption rate as in Equation 3:

$$Rate\ of\ adsorption = k_a \cdot C \cdot (1 - \Theta) \tag{3}$$

where C is the equilibrium surfactant concentration, Θ, is the fraction of the surface that is covered by surfactants and k_a is a rate constant. In the same manner, the rate of desorption is defined by Equation 4:

$$Rate\ of\ desorption = k_d \cdot \Theta \tag{4}$$

where k_d is a rate constant. When equilibrium is reached, the adsorption rate and the desorption rate are the same, and the Langmuir adsorption equation is obtained by Equation 5:

$$\Theta = \frac{K \cdot C}{1 + K \cdot C} \tag{5}$$

where K is defined as the equilibrium constant and is equal to the ratio between k_a and k_d [27].

2.6.3 The Four-Region Adsorption Isotherm

Surfactant adsorption at the solid-liquid interface has been studied for decades, and even though there is a general agreement regarding the interactions leading to adsorption, there is still much discussion concerning the structure of the surfactant surface aggregates. Many attempts has been done in order to fully describe the observed adsorption behavior in the adsorption isotherms. This has lead to the development of several different mathematical models. Currently, none of the models are able to fully describe all the phenomena that affect surfactant adsorption without having to introduce assumptions and adjustable parameters for the various systems. However, they do provide important and interesting information.

Most adsorption studies that have been conducted have used the surfactant depletion method with the results being presented as isotherms. Isotherms are plots of the amount of surfactant adsorbed (per gram or per surface area) versus the equilibrium surfactant concentration at a constant temperature, and are usually constructed using log-log scales. The mechanisms behind surfactant adsorption are usually discussed in terms of the four-region isotherms. A typical isotherm for a monoisomeric anionic surfactant consisting of four regions and constructed using a log-log scale is illustrated in Figure 2.6.3.1.

At very low surfactant concentrations (see region 1, Figure 2.6.3.1), the adsorption behavior is often described using Henry's law, in other words it is linear with a slope of one. This is the region where the theory of the electrical double layer is valid. The surfactant molecules adsorb as individual unimers with no interactions between the adsorbed molecules. The surface-surfactant interaction depends on the surface and type of surfactant. For non-ionics, the interactions involve hydrogen bonding between the hydrogen molecules at the surface and the proton acceptors in the head-group. Also, the hydrophobic bonding between the surface and tail-group of the surfactant

contributes to adsorption. For ionics, the driving force it the electrostatic interactions between the head-groups and charged sites at the surface.

The break between region I and II corresponds to the surfactant concentration at which the first surfactant aggregates from on the surface, and is often referred to as the hemimicelle concentration (HMC) or the critical admicelle concentration (CAC). These associations are often attributes to tail-tail interactions, which are the same hydrophobics interactions by which micelle formation is described by. The CAC/HMC will vary with the surfactant chain length and branching in the same manner as the CMC. If the system contains ionic surfactants, the addition of an electrolyte will lead to a decrease in the CAC, similar to what happens in the same case for CMC.

In region III there is observed a small increase in the slope compared to region II. Several theories have been proposed trying to explain this change. One theory says that the change in the slope is due to the surfactant ions having filled all of the surface sites during region II, and that further adsorption in region III is caused by association between the first and second layer of hydrocarbon chains. Another theory attributes the change in slope to a reversal in surface charge due to the adsorbed surfactant ions. It has also been suggested that bilayers were formed already in region II and continued to region III, but at a different rate.

Region IV usually begins at the point where CMC is obtained and is characterized as a plateau with little or no increase in adsorption as surfactant concentration rises. There is a general agreement among researchers that the surfactant aggregates have a bilayer structure above the CMC. The total adsorption above the CMC strongly depends on the surface charge and, thus, the pH.

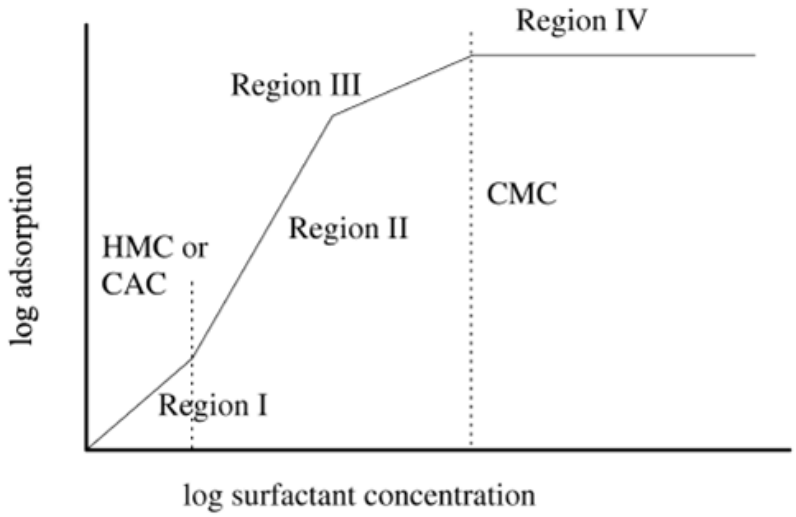

Figure 2.6.3.1: Schematic illustration of a typical four-region adsorption isotherm for a monoisomeric surfactant [28]

An important aspect concerning this topic is that the exact shape of the isotherm is dependent on factors such as the type of surfactant, the charge on the surface and the presence, or absence, of additives like electrolytes, co-surfactants, hydrotropes or alcohols. It should also be mentioned that not all log-log isotherms seen in the literature consist of four regions. In some of the earliest adsorption studies, surfactant concentrations well below the CMC were used. These studies resulted in isotherms with only two regions. By increasing the surfactant concentration, it was observed isotherms containing three regions, and by raising the concentration even further, four regions were obtained [28].

2.6.4 Mathematical Fitting

In this report, two different adsorption isotherms were used in order to create a mathematical fitting; the Langmuir adsorption isotherm and the Freundlich adsorption isotherm. These are two common isotherms which describes the equilibria between the amount of adsorbed surfactant and the concentration of the dissolved surfactant.

The Langmuir adsorption isotherm is, as mentioned earlier, based on the assumption of the existence of only a single adsorption layer, and is described by Equation 6:

$$q_e = \frac{Q_0 \cdot K \cdot C_e}{K \cdot C_e + 1} \tag{6}$$

where q_e is the amount of adsorbed surfactant per unit mass of Illite, Q_0 and K are empirical constants and C_e is the equilibrium concentration of surfactant in solution after adsorption. The equation above can be transformed into Equation 7:

$$\frac{1}{q_e} = \frac{1}{Q_0 \cdot K} \cdot \frac{1}{C_e} + \frac{1}{Q_0} \tag{7}$$

The empirical constants Q_0 and K can now be determined by plotting $\frac{1}{q_e}$ against $\frac{1}{C_e}$.

The Freundlich isotherm is defined by Equation 8, and usually proves to be a better relation:

$$q_e = K_f \cdot C_e^{\frac{1}{n}} \tag{8}$$

where K_f and n are constants. Further, Equation 8 can be transformed into Equation 9:

$$\log(q_e) = \log\left(K_f\right) + \frac{1}{n} \cdot \log(C_e) \tag{9}$$

The constants $\frac{1}{n}$ and K_f can now be determined by plotting $\log(q_e)$ against $\log(C_e)$ [29]

2.7 Surfactant/Chemical Flooding

Novosad et al. did early demonstrations of the technical feasibility of EOR by chemical flooding in the laboratory in 1982 and in field tests by Lake and Pope in 1979 and by Holm in 1982 [30].

Chemical flooding of oil reservoirs is one of the most successful methods for EOR in crude oil reservoirs. However, the process is not very beneficial from an economic point of view and in some cases it is directly uneconomical. Because of this, many research groups have tried to improve the technique by simplifying the flooding process, improving the efficiency of surfactants and developing new chemicals. Surfactants and polymers are the main chemicals used in chemical flooding. Surfactants reduce the interfacial tension between the reservoir oil and the injected water, while the polymer creates favorable viscosity conditions and good mobility control for the surfactant slug.

The economic feasibility depends on a several factors such as oil prices, international economics and the cost of surfactants. The cost of surfactant is usually the single most expensive item in the process of surfactant flooding, and include both the initial investment in purchasing the surfactant, as well as the cost of replacing the amount of surfactant lost due to adsorption. Generally, the amount of surfactant adsorbed accounts for most of the surfactant cost. The surfactants used in surfactant flooding are synthesized from petroleum. Thus, the surfactant cost will increase with the cost of the oil they are produced from. Hence, waiting for the oil prices to increase will not necessarily make EOR economically feasible. The amount of oil produced by surfactant flooding has to be great enough to replace the oil used for the manufacturing of the surfactant in order to pay for all the additional engineering, equipment and operating costs, and to provide a reasonable return on investment. All of these criteria must be satisfied in a volatile oil market in which oil prices may fluctuate between the

beginning of a surfactant flood and the time it takes before the tertiary oil is produced [30].

2.7.1 Traditional Surfactant Flooding

The capillary number, N_c, is related to the residual oil saturation through the desaturation curve illustrated by Figure 2.7.1.1, and is defined by Equation 10:

$$N_c = \frac{v \cdot \mu_w}{\sigma} \tag{10}$$

where v is the effective flow rate, μ_w is the viscosity of the displacing fluid and σ is the interfacial tension.

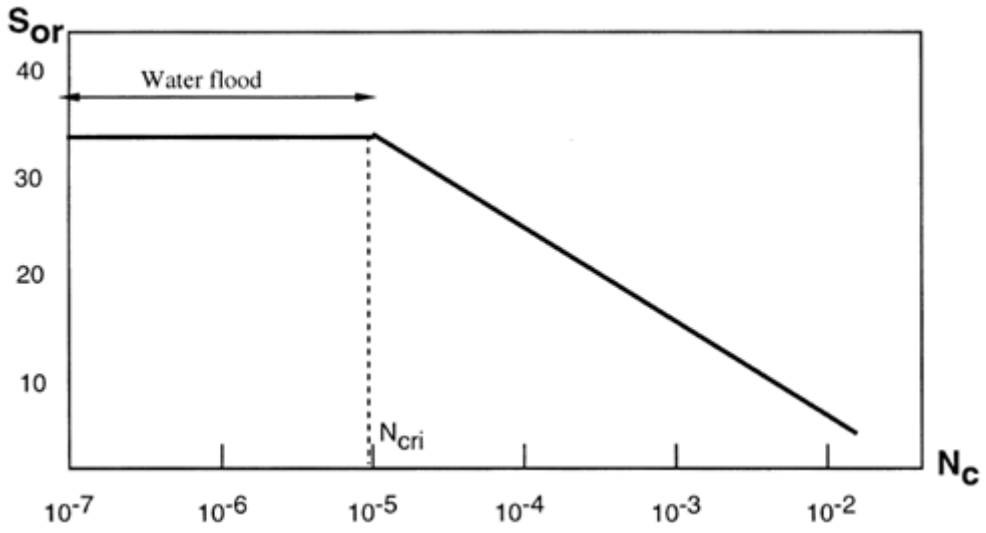

Figure 2.7.1.1: Schematic illustration of a capillary desaturation curve for a non-wetting phase [31]

The critical capillary number, N_{cri}, is the capillary number corresponding to the break in the desaturation curve seen in Figure 2.7.1.1. Thus, $N_c >> N_{cri}$ in order to improve the oil recovery relative to a water flood using chemicals. The critical capillary number and the shape of the desaturation curve are dependent on factors such as the rock properties, the ratio of body to pore throat diameter, pore size distribution and wettability.

The usual range of N_c for an ordinary water flood under water-wet conditions is 10^{-7} to 10^{-5}, for N_{cri} it is 10^{-5} to 10^{-4}, while for complete desaturation of the non-wetting phase, which is oil, it is 10^{-2} to 10^{-1}. The waterflooded residual oil saturation may be in the range of 30 to 40% [31]. This implies that there is 10 times more difficult to remobilize capillary trapped discontinuous oil than continuous oil. In order to be able to mobilize a significant amount of the waterflooded residual oil, it is expected that the capillary number must be increased by a factor of 10^3 to 10^4. This can be done by reducing the interfacial tension between the reservoir oil and the injected water by the same factor using surfactants. This will normally mean that the interfacial tension should be between 0.01 and 0.001 mN/m. Until recently, no single surfactant nor surfactant mixture has been able to lower the interfacial tension between water and oil down to this level by the addition of dilute surfactant concentrations to the injected water. This has led to complex injections due to the formation of a thermodynamically stable micro emulsion between the oil and water phase. At ideal conditions (equal solubilization of oil and water into this middle phase), the interfacial tension between the micro emulsion and the oil and water phase, is very low and equal, which satisfies the requirements for displacing most water flooded residual oil. The process is sensitive to many parameters including [31]:

- Rock type
- Mineral content
- Interstitial brine salinity and composition
- pH
- Injection rate
- Slug composition
- Polymer concentration and type
- Oil viscosity and composition
- Pressure
- Temperature
- Heterogeneities of the formation

The most common anionic surfactants extracts adsorbed multivalent cations into the micelles, which lead to a huge change in, phase properties. Thus, a pre-flush of water containing monovalent cations is normal procedure in order to obtain a cation exchange. To compensate for reservoir parameters, which are a disturbance to the phase behavior of the surfactant slug, an imposed phase gradient is often utilized. A loss of surfactants may take place due to phase trapping (surfactants are trapped in the oil or the micro emulsion phase) if the phase gradient is not working properly. The flow of three liquid phases through an inhomogeneous porous medium is very difficult to handle since the various fluids have various viscosities and the fact that mass transport may occur between the different phases. It is therefore desirable to make the chemical flood run in a two-phase mode. During the 1990's, the goal of many research groups was to develop surfactants that were able to recover additional oil in an economically feasible manner during a water flood consisting of produced brine or seawater. Since complicated chemical slugs with high surfactant concentration wanted to be avoid, there were some criteria set [31]:

- The only chemicals to be used was surfactants and polymers
- The chemical concentration had to be low (surfactant 0.1±0.5 wt% and polymer 5500 ppm)
- No imposed salinity gradient or other phase gradients
- The chemicals should be insensitive to multivalent cations
- The flooding conditions should be a two-phase flood with the surfactant/polymer present in the aqueous phase, forming an oil-in-water micro emulsion

2.8 Low Salinity Water Flooding

Injection off brines with low salinity content is a relatively new EOR method used in mixed-to-oil-wet sandstone reservoirs. The low salinity water flooding makes the rock surface more water-wet, decreases the remaining oil saturation and increases the oil recovery. This is due to desorption of heavy ends from the clay minerals present on the pore wall. The main benefits of the low salinity water flooding method are that the technique is quite similar to conventional water flooding and the fact that it does not require any expensive or toxic chemicals. The only major cost is related to the sourcing of low salinity water and the disposal of high salinity water [32].

It has been documented from both laboratory tests as well as in single well field tests that EOR can be achieved by performing a tertiary low saline water injection in a sandstone reservoir. The mechanism behind the low salinity EOR method is not fully understood and has been a topic of debate in literature for the last decades. This is primarily caused by the complexity of the interactions between the crude oil, brine and reservoir rock. Many suggestions have been proposed, both physical and chemical mechanisms, but none of which have been generally accepted as the main driving force behind the low salinity effect. Most likely, the low salinity effect is a result of various mechanisms acting together, each with its own contribution.

Based on published data and new experimental results on core flooding a new mechanism, which agrees with documented experimental facts, has been suggested. At sandstone reservoir conditions, the pH of produced water is approximately five due to the presence of dissolved acidic gases such as CO_2 and H_2S. At this pH, the clay minerals act as a cation exchange material and are adsorbed by acidic and protonated basic components from the crude oil. Injection of low saline water will promote desorption of Ca^{2+} and thereby increase the pH in the brine-clay interface, since Ca^{2+} is substituted by H^+-ions from the water. A rapid reaction between OH^--ions and the adsorbed acidic and protonated basic material will lead to an adsorption of organic material from the clay. The water wetness of the rock is thereby improved and increased oil recovery is observed. To be able to observe the effect of low salinity water flooding in sandstone reservoirs, a balanced initial adsorption of organic components and Ca^{2+} onto the clay is required. The amount of adsorption and pH range for adsorption/desorption of organic material varies for the different types of clay. It is possible to evaluate the potential for enhanced oil recovery by low salinity water flooding by having a detailed knowledge about the chemical mechanism together with information on the brine composition, oil properties and the type of clay present in the reservoir. Ligthelm et al. (2009) explained the alteration in wettability in terms of electrical double layer effects. He suggested that a decrease in salinity would increase the size of the double layer between the clay and oil interface, leading to the release of organic materials [33].

2.8.1 The Concepts of Wettability

As mentioned earlier, low salinity water flooding is a method to improve oil recovery by turning an oil-wet reservoir into a water-wet reservoir.

The wettability, W, of a reservoir rock can be defined as the fraction of the rock surface that is covered by hydrocarbons. For W = 0, the rock is completely water-wet and for W = 1, it is completely oil-wet. A so called mixed witness occurs at W = 0.5 [32].

The pH in sandstone reservoirs is typically five. At this pH value, both the silica surface of the reservoir rock and the crude oil has a negative charge, and one would expect the silica surface to remain water-wet (no hydrocarbon coating). However, there tend to be some contaminations present, such as clay minerals. Clay particles are very reactive, have a specific surface area and they behave as colloid particles. In the pH range encountered in the sandstone reservoirs, they often have a negative charge due to imperfections in the crystal lattice. Multivalent metal cations, such as Ca^{2+} and Mg^{2+}, act like bridges between the negatively charged oil and clay. In the presence of a high salinity level, positive cations are able to screen-off their negative electrical charges with suppression of the electrostatic repulsive forces and as a result, hydrocarbon particles will adsorb on the clays [32]

2.8.2 Change in Wettability due to Injection of Low-Salinity Water

Low salinity flooding is applied in mixed-to-oil-wet sandstone reservoirs. The oil-wet state can be caused by several factors: [30]

- Certain clay minerals, such as Kaolinite and Illite, may be distributed over the rock surface
- Water with high salinity, and particularly with bivalent cations, may be present in the reservoir
- The reservoir crude oil may contain surface-active components that promotes this state.

In high salinity environments, heavy ends in the oil can form a bond with the negatively charged clay minerals mentioned above via the presence of divalent cations. By

lowering the salinity and reducing the amount of divalent cations in the brine, the electrical diffuse double layers surrounding the negatively charged clay minerals and adsorbed hydrocarbons will expand. Further, this will lead to an increased electrostatic repulsion between the clay and the hydrocarbons. It is believed that when this electrostatic repulsion exceed the attractive forces via divalent cation bridging, the hydrocarbon particles are able to desorb from the clay surface. Since this will result in a reduction of the fraction of the rock surface that is covered by oil, a more water-wet state is obtained. From this, one can draw the conclusion that manipulation of the wettability in EOR depends on the amount and distribution of clay on the reservoir rock. In concept, low salinity injection changes the wettability characteristics of the reservoir rock towards more water wetness. The interfacial chemistry describing low salinity flooding is shown in Figure 2.8.2.1.

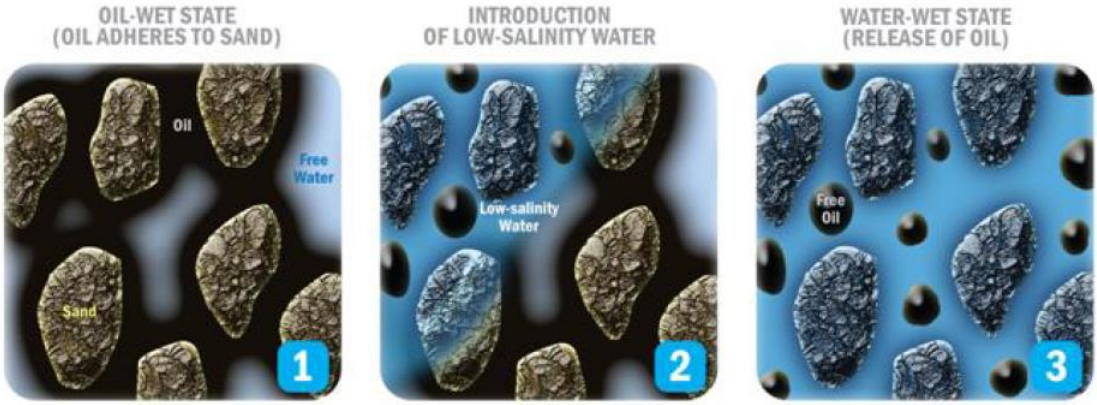

Figure 2.8.2.1: Water-oil-rock interfacial characteristics [32]

The process shown in Figure 2.8.2.1 can be described in the following manner:

1. Polar molecules in the crude oil attract to the negatively charged clay surface. Divalent cations (Ca^{2+}, Mg^{2+} etc.) act as bridges between the negatively charged molecules in the oil and the negatively charged clay surface.
2. Low-salinity water reduces the electrostatic forces holding the oil to the rock, resulting in the release of oil from the rock surface.
3. Low salinity water is injected and the ion exchange equilibrium changes. Trapped oil becomes mobile and oil recovery increases.

2.8.3 Properties of Clay Minerals

The presence of active clay minerals is necessary to obtain low salinity EOR effects. Typically, the crystal structure of clays found in sandstone reservoirs is made up of sheets of tetrahedral silica and octahedral aluminum layers. Clay minerals are often characterized as cation exchange materials due to their charge imbalance, either in the silica or in the aluminum layer and at the edge surfaces, which causes a negative charge on the clay surface. The replacing effect of cations can be ranked as follows: $Li^{+}<Na^{+}<K^{+}<Mg^{2+}<Ca^{2+}<H^{+}$. The magnitude of the selectivity of different cations toward different clays varies considerably. Illite clay is characterized as a 2:1 clay, which means that it consists of three layers where the octahedral aluminum layer lies between two tetrahedral silica layers. The charge imbalance is located in the silica layers where Al^{3+}, which results in a negatively charged surface, replaces Si^{4+} [34].

2.8.4 Previous Studies and Novel Techniques

Since the late 1990s, there have been numerous laboratory tests and field studies where low salinity water injection (LSWI) has resulted in increased oil recovery [2]. A great number of laboratory tests by Morrow and co-workers and by researchers at BP have confirmed that enhanced oil recovery can be obtained by a tertiary low salinity

water flood with salinity in the range of 1000-2000 ppm. Based on tests from different sandstone reservoirs, it was reported that the average increase in recovery was about 14%. The laboratory observations have even been confirmed by single well tests performed in an Alaskan reservoir [33]. On the other hand, research and demonstrations using core flow and single well chemical tracer (SWCT) tests have indicated oil recovery improvements of 5-10% OOIP with LWSI [32]. Thus, the observed oil recovery increase from low salinity water flooding varies with different literature sources.

There is currently a lot of work put into experimental and modeling studies in order to gain more insight into the underlying mechanism of the LSWI effect. A review of the LSWI effect on sandstone, both experimental and modeling work, is presented below.

The effect of fresh and salt water on oil recovery from synthetic and natural cores containing clays was investigated already in 1967 [35]. Both connate and invading brines have proven to alter the wettability and increase the oil recovery at reservoir temperature [36]. Suggested mechanisms behind the LSWI effect on sandstone include fine migration, pH increase, multi-ion exchange, salting-in and wettability alteration. However, some researchers have not observed fine migrations in their study, even though a low salinity effect has been determined [37].

As mentioned earlier, the wettability alteration leads to a low salinity effect since the decrease in salinity increases the size of the double layer between the clay and the oil interface, which in turn leads to organic material release. The expansion of the electric double layer has been investigated as the main mechanism by LSWI through different corefloods using Berea sandstone cores. The results of this study showed that the double layer expansion mechanism is indeed dominant in enhanced oil recovery by LSWI in the secondary flood. [38]

Several new studies has been published regarding simulation and modeling of the effect of LSWI on oil recovery on sandstones, some of which are described below.

A simple analytical fines migration model was made in order to justify incremental oil recovery due to LSWI. The model combined a modified particle-detachment model along with the Dietz model for waterflooding in a layer-cake reservoir. It was validated for a single phase flow by comparing laboratory corefloods. It was reported that the fines migration effect is more pronounced when the viscosity ratio and the heterogeneity of the reservoir increase. However, a model validation for a two-phased oil/water system is still required [39]. It was reported that the reservoir simulations in this study showed that incremental oil recovery depended on both initial and final wetting states; at strong water-wet conditions, the increase of oil relative permeability is the underlying recovery mechanism, while at weak water-wet conditions, the incremental oil recovery is driven by low capillary pressure. It was also reported that the intermediate wetting condition was the ideal wettability alteration condition, since the capillary pressure is low and the increase in oil relative permeability is the main recovery mechanism [40].

A novel water ionic composition optimizing technology, SmartWater, has been investigated using nanofiltration and reverse osmosis membrane processes in a parallel configuration. The advantage of this configuration is the fact that it can generate multiple product water streams to cover the entire range of ionic composition. Due to this flexibility, the desired composition and ionic content compatible for injection into the reservoir, either by itself or in combination with other EOR fluids, can be tailor-made. Low ionic strength water blends with the desired ratio of monovalent and divalent ions can be custom made using the investigated technology to suit SmartWater technology in both sandstone and carbonate reservoirs [41]. SmartWater can improve wetting properties of oil reservoirs and optimize fluid

flow/oil recovery in porous medium during production. It is made by modifying the ion composition, and is thereby free of expensive chemicals and environmental friendly.

2.9 Instrument Description

Theory regarding the instruments used in this experiment is described in the following sections.

2.9.1 Tensiometer

The sigma 700 tensiometer, which was used in this experiment, measures the interfacial tension between two fluids by measuring the force detected on a probe, which interacts with both fluids. The probe is placed on a balance, which measures the force required to detach the probe from a surface or interface. This force is further used to calculate the interfacial tension. The probe used in this experiment is a Du Noüy ring. Before conducting any experiments, the calibration of the Sigma 700 tensiometer had to be tested using a water test.

The Du Noüy ring method utilizes a platinum ring, which is lowered into the solution that is to be studied. It is important that the ring is fully submerged below the interface in the heavy phase. The ring is then carefully pulled upwards towards the interface and into the light face, which in this experiment is air. As the ring is pulled out of the heavy phase, a meniscus is formed which will exert a force onto the balance. Eventually, a maximum is achieved right before the meniscus breaks and the ring is returned to the heavy phase. A schematic illustration of the different steps are shown in Figure 2.9.1.1.

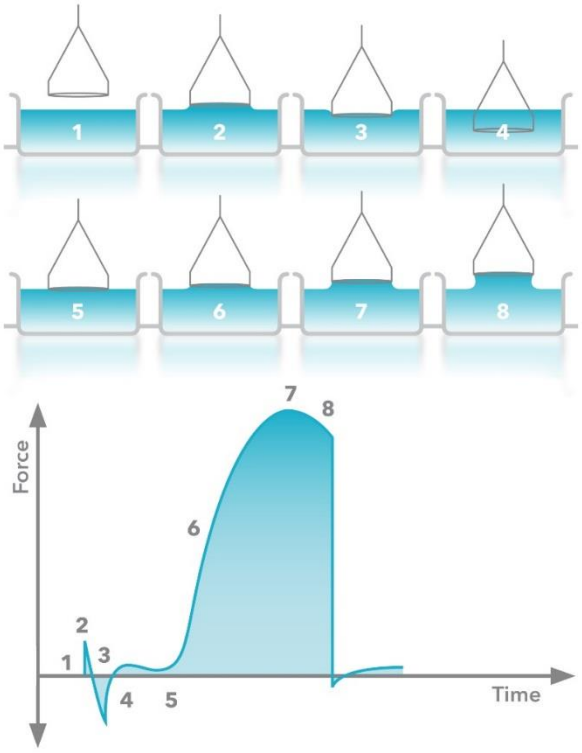

Figure 2.9.1.1: Schematic illustration of a Du Noüy ring tensiometer at various time intervals and the corresponding plot showing the force vs. the time [42]

An explanation of the different points in Figure 2.9.1.1 is given below:

1. The ring is above the surface and the balance observe zero force
2. The ring connects with the interface and there is a small increase in force caused by adhesive forces between the ring and the interface.
3. A small negative force is detected as the ring is pushed through the interface
4. After the ring has been pushed through the interface, a small positive force is measured due to the supporting wires of the ring
5. The ring re-enters the interface and the force starts to increase
6. The force continues to increase as the meniscus is pulled upwards
7. A peak in detected force is obtained
8. A small decrease in force is detected before the meniscus breaks.

The force detected by the platinum ring is, assuming that the ring is completely wetted by the solution, is given by Equation 11 [43]:

$$F_t = W_r - b + 2 \cdot (2 \cdot \pi \cdot r \cdot \gamma) \quad (11)$$

where F_t is the measured force inhibited on the ring, W_r is the weight of the ring in the light phase, b is the buoyancy, *r* is the radius of the ring and γ is the interfacial tension. The factor of two is because the liquid is in contact with the rings both inner and outer perimeter. In practical experiments, the weight of the ring and the buoyancy is corrected for by resetting the instrument before measuring. The net force can then be obtained by Equation 12:

$$F = 4 \cdot \pi \cdot r \cdot \gamma \quad (12)$$

The calculation of γ from the equation above is however prone to huge errors due to the complex nature of the meniscus. This error can be corrected for by defining a correction factor K, as shown in Equation 13:

$$\gamma = \frac{K \cdot F}{4 \cdot \pi \cdot r} \quad (13)$$

2.9.2 UV-vis Spectroscopy

All molecules are capable of absorbing electromagnetic radiation at their own characteristic wavelengths. This process will transfer energy to the molecule and lead to a decrease in the electromagnetic radiation [44].

In order to understand the fundamental principles of practical absorption spectrometry, it may be useful to make a short diversion into the world of quantum theory. In quantum theory, radiation is considered a stream of particles rather than

waves. Atoms and molecules exist in a number of defined energy states or levels and a change of level requires the absorption or emission of an integral number of a unit of energy called a quantum, in this context known as a photon.

The absorption law, also known as the Beer-Lambert law, states that the concentration, C, and the path length, l, of the absorbing medium is directly proportional to the absorbance, A. The law is only valid for monochromatic radiation (radiation of a single wavelength) and requires that the physical or chemical state of the absorbing molecule does not change with concentration.

The transmittance, T, of a solution is the fraction of incident radiation transmitted by the solution, and is defined as the ratio shown in Equation 14:

$$T = \frac{I}{I_0} \tag{14}$$

where I_0 is the intensity of the incident radiation and I is the intensity of the transmitted radiation. The transmission is often expressed as a percentage referred to as the percent transmittance.

The absorbance, A, of a solution relates to the percentage transmittance, T, and is expressed by Equation 15:

$$A = log\frac{I_0}{I} = -logT \tag{15}$$

It can be observed that as the absorbance of a solution increases, the transmittance decreases. The transmittance, T, and absorbance, A, are graphically illustrated in Figure 2.9.2.1.

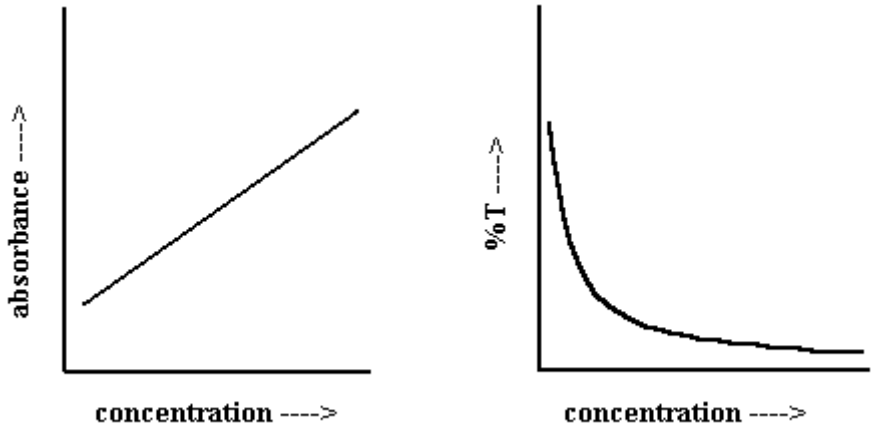

Figure 2.9.2.1: To the left: absorbance vs. concentration. To the right: percent transmittance vs concentration [45]

By including the definition of the Beer-Lambert law mentioned earlier in this chapter, we obtain Equation 16:

$$A = a \cdot l \cdot c \tag{16}$$

where a is a proportionality constant known as the absorptivity, l is the path length of the absorbing medium and c is the concentration of the absorbing substance (see Figure 2.9.2.2). The absorptivity is constant dependent only on the nature of the molecule and the wavelength of the radiation. Since absorbance is a unitless quantity, the absorptivity is required to have units that cancel out the units of the concentration and path length. If the concentration is expressed in moles per liter and b in centimeter, the absorptivity must have the unit L/mol·cm. In this specific case, the proportionality constant is referred to as the molar absorptivity.

Figure 2.9.2.2 shows the attenuation (the decrease in energy per unit area of a beam of radiation). The dark red incident beam signifies a higher radiant energy than the light red transmitted beam. When measuring transmittance and absorbance, the

solution to be studied has to be placed in a vessel made of transparent material, known as a cell or cuvette. The surfaces of these cells through which the radiation passes are highly polished to keep reflection and scatter losses to a minimum.

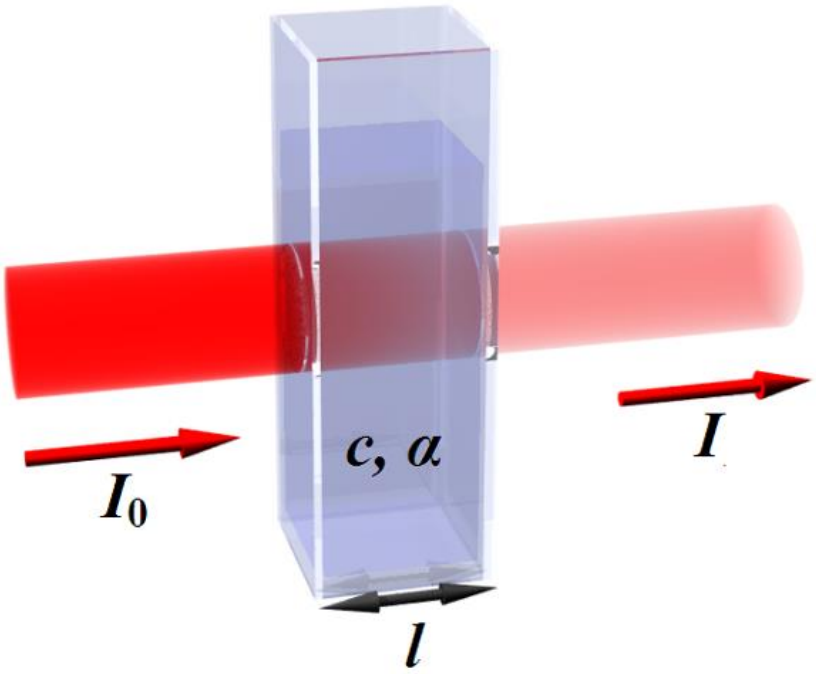

Figure 2.9.2.2: Attenuation of a beam of radiation by an adsorbing medium [46]

Reflection at the cell walls and scattering losses in the solution can cause substantial losses. As an example, approximately 8.5% of a beam of yellow light is lost by reflection when it passes through a glass cell. Light scattering in the solution is a consequence of large molecules or particles (such as dust) in the solvent. This will cause an increased attenuation of the beam as it goes through the solution. To prevent any inaccuracy, a cell containing only the solvent is compared with the cell containing the analyte solution. This will compensate the effects of the reflection and scattering losses.

Variables that influences the absorbance: Common variables that may influence the adsorption spectrum are the nature of the solvent, the pH of the solution, the temperature, high electrolyte concentrations and the presence of interfering

substances. It is therefore important that these variables are known and that the conditions of the experiments are chosen in such a manner that the absorbance will not be materially affected by minor, uncontrolled variations in their magnitudes [47]

3. Materials and Experimental Procedure

The materials and experimental procedures used in this experiment are described in the following sections.

3.1 Materials

3.1.1 Illite

The clay mineral used in this experiment was Illite, which is a layered alumino-silicate mineral. It has a structure that consists of repetitive layers of tetrahedron-octahedron-tetrahedron (TOT) and the chemical formula is given as $(K,H_3O)(Al,Mg,Fe)_2(Si,Al)_4O_{10}[(OH)_2,(H_2O)]$. The K and Mg interlayer cations prevent the entrance of water molecules into the structure. Thus, the Illite clay is non-expanding. It occurs as aggregates of small monoclinic grey crystals, as shown in Figure 3.1.1.1.

Figure 3.1.1.1: Illite clay [48]

The cation exchange capacity (CEC) of Illite is higher than that of kaolinite, typically around 20 – 30 mEq/100 g. The structure of the Illite clay will typically induce so called

pore bridging, which reduces the permeability within the clay [49]. This phenomenon is shown in Figure 3.1.1.2.

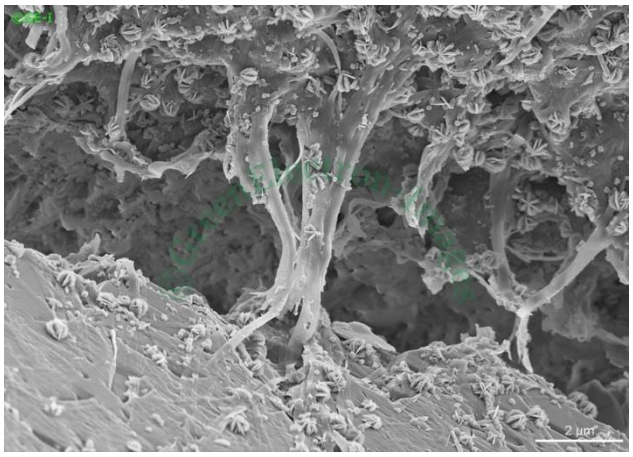

Figure 3.1.1.2: Pore bridging in Illite clay [50]

Pure Illite is typically hard to find. The Illite used in this experiment was purchased from The Clay Minerals Society's web shop.

3.1.2 SDBS

The surfactant used in this experiment is the anionic sodium dodecylbenzensulfonate (SDBS). It is a colorless salt with the molecular formula $C_{18}H_{29}NaO_3S$ and is displayed in Figure 3.1.2.1. The literature-reported value for the CMC of SDBS in water is $1.6 \cdot 10^{-3}$ M, and the presence of electrolytes is known to decrease the CMC of surfactants [51]. It should be mentioned that this value varies in different literature.

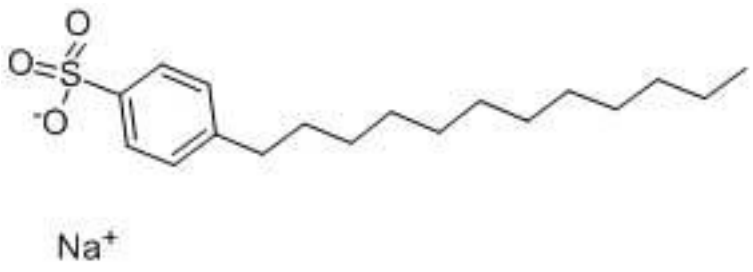

Figure 3.1.2.1: A schematic illustration of the linear dodecyl-4-benzenesulfonate anion [52]

Because of their excellent properties as surfactants in detergents and cleansing agents and their low production costs compared to other surfactants, the dodecylbenzenesulfonates are the most important group of synthetic surfactants in terms of quantity [53]

The reservoir rock in a crude oil reservoir usually consists of sand stone (SiO_2) or carbonate ($CaCO_3$). In Norway however, it consists only of sand stone. The surface of sand stone has a negative charge, thus an anionic surfactant is favorable due to repulsive forces.

3.1.3. NaCl and $CaCl_2$

The salts used in the various salinity solutions are natrium chloride (NaCl), which is a monovalent salt, and calcium chloride ($CaCl_2$), which is a divalent salt. It is expected that the divalent salt will lead to a reduction in CMC and thereby promote adsorption.

3.2 Experimental Procedure

3.2.1 Parameters

A literature study of similar projects and reservoir conditions was conducted before starting the experiment to make sure reasonable parameters was used. The type of clay and surfactant was determined prior to the project.

Salinity

The experiment was carried out using three different salinity concentrations. One medium salinity and one with low salinity, below 3000 ppm. In addition, two different salts were chosen since it was desirable to observe the effect of divalent cations. Thus,

two low salinity solutions were prepared, one with only NaCl and one with both NaCl and $CaCl_2$. The same was done for medium salinity. In addition, one high salinity condition was prepared. The latter was only prepared using NaCl due to precipitation when adding $CaCl_2$. This resulted in a total of five different salinity solutions. The exact concentrations were calculated using the pre-determined ratio between NaCl and $CaCl_2$ 45:1 and ionic strengths 0.02, 0.08 and 0.2 for low salinity, medium salinity and high salinity, respectively. The various electrolyte concentrations and compositions are shown in Table 3.2.1.1.

Table 3.2.1.1: Overview of the various electrolyte concentrations and compositions used in the experiment.

	Low salinity	**Low salinity with $CaCl_2$**	**Medium salinity**	**Medium salinity with $CaCl_2$**	**High salinity**
Ionic strength [M]	0.02	0.02	0.08	0.08	0.2
Concentration of NaCl [ppm]	1169	1096	4675.2	4.383	11688
Concentration of $CaCl_2$ [ppm]	-	61.3	-	0.245	-

Originally, it was the high salinity condition and the low salinity condition which was to be compared. However, due to the precipitation problem with the high salinity condition mentioned earlier, a medium salinity condition had to be prepared as well.

Surfactant concentration

The concentrations chosen for the adsorption isotherms in this experiment are shown in Table 3.2.1.2.

Table 3.2.1.2: Overview of the various surfactant concentrations used for the adsorption isotherms.

Sample	Surfactant concentration [M]
1	$5.00 \cdot 10^{-5}$
2	$7.50 \cdot 10^{-5}$
3	$1.00 \cdot 10^{-4}$
4	$2.50 \cdot 10^{-4}$
5	$5.00 \cdot 10^{-4}$
6	$7.50 \cdot 10^{-4}$
7	$1.00 \cdot 10^{-3}$
8	$2.50 \cdot 10^{-3}$

For the UV calibration curves and the CMC determination using the sigma tensiometer, slightly different concentrations were used. These concentrations are shown in Table 3.2.1.3 and Table 3.2.1.4, respectively.

Table 3.2.1.3: Overview of the various surfactant concentrations used for the UV calibration curves.

Sample	Surfactant concentration [M]
1	$5.00 \cdot 10^{-5}$
2	$1.00 \cdot 10^{-4}$
3	$2.00 \cdot 10^{-4}$
4	$4.00 \cdot 10^{-4}$
5	$6.00 \cdot 10^{-4}$
6	$8.00 \cdot 10^{-4}$
7	$1.00 \cdot 10^{-3}$
8	$1.20 \cdot 10^{-3}$

Table 3.2.1.4: Overview of the various surfactant concentrations used for the CMC determination using the Sigma tensiometer.

Sample	Surfactant concentration [M]
1	$5.00 \cdot 10^{-6}$
2	$1.00 \cdot 10^{-5}$
3	$5.00 \cdot 10^{-5}$
4	$1.00 \cdot 10^{-4}$
5	$5.00 \cdot 10^{-4}$
6	$1.00 \cdot 10^{-3}$
7	$5.00 \cdot 10^{-3}$
8	$1.00 \cdot 10^{-2}$

The reason why slightly different concentration ranges are used is the instruments varying abilities in certain concentrations. For example, a sample with the concentration $5 \cdot 10^{-6}$ would produce different absorption values on the UV when measured several times. Thus, measuring this concentration on the UV-vis would not produce liable results. The concentration range for the samples used in the adsorption experiments is also a bit different from the one used for the calibration curves. This is simply because the range for the adsorption experiments was chosen by analyzing the range from the calibration curve, and a few changes were made in order to get the best isotherms.

pH

The pH was measured using a pH meter in order to have a reference in case the experiment is to be repeated.

Mixing Ratio of Clay and Surfactant

The samples was prepared in 30 ml batches with three parallels. The batches were made by weighing out Illite clay (0.3g) in a centrifugal tube (45mL) and adding the different surfactant concentrations and salinity solutions (30mL).

Centrifugation and UV-vis Measurements

During the experiments, a time dependency was observed for the measured absorption values when using the UV-vis spectroscopy. Measurements of the exact same sample produced different results depending on how long after the preparation they were measured. Due to this, it became crucial to measure the samples straight away after preparation. Hence, only two by two different concentration could be prepared and measured at a time, which was a time demanding procedure.

Thus, six samples were prepared at a time (two different concentrations with three parallels each). After preparation they were agitated for 24 hours at 250 rpm. The centrifugal tubes were placed horizontally in the shaker to ensure an efficient mixing. After 24 hours, the samples were centrifuged for 15 minutes at 11 000 rpm. The supernatant was removed from the tube and placed in another 45mL centrifugal tube, which was centrifuged for another 15 minutes at 11 000 rpm. The supernatant was yet again removed and placed in a 15 mL centrifugal tube, which was centrifuged one last time at 15 minutes at 11 000 rpm. The remaining supernatant was kept for UV-vis measurements, which was conducted straight away after the centrifugation.

In addition, blank samples were made for each of the salinity solutions. These samples did not contain any surfactants, only brine and clay. The blank samples were prepared in the same manner as described in the section above. They were used as references and baseline solutions.

For the UV-vis measurements, a baseline close to that of the actual sample had to be chosen. For the samples which had not been in contact with Illite (which was used to calculate the concentration before contact with the clay), the respective salinity solution was used. For the samples which had been in contact with Illite, the respective blank sample was used. In this experiment, a wave length of 260nm was used.

Temperature and Pressure

The temperature and pressure were kept at normal conditions throughout the experiment. Room temperature and atmospheric pressure is therefore assumed.

3.2.2 Determination of CMC Using Sigma 700 Tensiometer

It was attempted to determine the CMC for each of the five different salinities. This was achieved by measuring the interfacial tension using a Sigma 700 Tensiometer in variuos surfactant concentrations. A calibration curve was made by plotting the interfacial tension versus the surfactant concentration. Microsoft Excel was used to obtain a mathematical equation for the trend line so the CMC could be calculated. The calculated CMC values are presented in the results.

3.2.3 Calibration Curves for the UV-vis

Five calibration curves were produced in this experiment; one for each salinity condition. The calibration curves were obtained by measuring the absorption of the various surfactant concentrations in each of the salinity solutions. The absorption was measured at a wavelength of 260 nm, since this wavelength produced the greatest absorption values.

3.2.4 Adsorption Isotherms

The amount of surfactant adsorbed was determined by measuring the absorption in all the different concentrations after contact with Illite using the UV-vis spectroscopy. These values were plotted into the respective trend line equations from the UV calibration curves. The concentration of the samples after contact with Illite could now be calculated. The concentration of the samples without Illite had to be calculated as well, since it deviated from the original concentration due to the time dependency mentioned earlier. This concentration is called the equilibrium concentration. The adsorption was determined as the difference between the concentration after contact with Illite and the equilibrium concentration. Further, the isotherms were obtained by constructing plots of the calculated adsorption versus the equilibrium concentration. The adsorption isotherms are presented in the results.

3.3 Clay Treatment

Before the main experiment was conducted, the clay was treated in several washing steps. The goal with these washing steps was to achieve equilibration of the Illite clay and its purified sodium form in water. This mechanism involves a rapid ion exchange and/or an electrostatic adsorption step and a slow step. The latter is most likely because of dissolution of aluminum particles due to prolonged contact of Illite and water. The various washing steps performed in this experiment are described in the following sections.

Water Wash

Illite clay (500g) was transferred to a large beaker and diluted with distilled water (500mL). The water was added during a time interval of 30 minutes and mixed with a magnetic stirrer. The clay/water mixture was left on the stirrer for two hours at 370 rpm. After mixing, the clay was left for sedimentation for two days. A small amount of the supernatant was kept for further analysis while the rest was removed using a

peristaltic pump and decantation. The supernatant was analyzed by conductivity measurements. This procedure was repeated until the conductivity of the supernatant was constant (three to four times in total).

NaCl Wash

NaCl (5.844g) was mixed with distilled water (500 mL). This mixture was added during a time interval of 30 minutes and mixed with a magnetic stirrer. The clay/salt water mixture was left on the stirrer for two hours at 370 rpm. After the mixing, the clay was left for sedimentation for approximately 5 hours. A small amount of the supernatant was kept for further analysis while the rest was removed using a peristaltic pump and decantation. The supernatant was analyzed by conductivity measurements. This procedure was repeated until the conductivity of the supernatant was constant (three times in total).

NaCl/HCl Wash

NaCl (2.922g) was mixed with distilled water (50mL). This mixture was added during a time interval of 15 minutes and mixed with a magnetic stirrer. pH was adjusted with concentrated HCl (37wt%) to pH 3 in order to remove $Al(OH)_2$ surface contamination. The product was diluted with distilled water (450mL) and left on the the stirrer for two hours at 370 rpm. After the mixing, the clay was left for sedimentation for approximately 5 hours. A small amount of the supernatant was kept for further analysis while the rest was removed using a peristaltic pump and decantation. The supernatant was analyzed by conductivity measurements. This procedure was repeated until the conductivity of the supernatant was constant (three times in total).

Weak NaCl Wash

NaCl (0.2922g) was mixed with distilled water (500mL). This mixture was added during a time interval of 30 minutes and mixed with a magnetic stirrer. The clay/salt water mixture was left on the stirrer for two hours at 370 rpm. After the mixing, the clay was

left for sedimentation for 24 hours. A small amount of the supernatant was kept for further analysis while the rest was removed using a peristaltic pump and decantation. The supernatant was analyzed by conductivity measurements. This procedure was repeated until the conductivity of the supernatant was constant (three times in total).

Filtering and Drying

The Na-clay product obtained was filtered by vacuum filtration using a Buchner funnel and dried in a drying cabinet at 50°C for three to five days.

Analysis of Treated Clay

The dry, treated clay (0.3g) was added to a centrifugal tube, which was filled with distilled water (30mL). The mixture was shaken for 24 hours at 250 rpm. The same procedure was carried out using a sample of untreated clay. The samples were centrifuged for 30 minutes at 7000 rpm and the supernatant was kept for further analysis. The supernatant of the two samples were analyzed by conductivity and surface tension measurements, and compared.

3.4 HSE

Before starting the experiment, a risk assessment had to be carried out. This risk assessment is found in appendix A, and evaluates the risk associated with the different chemicals and apparatus used in the experiment.

4. Results and Discussion

The experimental results are displayed and discussed in the following sections.

4.1 Determination of CMC using Sigma 700 Tensiometer

By analyzing the plots obtained using the tensiometer, an attempt was made to determine the CMC of the various salinity conditions. The results are shown in Table 4.1.1.

Table 4.1.1: Overview of the CMC for the different salinity conditions

Salinity condition	**CMC [M]**
Low salinity	$6.309 \cdot 10^{-4}$
Low salinity with $CaCl_2$	$2.249 \cdot 10^{-4}$
Medium salinity	$1.992 \cdot 10^{-4}$
Medium salinity with $CaCl_2$	$1.194 \cdot 10^{-4}$
High salinity	$1.090 \cdot 10^{-4}$

For the low salinity condition without $CaCl_2$, the CMC was determined to $6.309 \cdot 10^{-4}$ M from the calibration curve calculations. Compared to the literature value for the CMC for SDBS, which in Chapter 3.1.2 was said to be $1.6 \cdot 10^{-3}$, this value makes sense since adding electrolyte lower the CMC. For the low salinity condition with $CaCl_2$, the CMC was even lower at $2.249 \cdot 10^{-4}$, which also seems right from a theoretical aspect. For the two medium salinity conditions, the calculated CMC values are almost identical. These values seem to have decreased with the addition of electrolyte as well. This trend continues with the high salinity condition.

The plot used for determining the CMC value for the low salinity condition without calcium is displayed in the following section. The rest of the graphs and the values used for plotting them are found in Appendix C.

4.1.1 Low Salinity

The interfacial tension was measured using eight various surfactant concentrations. The results were analyzed by making a plot of the concentrations versus the interfacial tension. The plot is shown in Figure 4.1.1.1, and a clear breaking point in interfacial tension is observed. By using Microsoft Excel, an equation for each of the trend lines was obtained.

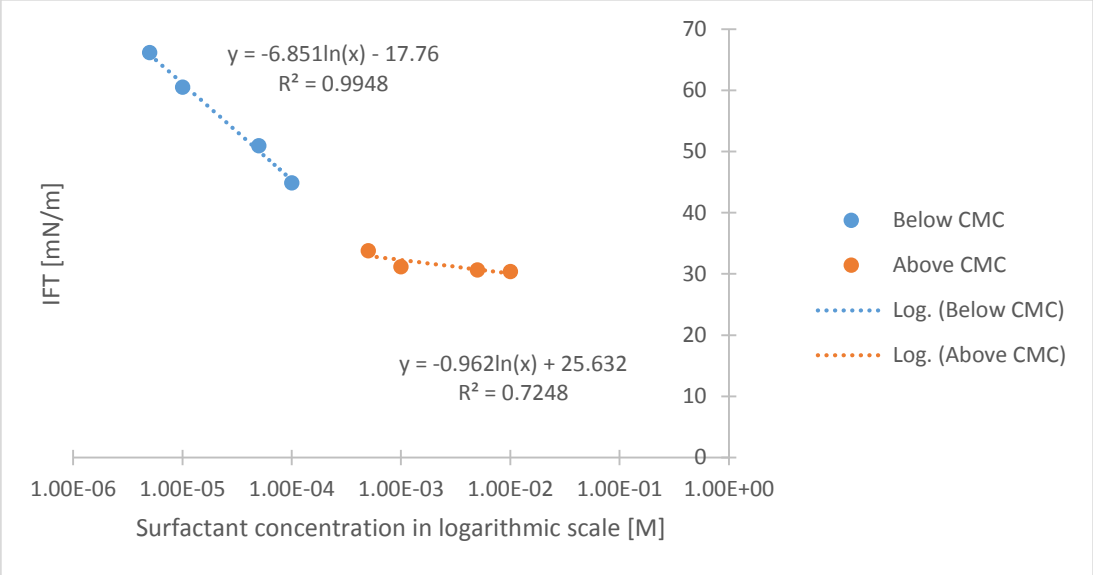

Figure 4.1.1.1: A plot of various surfactant concentrations versus the corresponding interfacial tension values in a low salinity solution. The trend line equations are included.

The CMC was obtained by putting the two equations in the graph equal to each other:

$$-6.851\ln(x) - 17.76 = -0.962\ln(x) + 25.632$$

and solving for x:

$$x = \frac{1}{e^{\frac{14464}{1963}}} = 6.309 \cdot 10^{-4}$$

This resulted in a CMC of $6.309 \cdot 10^{-4}$ M.

4.2 Calibration Curves Obtained Using UV-vis Spectroscopy

The absorption of SDBS could be determined by the UV method due to the benzene ring in the molecular structure of SDBS. The values used for plotting the following graphs were obtained at 260nm are found in Appendix D.

4.2.1 Low Salinity

The UV calibration curves were created by measuring the absorption for various surfactant concentrations. The results were plotted and the calibration curve for the low salinity condition is illustrated in Figure 4.2.1.1.

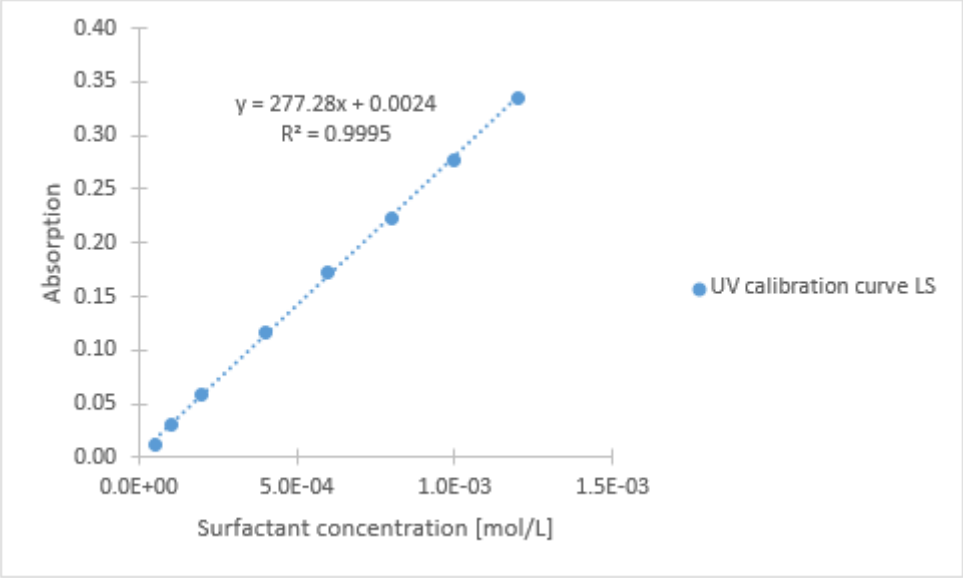

Figure 4.2.1.1: The UV calibration curve for the low salinity solution obtained at 260nm. The trend line equation is included.

The graph has a R^2 value of 0.9995, which correspond to a good straight-line approximation.

The rest of calibration curves are displayed in Appendix D. By analyzing these plots, it looks like the calcium-containing calibration curves have small deviations from a straight line. The deviations are slightly S-shaped and may be caused due to the fact that the samples did not get measured straight away after preparation. This time dependency is further discussed in Chapter 4.2.6

4.2.6 Time Dependency

As seen in the plot above and the plots in Appendix D, a time dependency was observed for the measured absorption values when using the UV-vis spectroscopy. This led to a S-shaped curve, and it seemed to influence the calcium-containing samples more than the one with only sodium chloride.

Because of this observation, a test was run in order to get a better understanding of the time dependancy. The result showed that measurements of the exact same sample produced different results depending on how long after the preparation they were measured. This phenomenon is shown in Figure 4.2.6.1. Here, a one-day-old sample of the low salinity condition with calcium is compared to a one-week-old sample.

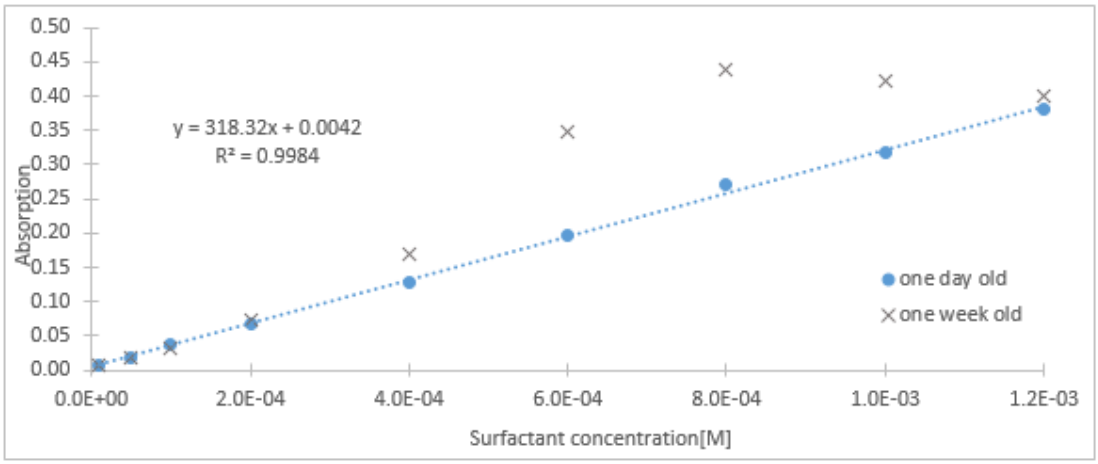

Figure 4.2.6.1: A calibration curve of low salinity with $CaCl_2$ showing the time dependency of measured absorbance.

The fact that the calcium-containing sample is more affected of this time dependency than the ones with only sodium chloride may be due to formation of a complex between calcium and surfactants, where one calcium ion bonds with two surfactants. This bonding might affect the absorption and lead to increasing adsorption for the calcium-containing samples over time.

4.2.7 UV-spectra

The UV-spectra obtained directly from the UV-vis spectroscopy show the wave length as a function of the absorption. The spectrum for low salinity is displayed in Figure 4.2.7.1 to show why the specific wavelength was chosen in the UV-vis experiments. Similar for all the plots is the absorption peak at approximately 260nm. This trend was

common to the spectra in the other salinities conditions as well, and 260nm was therefore chosen for all the experiments. The figure also shows how the absorption increases with increasing surfactant concentration. It looks like the absorption doubles in value when the surfactant concentration doubles.

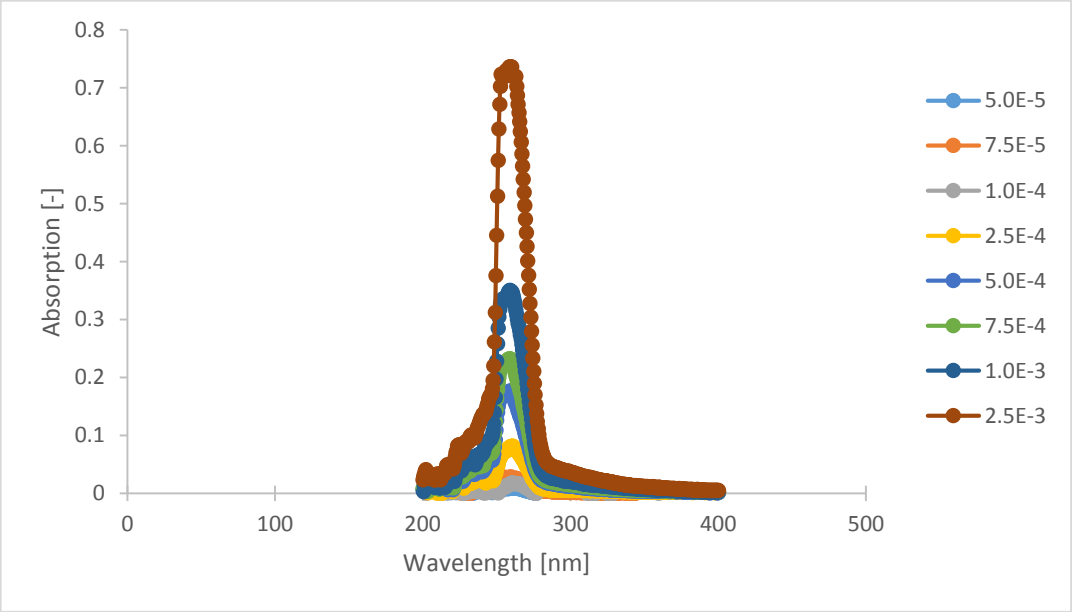

Figure 4.2.7.1: The UV-spectrum for the low salinity condition showing the absorption vs. the wavelength. The spectrum has an absorption peak at 260nm. To the right in the figure, the respective surfactant concentrations are displayed.

4.3 Adsorption Isotherms

Because of the time consuming experimental method that had to be carried out when creating the adsorption isotherms (due to the time dependency) using the UV-vis spectroscopy, there were not enough time to attempt the adsorption isotherms using the tensiometer. Also, the small attempt that was made did not produce liable results.

The adsorption isotherms were obtained by measuring the absorption after addition of Illite clay in a series of known surfactant concentrations. The measured absorption

values were plotted into the corresponding trend line equation, and the concentration after adsorption was calculated. The concentration of the samples without Illite had to be calculated as well, since it deviated from the original concentration due to the time dependency mentioned earlier. This concentration is called the equilibrium concentration. The adsorption was determined as the difference between the concentration after contact with Illite and the equilibrium concentration. Further, the isotherms were obtained by constructing plots of the calculated adsorption versus the equilibrium concentration. The values used for plotting the following graphs are found in Appendix B. All of the isotherms were plotted in a linear-linear scale. The following sections do only include the graphical illustrations of the isotherms, further description and discussion of them are found in Chapter 4.4.

4.3.1 Low Salinity

The adsorption curve for the low salinity condition is shown in Figure 4.3.1.1.

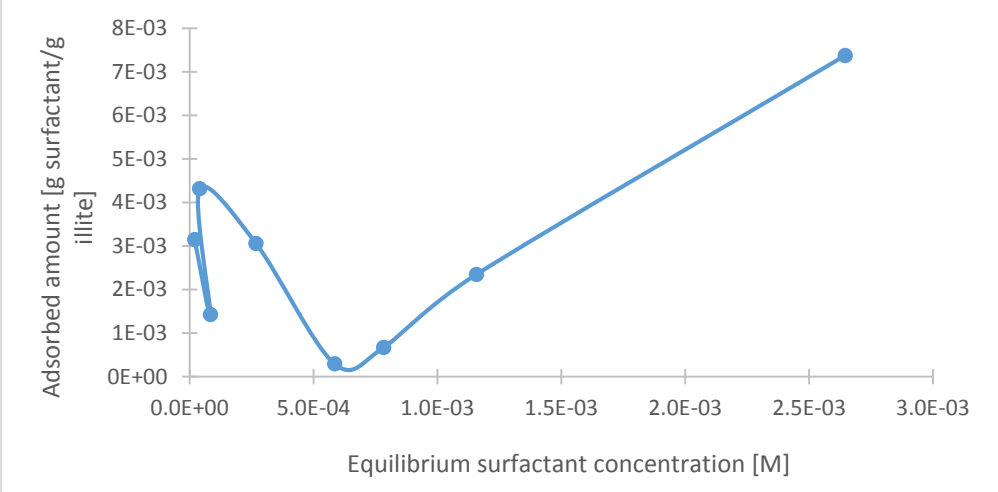

Figure 4.3.1.1: A plot of low salinity adsorption onto Illite clay versus the equilibrium concentration.

4.3.2 Low Salinity with $CaCl_2$

The adsorption curve for the low salinity condition with calcium is shown in Figure 4.3.2.1.

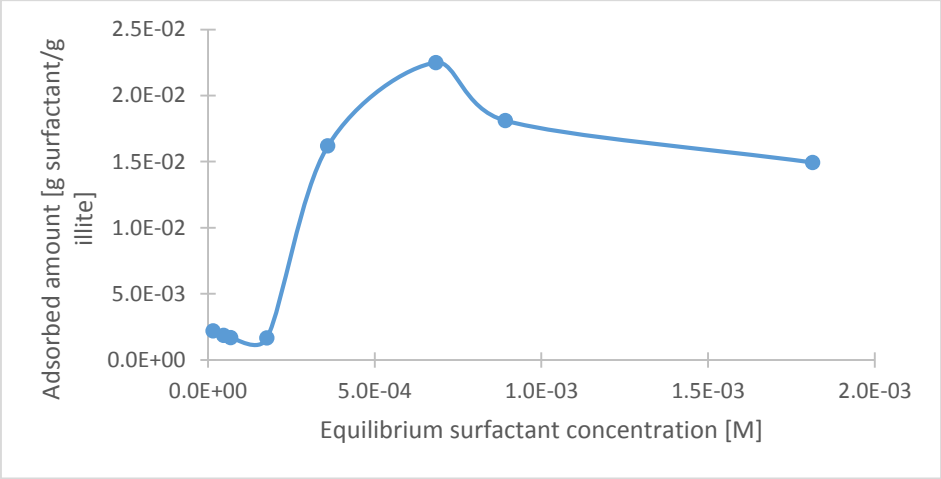

Figure 4.3.2.1: A plot of low salinity adsorption with $CaCl_2$ onto Illite clay versus the equilibrium concentration.

4.3.3 Medium Salinity

The adsorption curve for the medium salinity condition is shown in Figure 4.3.3.1.

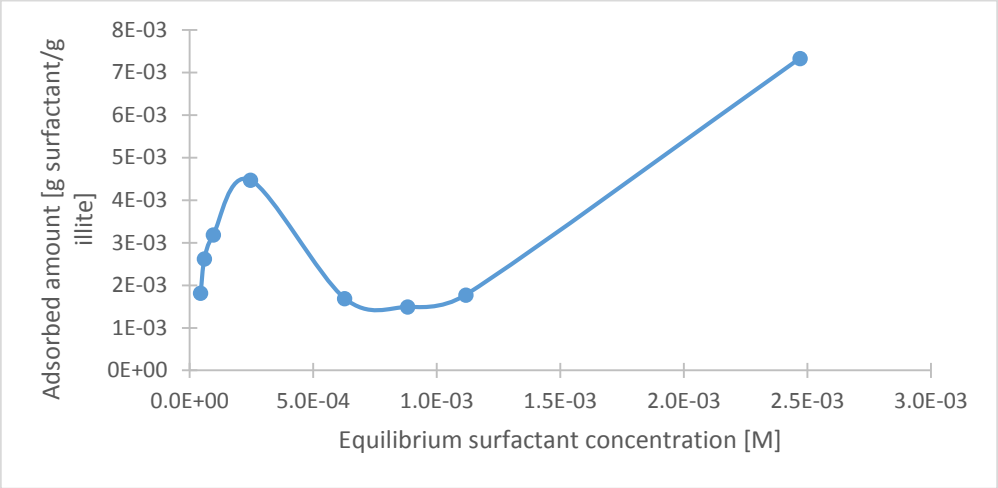

Figure 4.3.3.1: A plot of medium salinity adsorption onto Illite clay versus the equilibrium concentration.

4.3.4 Medium Salinity with $CaCl_2$

The adsorption curve for the low medium condition with calcium is shown in Figure 4.3.4.1.

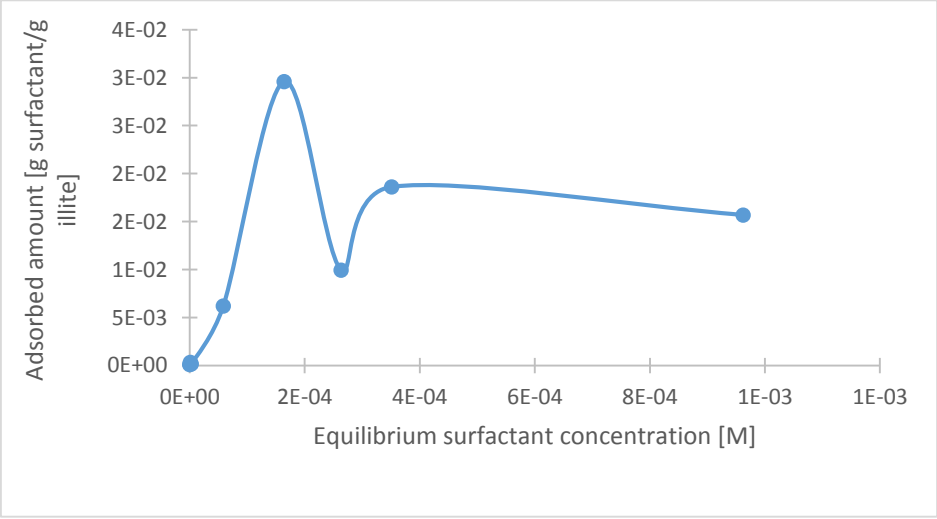

Figure 4.3.4.1: A plot of medium salinity adsorption with $CaCl_2$ onto Illite clay versus the equilibrium concentration.

4.3.5 High Salinity

The adsorption curve for the high salinity condition is shown in Figure 4.3.5.1.

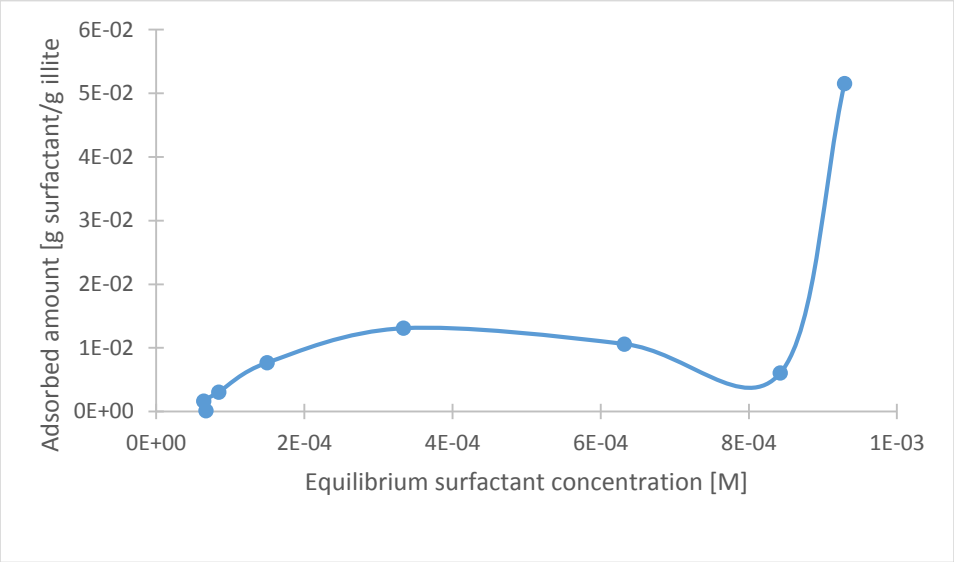

Figure 4.3.5.1: A plot of high salinity adsorption onto Illite clay versus the equilibrium concentration.

4.4 Comparison of Adsorption isotherms

The graphs displayed in Chapter 4.3 are compared and further discussed in the following sections.

4.4.1 Comparison of Adsorption Isotherms without $CaCl_2$

The adsorption isotherms of the low salinity, medium salinity and high salinity conditions without calcium are plotted together in Figure 4.4.1.1.

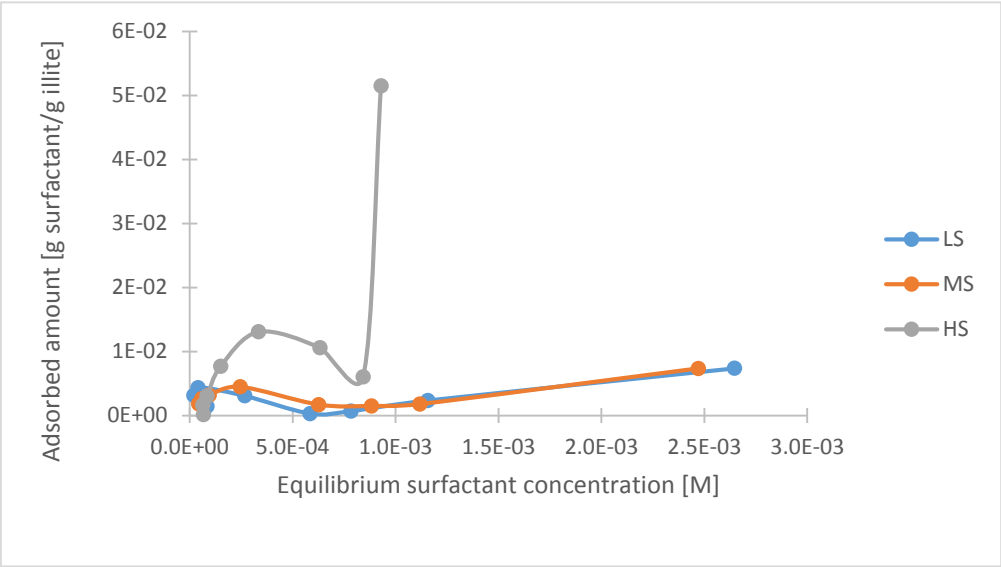

Figure 4.4.1.1: An overview of the adsorption isotherms of low salinity (LS), medium salinity (MS) and high salinity (HS) without calcium.

The actual values of the equilibrium concentrations and adsorbed amounts of surfactants onto Illite clay are displayed in Table 4.4.1.1.

Table 4.4.1.1: An overview of the values of the equilibrium concentrations and the corresponding adsorbed amounts for the different salinity conditions; low salinity (LS), medium salinity (MS) and high salinity (HS). The two maximum peaks for each salinity are written in bold.

LS		**MS**		**HS**	
Equilibrium surfactant concentration [M]	Adsorbed amount [g surf/g Illite]	Equilibrium surfactant concentration [M]	Adsorbed amount [g surf/g Illite]	Equilibrium surfactant concentration [M]	Adsorbed amount [g surf/g Illite]
$2.02 \cdot 10^{-5}$	$3.14 \cdot 10^{-3}$	$4.41 \cdot 10^{-5}$	$1.81 \cdot 10^{-3}$	$6.76 \cdot 10^{-5}$	$1.11 \cdot 10^{-4}$
$8.39 \cdot 10^{-5}$	$1.42 \cdot 10^{-3}$	$5.91 \cdot 10^{-5}$	$2.62 \cdot 10^{-3}$	$6.44 \cdot 10^{-5}$	$1.60 \cdot 10^{-3}$
$4.06 \cdot 10^{-5}$	$\mathbf{4.31 \cdot 10^{-3}}$	$9.49 \cdot 10^{-5}$	$3.18 \cdot 10^{-3}$	$8.45 \cdot 10^{-5}$	$3.04 \cdot 10^{-3}$
$2.68 \cdot 10^{-4}$	$3.06 \cdot 10^{-3}$	$2.45 \cdot 10^{-4}$	$\mathbf{4.47 \cdot 10^{-3}}$	$1.50 \cdot 10^{-4}$	$7.67 \cdot 10^{-3}$
$5.85 \cdot 10^{-4}$	$2.93 \cdot 10^{-4}$	$6.27 \cdot 10^{-4}$	$1.69 \cdot 10^{-3}$	$3.34 \cdot 10^{-4}$	$\mathbf{1.31 \cdot 10^{-2}}$
$7.84 \cdot 10^{-4}$	$6.70 \cdot 10^{-4}$	$8.82 \cdot 10^{-4}$	$1.49 \cdot 10^{-3}$	$6.32 \cdot 10^{-4}$	$1.06 \cdot 10^{-2}$
$1.16 \cdot 10^{-3}$	$2.35 \cdot 10^{-3}$	$1.12 \cdot 10^{-3}$	$1.77 \cdot 10^{-3}$	$8.43 \cdot 10^{-4}$	$6.03 \cdot 10^{-3}$
$2.65 \cdot 10^{-3}$	$\mathbf{7.37 \cdot 10^{-3}}$	$2.47 \cdot 10^{-3}$	$\mathbf{7.33 \cdot 10^{-3}}$	$9.29 \cdot 10^{-4}$	$\mathbf{5.15 \cdot 10^{-2}}$

From the graph and table above, it is clear that the low and medium salinity conditions have a much lower adsorption of surfactants onto Illite clay than high salinity, which is expected. This is due to the expansion of the electrical double layer when the salinity decreases, and thereby the decrease in adsorption. The highest adsorption value for the high salinity condition is almost ten times as great compared to the highest values of the other salinities. When comparing the low and medium salinity conditions, a lower adsorption should be observed for the low salinity case. However, the two isotherms are almost identical. This result does not match the theory and might be explained by the sources of error in Chapter 4.10.

One thing that all three isotherms seem to have in common is two maximum peaks, which are outlined in Table 4.4.1.1. These two peaks could indicate a two-step

adsorption mechanism, where the first step involves the surface active species being adsorbed through the interactions between the surface active species and the solid surface, and the second step in which the surface active species are adsorbed through the hydrophobic interaction between the adsorbed surface active species. As mentioned in the theory, two different structures are possible at high surfactant concentrations. If there are strong attractions between the polar head-groups and the surface, a monolayer is formed, in which the head-groups are facing towards the surface and the tails are oriented towards the solution. This will create a hydrophobic surface that will lead to further adsorption in the same manner as described for hydrophobic surfaces. Hence, at higher concentrations, a surfactant bilayer known as an admicelle is formed. At intermediate attraction forces between the polar head-groups and the surface, micelles or other surfactants aggregates will form at the surface. This is because attractions between tail-groups are stronger than the interaction of the head-groups with the surface. This could also explain why the adsorption continue to increase after the calculated CMC values are reached.

4.4.2 Comparison of Adsorption Isotherms with $CaCl_2$

The adsorption isotherms of the low salinity and medium salinity conditions with calcium are plotted together in Figure 4.4.2.1.

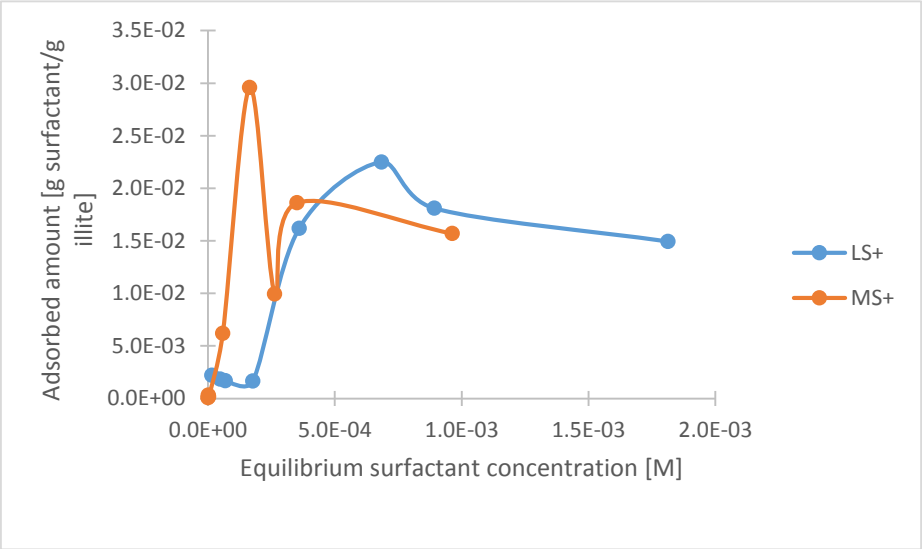

Figure 4.4.2.1: An overview of the adsorption isotherms of low salinity (LS) and medium salinity (MS) with calcium.

The actual values of the equilibrium concentrations and adsorbed amounts of surfactants onto Illite clay are displayed in Table 4.4.2.1.

Table 4.4.2.1: An overview of the values of the equilibrium concentrations and the corresponding adsorbed amounts for the different salinity conditions; low salinity with $CaCl_2$ (LS+) and medium salinity with $CaCl_2$ (MS+). The two maximum peaks for each salinity are written in bold.

LS+		**MS+**	
Equilibrium surfactant concentration [M]	Adsorbed amount [g surf/g Illite]	Equilibrium surfactant concentration [M]	Adsorbed amount [g surf/g Illite]
$1.57 \cdot 10^{-5}$	$\mathbf{2.20 \cdot 10^{-3}}$	$2.02 \cdot 10^{-7}$	$8.80 \cdot 10^{-5}$
$4.77 \cdot 10^{-5}$	$1.85 \cdot 10^{-}$	$1.21 \cdot 10^{-6}$	$3.17 \cdot 10^{-4}$
$6.88 \cdot 10^{-5}$	$1.69 \cdot 10^{-3}$	$2.73 \cdot 10^{-6}$	$1.58 \cdot 10^{-4}$
$1.77 \cdot 10^{-4}$	$1.66 \cdot 10^{-3}$	$5.83 \cdot 10^{-5}$	$6.20 \cdot 10^{-3}$
$3.59 \cdot 10^{-4}$	$1.62 \cdot 10^{-2}$	$1.64 \cdot 10^{-4}$	$\mathbf{2.96 \cdot 10^{-2}}$
$6.84 \cdot 10^{-4}$	$\mathbf{2.25 \cdot 10^{-2}}$	$2.63 \cdot 10^{-4}$	$9.95 \cdot 10^{-3}$
$8.92 \cdot 10^{-4}$	$1.81 \cdot 10^{-2}$	$3.51 \cdot 10^{-4}$	$\mathbf{1.86 \cdot 10^{-2}}$
$1.81 \cdot 10^{-3}$	$1.49 \cdot 10^{-2}$	$9.62 \cdot 10^{-4}$	$1.57 \cdot 10^{-2}$

From the graph and table above, it is observed that the two isotherms alter between having the highest adsorption, but when looking at the overall adsorption, the medium salinity is greater than the low salinity. This can be explained in terms of the electrical double layer, see Chapter 4.4.1.

Similar to the isotherms discussed in the previous chapter, these two isotherms seem to have two maximum peaks, which are outlined in Table 4.4.2.2, and increases after the calculated CMC values are reached.

4.4.3 Comparison of Adsorption Isotherms with and without $CaCl_2$

The adsorption isotherms of the low salinity conditions with and without calcium are plotted together in Figure 4.4.3.1.

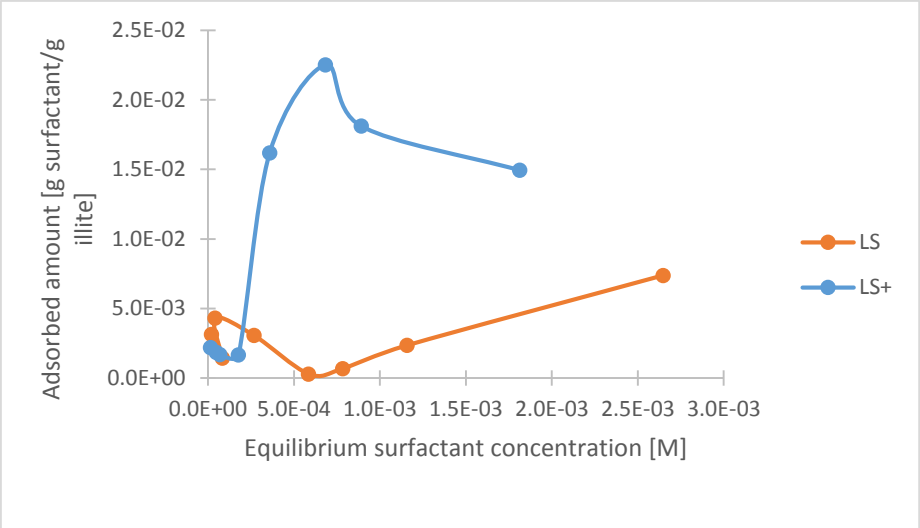

Figure 4.4.3.1: An overview of the adsorption isotherms of low salinity (LS) and low salinity with $CaCl_2$ (LS+).

From the graph above it is observed that the adsorption is much lower when $CaCl_2$ is not added, i.e. without the divalent cation, just like the theory predicts. The polar part of the surfactants attract to the negatively charged clay surface. Divalent cations, such as Ca^{2+}, act as bridges between the negatively charged surfactants and the negatively charged clay surface. By lowering the salinity and reducing the amount of divalent cations in the brine, the electrical diffuse double layers surrounding the negatively charged clay minerals and adsorbed surfactants will expand. More theory surrounding this topic is explained in Chapter 2.8.

The actual values of the equilibrium concentrations and adsorbed amounts of surfactants onto Illite clay are displayed in Table 4.4.3.1. From this table it is observed that the surfactant adsorption in low salinity without calcium is at its lowest, $2.93 \cdot 10^{-4}$ g surfactant/g Illite, at a surfactant concentration of $5.85 \cdot 10^{-4}$ M.

Table 4.4.3.1: An overview of the values of the equilibrium concentrations and the corresponding adsorbed amounts for the different salinity conditions; low salinity (LS) and low salinity with $CaCl_2$ (LS+). The two maximum peaks for each salinity are written in bold.

LS+		**LS**	
Equilibrium surfactant concentration [M]	Adsorbed amount [g surf/g Illite]	Equilibrium surfactant concentration [M]	Adsorbed amount [g surf/g Illite]
1.57E-05	**$2.20 \cdot 10^{-3}$**	$2.02 \cdot 10^{-5}$	$3.14 \cdot 10^{-3}$
4.77E-05	$1.85 \cdot 10^{-3}$	$8.39 \cdot 10^{-5}$	$1.42 \cdot 10^{-3}$
6.88E-05	$1.69 \cdot 10^{-3}$	$4.06 \cdot 10^{-5}$	**$4.31 \cdot 10^{-3}$**
1.77E-04	$1.66 \cdot 10^{-3}$	$2.68 \cdot 10^{-4}$	$3.06 \cdot 10^{-3}$
3.59E-04	$1.62 \cdot 10^{-2}$	$5.85 \cdot 10^{-4}$	$2.93 \cdot 10^{-4}$
6.84E-04	**$2.25 \cdot 10^{-2}$**	$7.84 \cdot 10^{-4}$	$6.70 \cdot 10^{-4}$
8.92E-04	$1.81 \cdot 10^{-2}$	$1.16 \cdot 10^{-3}$	$2.35 \cdot 10^{-3}$
1.81E-03	$1.49 \cdot 10^{-2}$	$2.65 \cdot 10^{-3}$	**$7.37 \cdot 10^{-3}$**

The adsorption isotherms of the medium salinity conditions with and without calcium are plotted together in Figure 4.4.3.2.

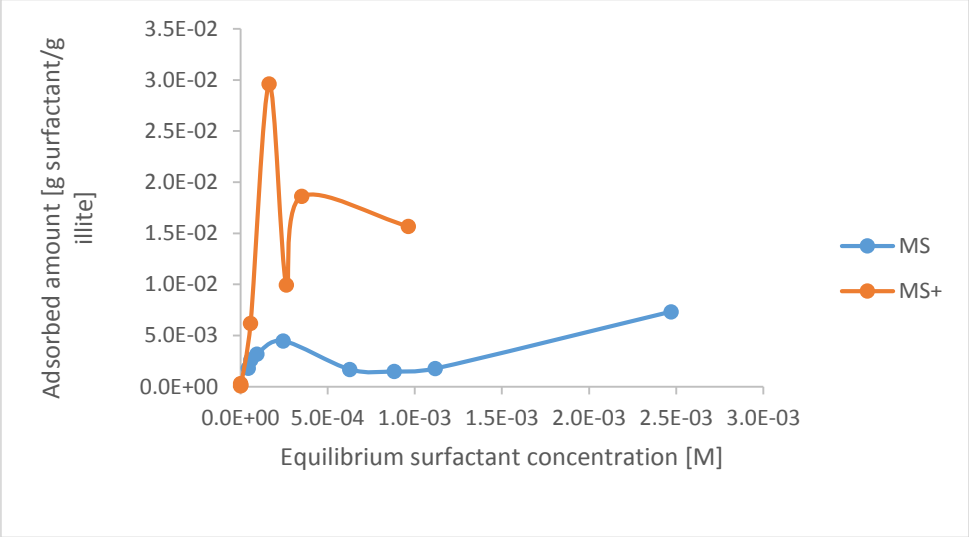

Figure 4.4.3.2: An overview of the adsorption isotherms of medium salinity (MS) and medium salinity with $CaCl_2$ (MS+).

The same phenomenon is observed in the graph above as in Figure 4.4.3.1. The adsorption is much higher for the samples containing $CaCl_2$. The actual values of the equilibrium concentrations and adsorbed amounts of surfactants onto Illite clay are displayed in Table 4.4.3.2. From this table it is observed that the surfactant adsorption in medium salinity without calcium is at its lowest, $1.49 \cdot 10^{-3}$ g surfactant/g Illite, at a surfactant concentration of $8.82 \cdot 10^{-4}$ M.

Table 4.4.3.2: An overview of the values of the equilibrium concentrations and the corresponding adsorbed amounts for the different salinity conditions; *medium salinity (MS) and medium salinity with $CaCl_2$ (MS+)*. The two maximum peaks for each salinity are written in bold.

MS+		**MS**	
Equilibrium surfactant concentration [M]	Adsorbed amount [g surf/g Illite]	Equilibrium surfactant concentration [M]	Adsorbed amount [g surf/g Illite]
$2.02 \cdot 10^{-7}$	$8.80 \cdot 10^{-5}$	$4.41 \cdot 10^{-5}$	$1.81 \cdot 10^{-3}$
$1.21 \cdot 10^{-6}$	$3.17 \cdot 10^{-4}$	$5.91 \cdot 10^{-5}$	$2.62 \cdot 10^{-3}$
$2.73 \cdot 10^{-6}$	$1.58 \cdot 10^{-4}$	$9.49 \cdot 10^{-5}$	$3.18 \cdot 10^{-3}$
$5.83 \cdot 10^{-5}$	$6.20 \cdot 10^{-3}$	$2.45 \cdot 10^{-4}$	**$4.47 \cdot 10^{-3}$**
$1.64 \cdot 10^{-4}$	**$2.96 \cdot 10^{-2}$**	$6.27 \cdot 10^{-4}$	$1.69 \cdot 10^{-3}$
$2.63 \cdot 10^{-4}$	$9.95 \cdot 10^{-3}$	$8.82 \cdot 10^{-4}$	$1.49 \cdot 10^{-3}$
$3.51 \cdot 10^{-4}$	**$1.86 \cdot 10^{-2}$**	$1.12 \cdot 10^{-3}$	$1.77 \cdot 10^{-3}$
$9.62 \cdot 10^{-4}$	$1.57 \cdot 10^{-2}$	$2.47 \cdot 10^{-3}$	**$7.33 \cdot 10^{-3}$**

4.4.4 Calculation of the Debye Length

The Debye length was calculated for the various salinity solutions in order to achieve a more quantitative understanding of the compression/expansion of the electrical double layer. The values are displayed in Table 4.4.4.1 and the calculations are shown in Appendix E.

Table 4.4.4.1: The calculated Debye length for the various salinities.

	Low Salinity	**Medium Salinity**	**High Salinity**
Debye Length, k_D^{-1} [nm]	2.16	1.08	0.68

According to the literature, the Debye length is typically on the scale of a few nanometers in aqueous solutions. Thus, the values displayed in the table above seem

reasonable. It is observed that the Debye length decrease with increasing electrolyte concentration, which is an indication of the compression of the electrical double layer. The compression of the electrical double layer when the electrolyte concentration increases leads to higher adsorption, while the expansion on the electrical double layer when the electrolyte concentration decreases leads to lower adsorption. This is consistent with the results achieved earlier in the chapter.

It is known that the effectiveness of multivalent electrolytes in destabilizing colloidal dispersions is reduced in the presence of moderate amounts of a second electrolyte [54]. It has been suggested that this could be due to the large deviations from ideal behavior observed in solutions of multivalent electrolytes, implying that activities should be used instead of concentrations in the formula for the Debye length. At concentrations normally encountered in colloidal systems, the activity of an ion is less than its concentration (the activity coefficient, γ, is less than 1). If activities were used in the Debye length equation instead of concentration, the predicted Debye length would be longer, and the electrical double layer force would be expected to decay less rapidly [22].

4.5 Mathematical Fitting

The Langmuir and Freundlich isotherms were used to create a mathematical fit to each of the adsorption isotherms obtained in this experiment. The intentions of this modelling was to investigate the degree of correlation of the obtained adsorption isotherms from experimental studies with the theoretical models; the higher the R^2 value, the better the fit. The R^2 values obtained from the two mathematical models are displayed in Table 4.5.1.

Table 4.5.1: An overview of the R^2 values obtained from the different mathematical models for low salinity (LS), low salinity with $CaCl_2$ (LS+), medium salinity (MS), medium salinity with $CaCl_2$ (MS+) and high salinity (HS).

Isotherm	Salinity	R^2 value
Freundlich	LS	0.0176
	LS+	0.6980
	MS	0.1706
	MS+	0.9132
	HS	0.5816
Langmuir	LS	0.1042
	LS+	0.2296
	MS	0.0455
	MS+	0.7959
	HS	0.8406

The mathematical fitting was supposed to yield a straight line. Unfortunately, this is not obtained for many of these cases. About half of the isotherms produced very low R^2 values (see Table 4.5.1), thus they do not seem as a good mathematical fits. In general, a model fits the data well if the differences between the observed values and the model's predicted values are small and unbiased.

Due to the consistently poor results from the mathematical fitting, it is hard to interpret the results in a good way. However, it does seem like the calcium containing salinities overall produce better fits than the ones containing only sodium chloride. This might be explained by the decreasing adsorption isotherms observed for the non-calcium containing salinities.

The graphical illustrations of the mathematical fittings are shown in the following sections, and the data presented on these plots show the linear relationship between

the surfactant equilibrium concentration and adsorption of surfactant onto Illite clay. The values used for plotting the graphs are found in Appendix E.

4.5.1 Low Salinity

The mathematical fitting using the Langmuir isotherm was obtained by plotting the reciprocal of the amount adsorbed per unit mass of adsorbent against the reciprocal of the equilibrium concentration. The Langmuir fitting of the low salinity condition is shown in Figure 4.5.1.1.

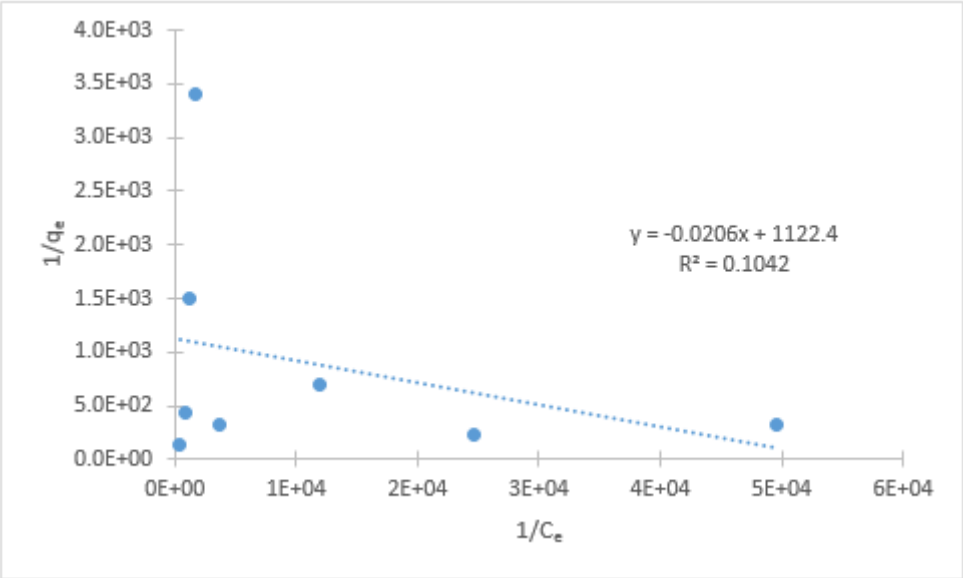

Figure 4.5.1.1: Mathematical fitting of the low salinity condition using the Langmuir isotherm.

The mathematical fitting using the Freundlich isotherm was obtained by plotting the logarithm of the amount adsorbed per unit mass of adsorbent against the logarithm of the equilibrium concentration. The Freundlich fitting of the low salinity condition is shown in Figure 4.5.1.2.

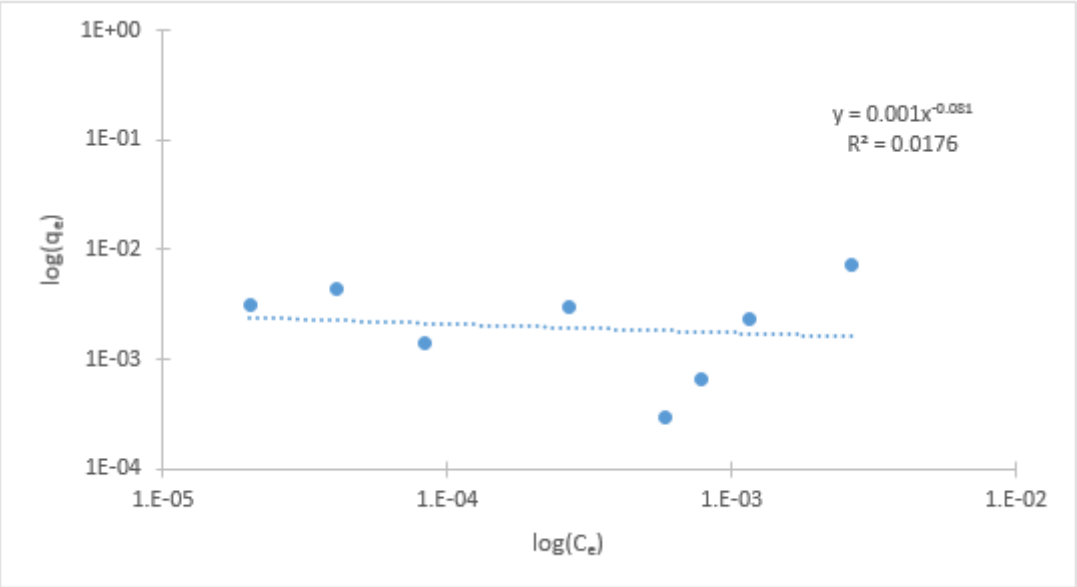

Figure 4.5.1.2: Mathematical fitting of the low salinity condition using the Freundlich isotherm.

4.5.2 Low Salinity with $CaCl_2$

The mathematical fittings for the low salinity condition with $CaCl_2$ using the Langmuir and Freundlich isotherm was obtained using the same procedure as described for the low salinity condition without calcium, and are shown in Figure 4.5.2.1 and Figure 4.5.2.2, respectively.

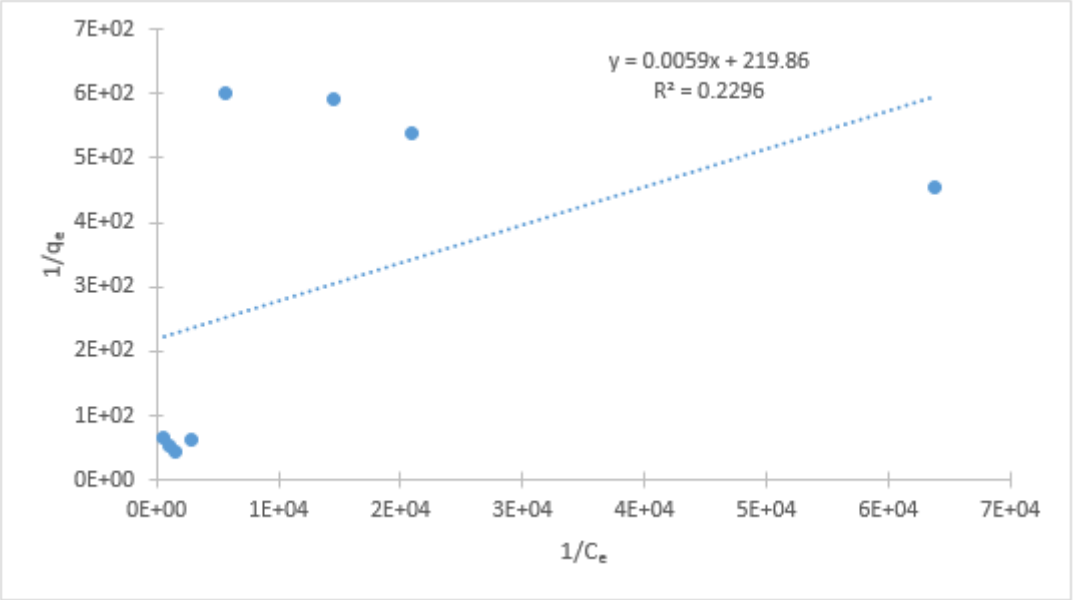

Figure 4.5.2.1: Mathematical fitting of the low salinity condition with $CaCl_2$ using the Langmuir isotherm.

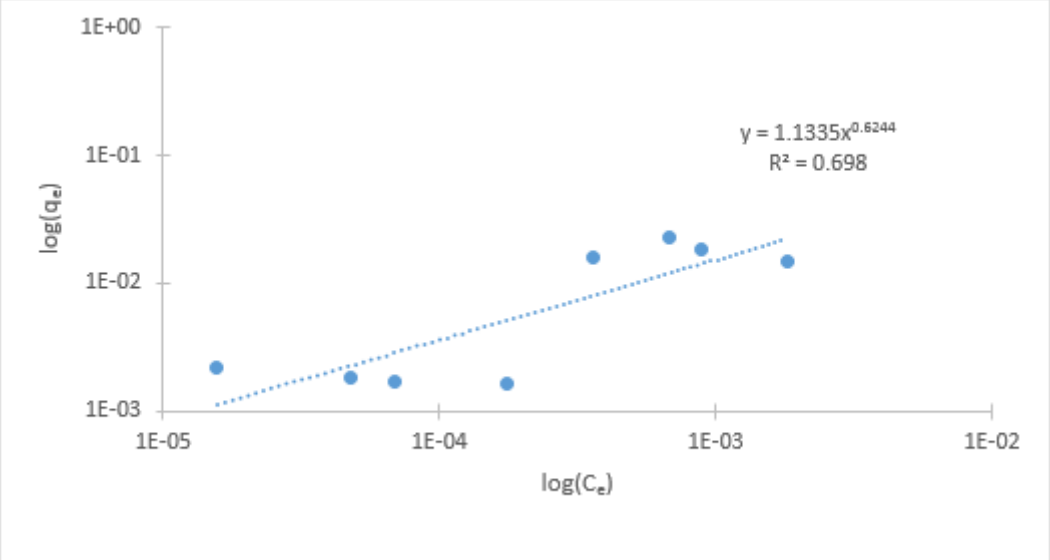

Figure 4.5.2.2: Mathematical fitting of the low salinity condition with $CaCl_2$ using the Freundlich isotherm.

4.5.3 Medium Salinity

The mathematical fittings for the medium salinity condition using the Langmuir and Freundlich isotherm was obtained using the same procedure as described for the low salinity condition without calcium, and are shown in Figure 4.5.3.1 and Figure 4.5.3.2, respectively.

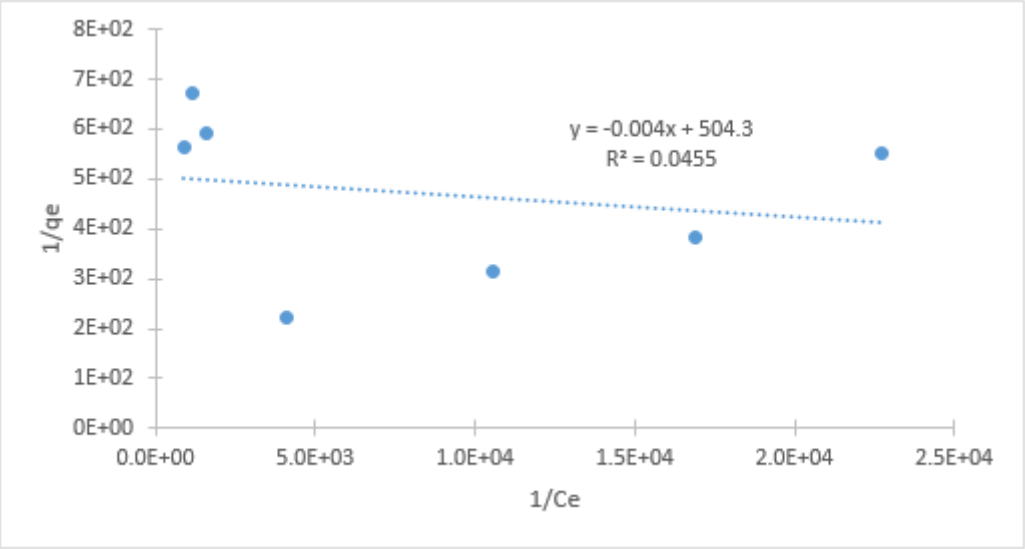

Figure 4.5.3.1: Mathematical fitting of the medium salinity condition using the Langmuir isotherm.

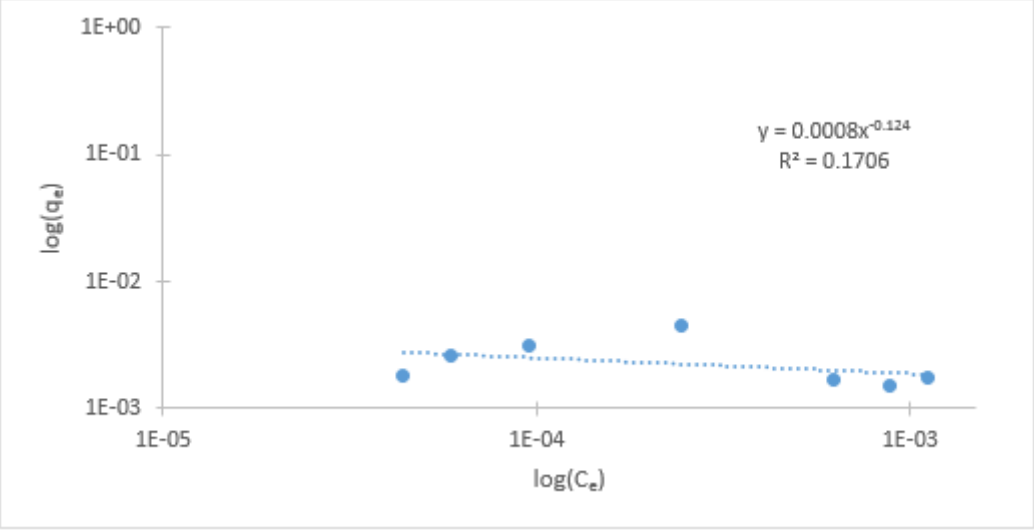

Figure 4.5.3.2: Mathematical fitting of the medium salinity condition using the Freundlich isotherm.

4.5.4 Medium Salinity with $CaCl_2$

The mathematical fittings for the medium salinity condition with $CaCl_2$ using the Langmuir and Freundlich isotherm was obtained using the same procedure as described for the low salinity condition without calcium, and are shown in Figure 4.5.4.1 and Figure 4.5.4.2, respectively.

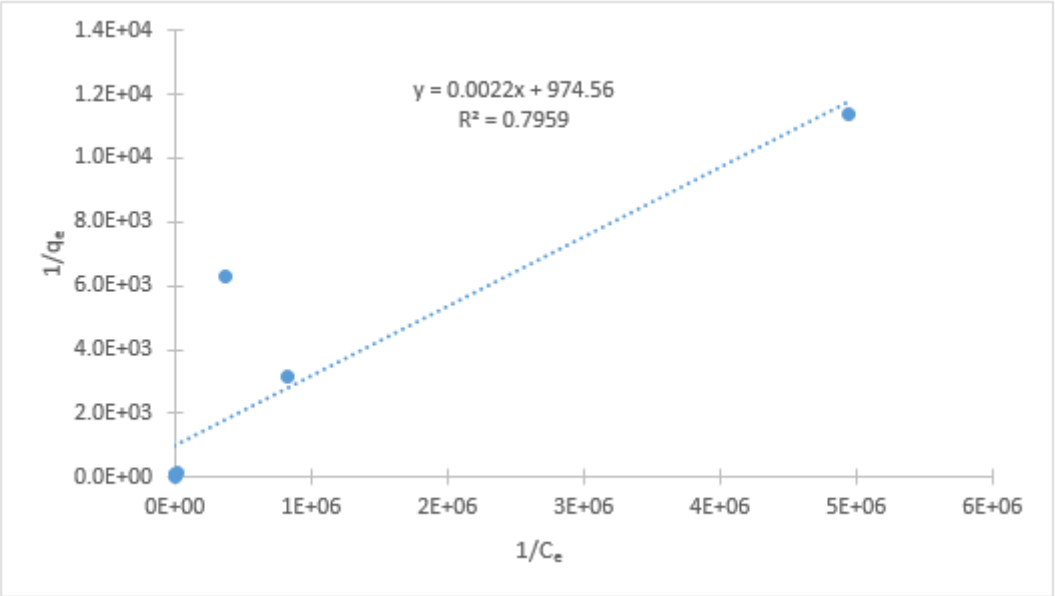

Figure 4.5.4.1: Mathematical fitting of the medium salinity condition with $CaCl_2$ using the Langmuir isotherm.

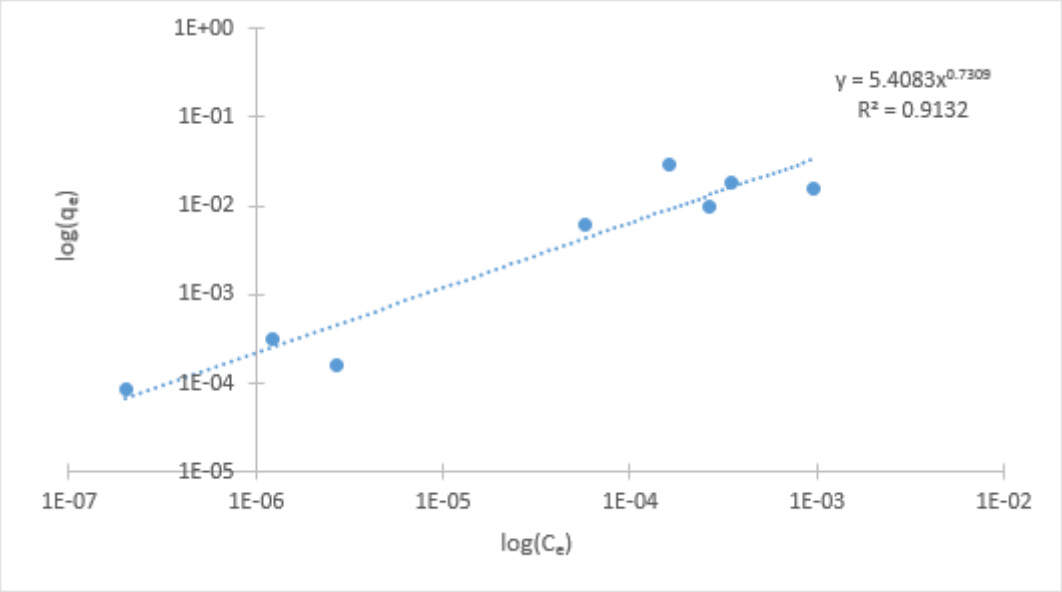

Figure 4.5.4.2: Mathematical fitting of the medium salinity condition with $CaCl_2$ using the Freundlich isotherm.

4.5.5 High Salinity

The mathematical fittings for the high salinity condition using the Langmuir and Freundlich isotherm was obtained using the same procedure as described for the low salinity condition without calcium, and are shown in Figure 4.5.5.1 and Figure 4.5.5.2, respectively.

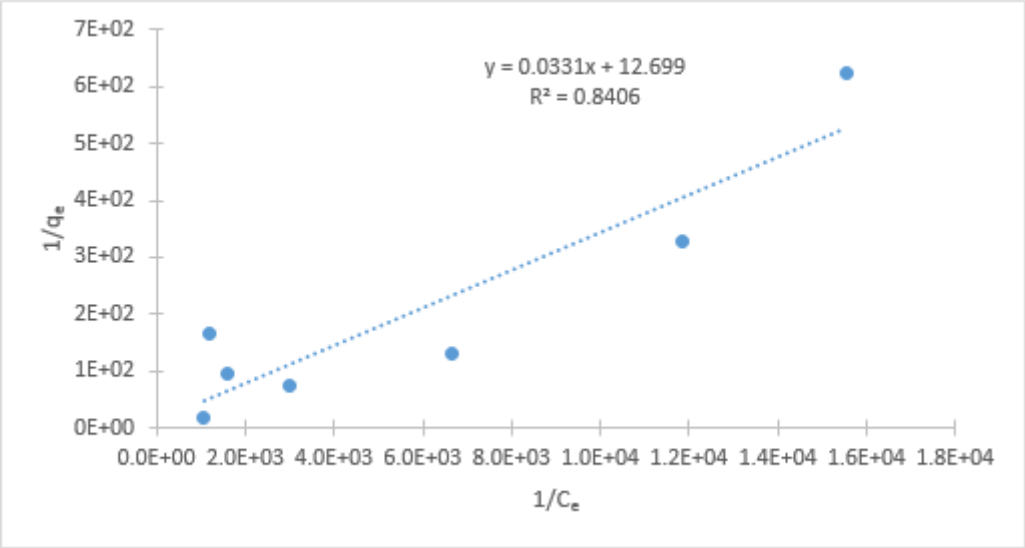

Figure 4.5.5.1: Mathematical fitting of the high salinity condition using the Langmuir isotherm.

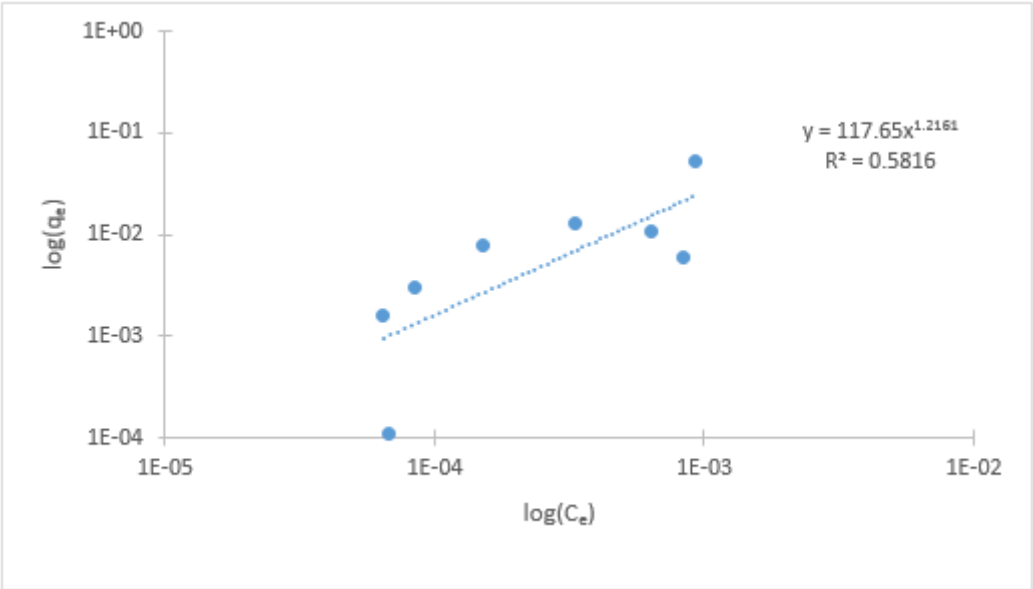

Figure 4.5.5.2: Mathematical fitting of the high salinity condition using the Freundlich isotherm.

4.5.6 Two-Step Adsorption Mechanism

In the Langmuir and Freundlich isotherms, a one-step adsorption mechanism is assumed. However, from the adsorption isotherms it is reason to believe that a two-step adsorption, as described in Chapter 4.4.1, occurs. If this is the case, it would be

more correct to use a model that takes this into account. For example the model described by Equation 17:

$$\Gamma = \frac{\Gamma_\infty \cdot k_1 \cdot C(\frac{1}{n} + k_2 \cdot C^{n-1})}{1 + k_1 \cdot C(1 + k_2 \cdot C^{n-1})} \quad (17)$$

where Γ is the amount of surfactant adsorbed at a concentration C, Γ_∞ is the limiting adsorption at high concentrations, k_1 and k_2 are the equilibrium constants for the first and second step, respectively, and n is the aggregation number of surface hydrophobic aggregated or hemimicelles [55]. This model was not included in this report since it would have been a very difficult and time demanding process to solve the equation regarding all the unknown parameters and the complicity of the equation.

4.6 Clay Treatment

The clay was treated and measured as described in Chapter 3.3. The results are shown in Table 4.6.1.

Table 4.6.1: The results of clay treatment

Clay	**Conductivity [mS/cm]**	**IFT [mN/m]**
Untreated	69.40	71.34
Treated	10.90	70.92

The surface tension did not change remarkably, but the conductivity decreased quite a bit, which suggests that the clay treatment was successful.

4.7 Test of Blank Samples

A test of blank samples was conducted in order to see if, and how much, the absorption would change after contact with the clay. The absorption of the blank samples, which consisted of the various salt solutions, were measured using the UV-vis. Further, clay was added and the sample was treated as described in Chapter 3.2. The absorption was measured one more time after removal of the clay. The values obtained from this test are shown in Table 4.7.1.

Table 4.7.1: An overview of the difference in absorption in the various salt solutions before and after contact with Illite clay.

	Absorption before contact with clay [-]	**Absorption after contact with clay [-]**
Low salinity	0.001	0.013
Low salinity with $CaCl_2$	0.003	0.014
Medium salinity	0.002	0.011
Medium salinity with $CaCl_2$	0.004	0.019
High salinity	0.005	0.019

The table above shows that the absorption does in fact increase a bit after being in contact with Illite. This may suggest that not all clay particles has been successfully removed, and can lead to some errors in the adsorption isotherms.

4.8 pH Measurements

The pH was measured in order to have a reference in case the experiment is to be repeated. The results are presented in Appendix G.

4.9. Density Measurements

The densities of the samples used for the tensiometer were measured using a density meter. The results are presented in Appendix H.

4.10 Sources of Error

The performance of low salinity water injection in sandstones is strongly dependent on the composition of crude oil, clay content, formation water salinity and wettability of the rock surface. Based on this, there are some sources of errors that may have contributed to inaccurate results in this experiment. The concentrated SDBS solutions contained a lot of foam, which made it difficult to spot the meniscus. Therefore, some of the samples used in the calibration curves might have been inaccurate. In addition, the foam made it difficult to transfer the entire solution from the pipette and into the sample.

When using the tensiometer, it was difficult to know when the solution had reached equilibrium. The interfacial tension do not stabilize before this is reached, so if the samples did not get enough time to reach equilibrium, the values of the interfacial tension are inaccurate. In this experiment, the samples were left for 30 minutes, which might have been a short time interval. The measurements conducted on the Sigma 700 Tensiometer may also be a significant source of error. According to the apparatus manual, the tensiometer should be calibrated to +/- 1 [mN/m], which allows for a noteworthy error at higher surfactant concentrations. However, due to an old and well used ring, the apparatus was calibrated to +/- 2, whics allows for an even higher error.

The Illite clay used in this experiment was ordered from The Clay Minerals Society's web shop. The purity of this clay was not mentioned on the package, so there might have been some contaminants present in the clay that could have influenced the adsorption.

As shown in Chapter 4.7, the blank sample test indicated that the absorption increased in the samples that did not contain any surfactants. This may suggest that not all clay particles was successfully removed in the centrifugation process, which could have led to errors in the adsorption experiments. Some samples were filtered after the centrifugation process using filtration syringes. A zetasizer analysis of these samples indicated that this procedure removed more particles from the solution than the centrifugal process alone. However, since the laboratory ran out of these filters early in the process and they were too expensive to order in larger quantities, this procedure was not used for the samples described in this report.

5. Conclusion

The adsorption of the anionic surfactant SDBS onto Illite clay has been investigated in various salinity solutions. The method used for determination of the surfactant adsorption was UV-vis spectroscopy.

The results showed that the high salinity condition had a much higher adsorption than medium and low salinity. The high salinity experienced the highest surfactant adsorption value of all the salinities, $5.15 \cdot 10^{-2}$ g surfactant/g Illite at a concentration of $9.29 \cdot 10^{-4}$ M. The adsorption isotherms for medium and low salinity without calcium were nearly identical. Thus, the low salinity condition did not reveal any remarkably lower surfactant adsorption in this specific case, which had been expected. However, the low salinity condition with calcium produced lower surfactant adsorption than the medium salinity with calcium, which was consistent with the theory. When comparing the salinity conditions without calcium with the ones containing calcium, the trend was clear. The solutions containing calcium experienced a much higher surfactant adsorption than the ones without. The surfactant adsorption in low salinity without calcium was at its lowest, $2.93 \cdot 10^{-4}$ g surfactant/g Illite, at a surfactant concentration of $5.85 \cdot 10^{-4}$ M.

Thus, the trends indicates that low salinity combined with surfactant flooding indeed reduces the amount of surfactant adsorption onto Illite clay. The adsorption is further reduced by lowering the concentration of divalent cations.

Due to all the mentioned sources of errors in the discussion, the adsorption isotherms and calibration curves presented in this report can not be considered exact, even though most of the trends seem to match the theory. Several experiments should be conducted before a valid conclusion can be drawn.

6. Further Work

In the light of the conclusions made in this report, it would be beneficial to conduct the experiments several times while taking the sources of error into account. This would produce improved adsorption isotherms and a more correct picture of how the adsorption alters when specific parameters are changed.

It would also be desirable to conduct the adsorption experiment using the surface tension method as well, like described in the original agenda. This would produce several adsorption isotherms, which further could be compared to the isotherms obtained from the UV measurements. By doing this, a better understanding of the results would be achieved and the trend of the isotherms could be easier to interpret.

An analysis of the clay remains after the removal the supernatant should also be carried out in order to double check the produced adsorption isotherms. This could be carried out by measuring the clay's zeta potential and contact angle. It is expected that the zeta potential will decrease with increasing surfactant adsorption, and that the contact angle will increase with increasing surfactant adsorption. The latter may show the same trend as the isotherms.

Bibliography

1. Enhanced Oil Recovery Conferance. *Enhanced Oil Recovery Conferance*. 2013 [cited 2013 20. 10]; Available from: http://www.spe.org/events/eorc/2013/.
2. Henthorne, L., M. Hartman, and A. Hayden, *Improving Chemical EOR economics by Optimizing Water Quality.* 2011: p. 1-3.
3. Kosswig, K., *Ullmann's encyclopedia of industrial chemistry; Surfactants*. 2000, Wiley-VCH Verlag GmbH & Co. KGaA. p. 431.
4. Mørk, P.C., *Overfalte og Kolloidkjemi*. 2004. p. 48-50.
5. SITA Process Solutions. *Process parameter surface tension*. 2013 [cited 2014 30.04]; Available from: http://surface-tension.sita-process.com/overview/.
6. Holmberg, K., et al., *Surfactants and Polymers in Aqueous Solution*. 2002, John Wiley & Sons, Ltd. p. 337-350.
7. Holmberg, K., et al., *Surfactants and polymers in aqueous solution*. 2002, John Wiley & Sons, Ltd. p. 1-4.
8. University of Waikato. *Surfactants,*. 2012 [cited 2014 30.04]; Available from: http://www.sciencelearn.org.nz/Science-Stories/Where-Land-Meets-Sea/Sci-Media/Images/Surfactants.
9. Holmberg, K., et al., *Surfactants and polymers in aqueous solution,* . 2002, John Wiley & Sons, Ltd. p. 6.
10. Holmberg, K., et al., *Surfactants and polymers in aqueous solution*. 2002, John Wiley & Sons, Ltd. p. 10-14.
11. Schramms, L.L., *Surfactants: Fundamentals and Applications in the Petroleum Industry*. 2000, Cambridge University press. p. 121-123.
12. Mandavi, R., *Kinetic studies of some Esters and Amides in presence of micelles*. 2012. p. 59.
13. Schramms, L.L., *Surfactants: Fundamentals and Applications in the Petroleum Industry*. 2000, Cambridge University press. p. 9-14.
14. Biolin Scientific. *Critical Micelle Concentration*. 2014 [cited 2014 05.05]; Available from: http://www.attension.com/applications/measurements/critical-micelle-concentration.
15. Holmberg, K., et al., *Surfactants and polymers in aqueous solution*. 2002, John Wiley & Sons, Ltd. p. 44.
16. Holmberg, K., et al., *Surfactants and polymers in aqueous solution*. 2002, John Wiley & Sons, Ltd. p. 47.
17. Holmberg, K., et al., *Surfactants and polymers in aqueous solution*. 2002, John Wiley & Sons, Ltd. p. 49.
18. Shirinsky, V.P. *Krafft temperature,*. 2011 [cited 2014 05.05]; Available from: http://eng.thesaurus.rusnano.com/wiki/article1057.
19. Lv, W., et al., *Static and dynamic adsorption of anionic and amphoteric surfactants with and without the presence of alkali.* 2011: p. 1-2.

20. Schramms, L.L., *Surfactants: Fundamentals and Applications in the Petroleum Industry*. 2000, Cambridge University press. p. 123-125.
21. Schramms, L.L., *Surfactants: Fundamentals and Applications in the Petroleum Industry*. 2000, Cambridge University press. p. 126-128.
22. Kohonen, M.M., M.E. Karaman, and R.M. Pashely, *Debye Length in Multivalent Electrolyte Solutions.* 2000.
23. Cooper, S. *Interfaces, Colloids and Gels*. Available from: http://community.dur.ac.uk/sharon.cooper/lectures/colloids/interfacesweb1.html.
24. Kriaa, A., N. Hamdi, and E. Srasra, *Proton adsorption and acid-base properties of Tunisian illites in aqueous solution.* Journal of Structural Chemistry, 2009. **50**(2): p. 273-287.
25. Holmberg, K., et al., *Surfactants and polymers in aqueous solution*. 2002, John Wiley & Sons, Ltd. p. 357.
26. Holmberg, K., et al., *Surfactants and polymers in aqueous solution*. 2002, John Wiley & Sons, Ltd. p. 358.
27. Holmberg, K., et al., *Surfactants and polymers in aqueous solution*. 2002, John Wiley & Sons, Ltd. p. 360-365.
28. Schramms, L.L., *Surfactants: Fundamentals and Applications in the Petroleum Industry*. 2000, Cambridge University press. p. 129-131.
29. Salari, Z., et al., *Experimental Studies of Cationic Surfactant Adsorption onto Carbonate Rocks.* Australian Journal of Basic and Applies Sciences, 2011: p. 811.
30. Schramms, L.L., *Surfactants: Fundamentals and Applications in the Petroleum Industry*. 2000, Cambridge University press. p. 122-123.
31. Schramms, L.L., *Surfactants: Fundamentals and Applications in the Petroleum Industry*. 2000, Cambridge University press. p. 205-209.
32. Vledder, P., et al., *Low salinity water flooding: Proof of wettability alteration on a field wide scale*. 2010, Society of Petroleum Engineers. p. 1-4.
33. Austad, T., A.R. Doust, and T. Puntervold, *Chemical mechanism of low salinity water flooding in sandstone*. 2010, Society of Petroleum Engineers. p. 1-2.
34. Austad, T., A.R. Doust, and T. Puntervold, *Chemical mechanism of low salinity water flooding in sandstone*. 2010, Society of Petroleum Engineers. p. 5-6.
35. Bernard, G.G., *Effect of Floodwater Salinity on Recovery of Oil from Cores Containing Clay*, in *SPE California Regional Meeting*. 1967, Society of Petroleum Engineers: Los Angeles, California.
36. Tang, G.Q. and N.R. Morrow, *Influence of brine composition and fines migration on crude oil/brine/rock interactions and oil recovery.* Journal of Petroleum Science and Engineering, 1999. **24**(2-4).
37. Lager, A., et al., *LoSal Enhanced Oil Recovery: Evidence og Enhanced Oil Recovery at the Reservoir Scale*, in *SPE Symposium on Improved Oil Recovery*. 2008: Tulsa, Oklahoma, USA.

38. Nasralla, R.A., M.A. Bataweel, and H.A. Nasr-El-Din, *Investigation of Wettability Alteration and Oil-Recovery Improvement by Low-Salinity Water in Sandstone ROck.* Journal of Canadian Petroleum Technology, 2013. **52**(02).
39. Zeinijahromi, A., P. Lemon, and B. P, *Effects of induced fines migration on water cut during waterflooding*. Journal of Petroleum Science and Engineering, 2011. **78**(3-4).
40. Al-adasani, A., B. Bai, and Y. Wu, *Investigation Low Salinity Waterflooding Recovery Mechanisms in Carbonate Reservoirs*, in *SPE EOR Conference*. 2012, Society of Petroleum Engineers: Muscat, Oman.
41. Yousef, A.A. and S.C. Ayirala, *A Novel Water Ionic Composition Optimizing Technology for SmartWater Flooding Application in Carbonate Reservoirs*, in *SPE Improved Oil Recovery Symposium*. 2014, Society of Petroleum Engineers: Tulsa, Oklahoma, USA.
42. Biolin Scientific. *Surface Tension*. 2014 [cited 2014 05.05]; Available from: http://www.attension.com/applications/measurements/surface-tension.
43. Mørk, P.C., *Overfalte og Kolloidkjemi*. 2004. p. 72.
44. Skoog, D.A., et al., *Fundamentals of analytical chemistry*. 2004, Cengage Learning. p. 718-727.
45. Seton Hall University. *Quantitative Colorimetry and the Biuret Test*. 2014 [cited 2014 05.05]; Available from: http://pirate.shu.edu/~rawncarr/biurettest/biurettest.htm.
46. Larsen, D. *The Dynamic Chemistry E-textbook: Spectrophotometry*. 2013 [cited 2014 05.05]; Available from: http://chemwiki.ucdavis.edu/Physical_Chemistry/Kinetics/Reaction_Rates/Experimental_Determination_of_Kinetcs/Spectrophotometry.
47. Skoog, D.A., et al., *Fundamentals of analytical chemistry*. 2004, Cengage Learning. p. 791.
48. USGS. *Illite,*. 1990 [cited 2014 05.05]; Available from: http://speclab.cr.usgs.gov/spectral.lib06/ds231/DESCRIPT/M/illite_gds4.html.
49. Poppe, L.J., et al. *A Laboratory Manual for X-Ray Powder Diffraction,*. 29.04.2014 [cited 2014 25.04]; Available from: http://pubs.usgs.gov/of/2001/of01-041/htmldocs/clays/illite.htm.
50. Green Electron Images. *Illite Bridge,*. 2008 [cited 2014 05.05]; Available from: http://www.greenelectron-images.co.uk/sem/illite/illite-4.html.
51. Nasiru, T., L. Avila, and M. Levine, *Determination of Critical Micelle Concentrations Using UV-Visible Spectroscopy.* 2011: p. 1-4.
52. IRO Group Inc. *Sodium Dodecyl Benzene Sulphonate*. 2013 [cited 2014 05.05]; Available from: http://www.irochemical.com/product/Surfactants/LAS.htm.
53. Kosswig, K., *Ullmann's encyclopedia of industrial chemistry; Surfactants*. 2000, Wiley-VCH Verlag GmbH & Co. KGaA. p. 450.
54. Overbeek, J.T.G., *The interaction between colloidal particles in colloid science*, Elsevier, Editor. 1952: Amsterdam.

55. Zhu, B.Y. and T. Gu, *General Isotherm Equation for Adsorption of Surfactants at Solid/Liquid Interfaces.* 1989.

List of Appendices

Appendix A Risk Assessment

Figure A.1, A2. and A.3 shows the HSE analysis carried out in conjunction with this experiment.

NTNU

HMS /KS

Risk assessment

Prepared by	Nummer	Date
HSE section	HMSRV2603	04.02.2011
Approved by	Page	Replaces
The Rector		09.02.2010

Unit: *(Institute)* *IKP* **Date:** 15.01.2014

Line manager: *Edd Blekkan*

Participants in the identification process (incl. function): *Gisle Øye, Ingrid K. Hov, Meysam Nourani*

(supervisor, student, co-supervisor, others)

Risk assessment of: Specialization project, investigation of loss of surfactants

Signatures: *Responsible supervisor:* *Student:*

ID nr.	Activity from the identification process form	Potential undesirable incident/strain	Likeli-hood: (1-5)	Consequence: Human (A-E)	Enviroment (A-E)	Economy/ material (A-E)	Risk value (human)	Comments/status Suggested measures
1	Preparing solutions with SDBS	Spill may irritate skin, cause eye injury. Inhalation may cause intoxication.	2	A			A2	
2	Preparing solutions with kaolinite/illiite	No potential risk	1	A			A1	
3	Preparing solutions with NaCl	No potential risk	1	A			A1	
4	Preparing solution with HCl	Spill have a corrosive effect on human tissue, with the potential to damage respiratory organs, eyes, skin, and intestines irreversibly	2	C			C2	
5	Preparing solutions with CaCl2	No potential risk	1	A			A1	
6	Cleaning of equipment with acetone	Spill may irritate skin, cause eye injury. Inhalation may cause intoxication.	2	A			A2	Be careful to change gloves if spill occurs.
7	Cleaning of equipment with toluene	Spill may irritate skin, cause eye injury. Inhalation may cause intoxication.	2	B			B2	Be careful to change gloves if spill occurs.
8	Use of tensiometer	Cleaning of ring with open fire may cause skin burn, spill when transferring sample to beaker	2	B			B2	
9	Use of UV-spectrophotmeter	No potential risk	1	A			A1	

Figure A.1: Risk assessment sheet.

Risk value = Likelihood (1, 2 ...) x consequence (A, B ...). Risk value A1 means very low risk. Risk value E5 means very large and serious risk

Likelihood		Consequence					
Value	Criteria	Grading		Human	Environment	Economy/material	
1	**Minimal**: Once every 50 year or less	E	Very critical	May produce fatality/ies	Very prolonged, non-reversible damage	Shutdown of work >1 year.	
2	**Low**: Once every 10 years or less	D	Critical	Permanent injury, may	Prolonged damage.	Shutdown of work 0.5-1	
3	**Medium**: Once a year or less	C	Dangerous	Serious personal injury	Minor damage. Long recovery time	Shutdown of work < 1 month	
4	**High**: Once a month or less	B	Relatively safe	Injury that requires medical treatment	Minor damage. Short recovery time	Shutdown of work < 1week	
5	**Very high**: Once a week	A	Safe	Injury that requires first	Insignificant damage.	Shutdown of work <	

MATRIX FOR RISK ASSESSMENT

CONSEQUENCE						
	Very critical	E1	E2	E3	E4	E5
	Critical	D1	D2	D3	D4	D5
	Dangerous	C1	C2	C3	C4	C5
	Relatively safe	B1	B2	B3	B4	B5
	Safe	A1	A2	A3	A4	A5
		Minimal	Low	Medium	High	Very high
		LIKELIHOOD				

Explanation of the colors used in the risk matrix.

Color	Description
Red	Unacceptable risk. Safety measures must be implemented.
Yellow	Measures to reduce risk shall be considered.
Green	Acceptabel risk.

Figure A.2: Risk definitions.

NTNU

HSE

Hazardous activity identification process

Prepared by	Number	Date
HSE section	HMSRV2601	22.03.2011
Approved by	Page	Replaces
The Rector		01.12.2006

Unit: *(Institute)* IKP **Date:** 15.01.2014

Line manager: Edd Blekkan

Participants in the identification process (incl. function):
(supervisor, student, co-supervisor, others) Gisle Øye, Ingrid K. Hov, Meysam Nourani

Short description of the main activity/main process: Specialization project, investigation of loss of surfactants

Is the project work purely theoretical? (YES/NO) NO

Answer "YES" implies that ***supervisor is assured that no activities requiring risk assessment are involved in the work****. If YES, skip rest of the form.*

Signatures: *Responsible supervisor:* _____ *Student:* _____

ID nr.	Activity/process	Responsible person	Existing documentation	Existing safety measures	Laws, regulations etc.	Comment
1	Preparing solutions with SDBS	Ingrid K. Hov	HSE-datasheet	Gloves, safety glasses, fume hood	Arbeidsmiljøloven, Kjemikalieforskrifter og Laboratorie- og verkstedhåndbok for NTNU	
2	Preparing solutions with kaolinite/illite	Ingrid K. Hov	HSE-datasheet	Safety glasses	Arbeidsmiljøloven, Kjemikalieforskrifter og Laboratorie- og verkstedhåndbok for NTNU	
3	Preparing solutions with NaCl	Ingrid K. Hov	HSE-datasheet	Safety glasses	Arbeidsmiljøloven, Kjemikalieforskrifter og Laboratorie- og verkstedhåndbok for NTNU	
4	Preparing solution with HCl	Ingrid K. Hov	HSE-datasheet	Gloves, safety glasses, lab coat	Arbeidsmiljøloven, Kjemikalieforskrifter og Laboratorie- og verkstedhåndbok for NTNU	
5	Preparing solutions with CaCl2	Ingrid K. Hov	HSE-datasheet	Safety glasses	Arbeidsmiljøloven, Kjemikalieforskrifter og Laboratorie- og verkstedhåndbok for NTNU	
6	Cleaning of equipment with acetone	Ingrid K. Hov	HSE-datasheet	Gloves, safety glasses, fume hood	Arbeidsmiljøloven, Kjemikalieforskrifter og Laboratorie- og verkstedhåndbok for NTNU	
7	Cleaning of equipment with toluene	Ingrid K. Hov	HSE-datasheet	Gloves, safety glasses, fume hood	Arbeidsmiljøloven, Kjemikalieforskrifter og Laboratorie- og verkstedhåndbok for NTNU	Need to be cleaned with open fire after each sample. Extra care must be taken.
8	Use of UV-spectrophotmeter	Ingrid K. Hov	Instrument card / User manual	Gloves, safety glasses, fume hood	Arbeidsmiljøloven, Kjemikalieforskrifter og Laboratorie- og verkstedhåndbok for NTNU	
8	Use of tensiometer	Ingrid K. Hov	Instrument card / User manual	Gloves, safety glasses, fume hood, lab coat	Arbeidsmiljøloven, Kjemikalieforskrifter og Laboratorie- og verkstedhåndbok for NTNU	

Figure A.3: Hazardous activity process sheet.

Appendix B Adsorption Data

Table B.1-B.5 shows the absorption data from the UV measurements of the samples after they have been in contact with Illite clay. The absorption values originates from three different parallels for each concentration and they are obtained at 260 nm. The average values from the tables are the values used in the adsorption isotherms in the report.

Table B.1: Overview of the surfactant concentrations and the absorption at the low salinity condition

Surfactant concentration [M]	Parallel	Absorption	Average
$5 \cdot 10^{-5}$	1	0.004	0.008
	2	0.001	
	3	0.019	
$7.5 \cdot 10^{-5}$	1	0.026	0.026
	2	0.025	
	3	0.026	
$1 \cdot 10^{-4}$	1	0.014	0.014
	2	0.015	
	3	0.012	
$2.5 \cdot 10^{-4}$	1	0.070	0.077
	2	0.080	
	3	0.080	
$5 \cdot 10^{-4}$	1	0.170	0.165
	2	0.161	
	3	0.163	
$7.5 \cdot 10^{-4}$	1	0.218	0.220
	2	0.215	
	3	0.226	
$1 \cdot 10^{-3}$	1	0.339	0.342
	2	0.346	
	3	0.341	
$2.5 \cdot 10^{-3}$	1	0.735	0.736
	2	0.738	
	3	0.736	

Table B.2: Overview of the surfactant concentrations and the absorption at the low salinity condition with $CaCl_2$.

Surfactant concentration [M]	Parallel	Absorption	Average
$5 \cdot 10^{-5}$	1	0.011	0.009
	2	0.007	
	3	0.009	
$7.5 \cdot 10^{-5}$	1	0.020	0.021
	2	0.022	
	3	0.020	
$1 \cdot 10^{-4}$	1	0.035	0.028
	2	0.024	
	3	0.026	
$2.5 \cdot 10^{-4}$	1	0.069	0.068
	2	0.066	
	3	0.068	
$5 \cdot 10^{-4}$	1	0.136	0.134
	2	0.132	
	3	0.134	
$7.5 \cdot 10^{-4}$	1	0.256	0.252
	2	0.250	
	3	0.250	
$1 \cdot 10^{-3}$	1	0.325	0.328
	2	0.329	
	3	0.330	
$2.5 \cdot 10^{-3}$	1	0.660	0.663
	2	0.664	
	3	0.665	

Table B.3: Overview of the surfactant concentrations and the absorption at the medium salinity condition.

Surfactant concentration [M]	Parallel	Absorption	Average
$5 \cdot 10^{-5}$	1	0.003	0.006
	2	0.005	
	3	0.001	
$7.5 \cdot 10^{-5}$	1	0.007	0.010
	2	0.012	
	3	0.012	
$1 \cdot 10^{-4}$	1	0.021	0.021
	2	0.020	
	3	0.021	
$2.5 \cdot 10^{-4}$	1	0.064	0.064
	2	0.061	
	3	0.067	
$5 \cdot 10^{-4}$	1	0.173	0.174
	2	0.174	
	3	0.175	
$7.5 \cdot 10^{-4}$	1	0.256	0.248
	2	0.247	
	3	0.240	
$1 \cdot 10^{-3}$	1	0.301	0.315
	2	0.322	
	3	0.323	
$2.5 \cdot 10^{-3}$	1	0.714	0.705
	2	0.701	
	3	0.701	

Table B.4: Overview of the surfactant concentrations and the absorption at the medium salinity condition with $CaCl_2$

Surfactant concentration [M]	Parallel	Absorption	Average
$5 \cdot 10^{-5}$	1	0.025	0.028
	2	0.025	
	3	0.035	
$7.5 \cdot 10^{-5}$	1	0.026	0.029
	2	0.025	
	3	0.036	
$1 \cdot 10^{-4}$	1	0.028	0.030
	2	0.025	
	3	0.037	
$2.5 \cdot 10^{-4}$	1	0.068	0.067
	2	0.066	
	3	0.066	
$5 \cdot 10^{-4}$	1	0.137	0.137
	2	0.137	
	3	0.136	
$7.5 \cdot 10^{-4}$	1	0.215	0.202
	2	0.193	
	3	0.197	
$1 \cdot 10^{-3}$	1	0.264	0.260
	2	0.255	
	3	0.260	
$2.5 \cdot 10^{-3}$	1	0.677	0.663
	2	0.652	
	3	0.660	

Table B.5: Overview of the surfactant concentrations and the absorption at the high salinity condition

Surfactant concentration [M]	Parallel	Absorption	Average
$5 \cdot 10^{-5}$	1	0.018	0.018
	2	0.018	
	3	0.018	
$7.5 \cdot 10^{-5}$	1	0.025	0.025
	2	0.025	
	3	0.025	
$1 \cdot 10^{-4}$	1	0.039	0.037
	2	0.035	
	3	0.036	
$2.5 \cdot 10^{-4}$	1	0.094	0.094
	2	0.094	
	3	0.094	
$5 \cdot 10^{-4}$	1	0.179	0.178
	2	0.178	
	3	0.178	
$7.5 \cdot 10^{-4}$	1	0.236	0.241
	2	0.247	
	3	0.240	
$1 \cdot 10^{-3}$	1	0.264	0.262
	2	0.260	
	3	0.261	
$2.5 \cdot 10^{-3}$	1	0.631	0.630
	2	0.628	
	3	0.630	

The surfactant concentration after addition of Illite was obtained using the trend line equations from the calibration curves and absorption values from Table B.1-B.5. The difference in concentration before and after adding Illite is the adsorption of surfactant onto the clay. In addition, the real concentration before adsorption had to be calculated. By measuring the absorption of the samples that had not been in contact with Illite, the real surfactant concentration before adsorption could be calculated. All of this is shown in Table B.6-B.11.

Table B.6: Overview of the surfactant concentration before and after adsorption onto Illite and the difference in concentration, which corresponds to the adsorption, for the low salinity condition.

Theoretical surfactant concentration before adsorption [M]	**Calculated/real surfactant concentration before adsorption [M]**	**Surfactant concentration after adsorption [M]**	**Difference in surfactant concentration [M]**	**Adsorbed amount [g surf/g Illite]**
$5.00 \cdot 10^{-5}$	$1.10 \cdot 10^{-4}$	$2.02 \cdot 10^{-5}$	$9.02 \cdot 10^{-5}$	$3.14 \cdot 10^{-3}$
$7.50 \cdot 10^{-5}$	$1.25 \cdot 10^{-4}$	$8.39 \cdot 10^{-5}$	$4.09 \cdot 10^{-5}$	$1.42 \cdot 10^{-3}$
$1.00 \cdot 10^{-4}$	$1.64 \cdot 10^{-4}$	$4.06 \cdot 10^{-5}$	$1.24 \cdot 10^{-4}$	$4.31 \cdot 10^{-3}$
$2.50 \cdot 10^{-4}$	$3.56 \cdot 10^{-4}$	$2.68 \cdot 10^{-4}$	$8.78 \cdot 10^{-5}$	$3.06 \cdot 10^{-3}$
$5.00 \cdot 10^{-4}$	$5.94 \cdot 10^{-4}$	$5.85 \cdot 10^{-4}$	$8.42 \cdot 10^{-6}$	$2.93 \cdot 10^{-4}$
$7.50 \cdot 10^{-4}$	$8.03 \cdot 10^{-4}$	$7.84 \cdot 10^{-4}$	$1.92 \cdot 10^{-5}$	$6.70 \cdot 10^{-4}$
$1.00 \cdot 10^{-3}$	$1.38 \cdot 10^{-3}$	$1.16 \cdot 10^{-3}$	$2.22 \cdot 10^{-4}$	$7.75 \cdot 10^{-3}$
$2.50 \cdot 10^{-3}$	$2.86 \cdot 10^{-3}$	$2.65 \cdot 10^{-3}$	$2.12 \cdot 10^{-4}$	$7.37 \cdot 10^{-3}$

Table B.7: Overview of the surfactant concentration before and after adsorption onto Illite and the difference in concentration, which corresponds to the adsorption, for the low salinity condition with $CaCl_2$.

Surfactant concentration before adsorption [M]	Calculated /real surfactant concentration before adsorption [M]	Surfactant concentration after adsorption [M]	Difference in surfactant concentration [M]	Adsorbed amount [g surf/g Illite]
$5.00 \cdot 10^{-5}$	$7.89 \cdot 10^{-5}$	$1.57 \cdot 10^{-5}$	$6.32 \cdot 10^{-5}$	$2.20 \cdot 10^{-3}$
$7.50 \cdot 10^{-5}$	$1.01 \cdot 10^{-4}$	$4.77E \cdot 10^{-5}$	$5.31 \cdot 10^{-5}$	$1.85 \cdot 10^{-3}$
$1.00 \cdot 10^{-4}$	$1.17 \cdot 10^{-4}$	$6.88 \cdot 10^{-5}$	$4.86 \cdot 10^{-5}$	$1.69 \cdot 10^{-3}$
$2.50 \cdot 10^{-4}$	$2.25 \cdot 10^{-4}$	$1.77 \cdot 10^{-5}$	$4.76 \cdot 10^{-5}$	$1.66 \cdot 10^{-3}$
$5.00 \cdot 10^{-4}$	$8.24 \cdot 10^{-4}$	$3.59 \cdot 10^{-4}$	$4.65 \cdot 10^{-4}$	$1.62 \cdot 10^{-2}$
$7.50 \cdot 10^{-4}$	$1.33 \cdot 10^{-3}$	$5.67 \cdot 10^{-4}$	$7.62 \cdot 10^{-4}$	$2.66 \cdot 10^{-2}$
$1.00 \cdot 10^{-3}$	$1.41 \cdot 10^{-3}$	$7.40 \cdot 10^{-4}$	$6.72 \cdot 10^{-4}$	$2.34 \cdot 10^{-2}$
$2.50 \cdot 10^{-3}$	$2.24 \cdot 10^{-3}$	$1.81 \cdot 10^{-3}$	$4.29 \cdot 10^{-4}$	$1.49 \cdot 10^{-2}$

Table B.8: Overview of the surfactant concentration before and after adsorption onto Illite and the difference in concentration, which corresponds to the adsorption, for the medium salinity condition.

Surfactant concentration before adsorption [M]	Calculated /real surfactant concentration before adsorption [M]	Surfactant concentration after adsorption [M]	Difference in surfactant concentration [M]	Adsorbed amount [g surf/g Illite]
$5.00 \cdot 10^{-5}$	$9.61 \cdot 10^{-5}$	$4.41 \cdot 10^{-5}$	$5.20 \cdot 10^{-5}$	$1.81 \cdot 10^{-3}$
$7.50 \cdot 10^{-5}$	$1.34 \cdot 10^{-4}$	$5.91 \cdot 10^{-5}$	$7.52 \cdot 10^{-5}$	$2.62 \cdot 10^{-3}$
$1.00 \cdot 10^{-4}$	$1.86 \cdot 10^{-4}$	$9.49 \cdot 10^{-5}$	$9.14 \cdot 10^{-5}$	$3.18 \cdot 10^{-3}$
$2.50 \cdot 10^{-4}$	$3.74 \cdot 10^{-4}$	$2.45 \cdot 10^{-4}$	$1.28 \cdot 10^{-4}$	$4.47 \cdot 10^{-3}$
$5.00 \cdot 10^{-4}$	$6.75 \cdot 10^{-4}$	$6.27 \cdot 10^{-4}$	$4.86 \cdot 10^{-5}$	$1.69 \cdot 10^{-3}$
$7.50 \cdot 10^{-4}$	$9.25 \cdot 10^{-4}$	$8.82 \cdot 10^{-4}$	$4.28 \cdot 10^{-5}$	$1.49 \cdot 10^{-3}$
$1.00 \cdot 10^{-3}$	$1.17 \cdot 10^{-3}$	$1.12 \cdot 10^{-3}$	$5.09 \cdot 10^{-5}$	$1.77 \cdot 10^{-3}$
$2.50 \cdot 10^{-3}$	$2.68 \cdot 10^{-3}$	$2.47 \cdot 10^{-3}$	$2.10 \cdot 10^{-4}$	$7.33 \cdot 10^{-3}$

Table B.9: Overview of the surfactant concentration before and after adsorption onto Illite and the difference in concentration, which corresponds to the adsorption, for the medium salinity condition with $CaCl_2$.

Surfactant concentration before adsorption [M]	Calculated /real surfactant concentration before adsorption [M]	Surfactant concentration after adsorption [M]	Difference in surfactant concentration [M]	Adsorbed amount [g surf/g Illite]
$5.00 \cdot 10^{-5}$	$2.73 \cdot 10^{-6}$	$2.02 \cdot 10^{-7}$	$2.53 \cdot 10^{-6}$	$8.80 \cdot 10^{-5}$
$7.50 \cdot 10^{-5}$	$1.03 \cdot 10^{-5}$	$1.21 \cdot 10^{-6}$	$9.09 \cdot 10^{-6}$	$3.17 \cdot 10^{-4}$
$1.00 \cdot 10^{-4}$	$7.28 \cdot 10^{-6}$	$2.73 \cdot 10^{-6}$	$4.55 \cdot 10^{-6}$	$1.58 \cdot 10^{-4}$
$2.50 \cdot 10^{-4}$	$2.36 \cdot 10^{-4}$	$5.83 \cdot 10^{-5}$	$1.78 \cdot 10^{-4}$	$6.20 \cdot 10^{-3}$
$5.00 \cdot 10^{-4}$	$1.01 \cdot 10^{-3}$	$1.64 \cdot 10^{-4}$	$8.49 \cdot 10^{-4}$	$2.96 \cdot 10^{-2}$
$7.50 \cdot 10^{-4}$	$5.48 \cdot 10^{-4}$	$2.63 \cdot 10^{-4}$	$2.85 \cdot 10^{-4}$	$9.95 \cdot 10^{-3}$
$1.00 \cdot 10^{-3}$	$8.85 \cdot 10^{-4}$	$3.51 \cdot 10^{-4}$	$5.34 \cdot 10^{-4}$	$1.86 \cdot 10^{-2}$
$2.50 \cdot 10^{-3}$	$1.41 \cdot 10^{-3}$	$9.62 \cdot 10^{-4}$	$4.50 \cdot 10^{-4}$	$1.57 \cdot 10^{-2}$

Table B.10: Overview of the surfactant concentration before and after adsorption onto Illite and the difference in concentration, which corresponds to the adsorption, for the high salinity condition.

Surfactant concentration before adsorption [M]	**Calculated /real surfactant concentration before adsorption [M]**	**Surfactant concentration after adsorption [M]**	**Difference in surfactant concentration [M]**	**Adsorbed amount [g surf/g Illite]**
$5.00 \cdot 10^{-5}$	$7.07 \cdot 10^{-5}$	$6.76 \cdot 10^{-5}$	$3.17 \cdot 10^{-6}$	$1.11 \cdot 10^{-4}$
$7.50 \cdot 10^{-5}$	$1.10 \cdot 10^{-4}$	$6.44 \cdot 10^{-5}$	$4.60 \cdot 10^{-5}$	$1.60 \cdot 10^{-3}$
$1.00 \cdot 10^{-4}$	$1.72 \cdot 10^{-4}$	$8.45 \cdot 10^{-5}$	$8.72 \cdot 10^{-5}$	$3.04 \cdot 10^{-3}$
$2.50 \cdot 10^{-4}$	$3.70 \cdot 10^{-4}$	$1.50 \cdot 10^{-4}$	$2.20 \cdot 10^{-4}$	$7.67 \cdot 10^{-3}$
$5.00 \cdot 10^{-4}$	$7.09 \cdot 10^{-4}$	$3.34 \cdot 10^{-4}$	$3.75 \cdot 10^{-4}$	$1.31 \cdot 10^{-2}$
$7.50 \cdot 10^{-4}$	$9.36 \cdot 10^{-4}$	$6.32 \cdot 10^{-4}$	$3.04 \cdot 10^{-4}$	$1.06 \cdot 10^{-2}$
$1.00 \cdot 10^{-3}$	$1.02 \cdot 10^{-3}$	$8.43 \cdot 10^{-4}$	$1.73 \cdot 10^{-4}$	$6.03 \cdot 10^{-3}$
$2.50 \cdot 10^{-3}$	$2.41 \cdot 10^{-3}$	$9.29 \cdot 10^{-4}$	$1.48 \cdot 10^{-3}$	$5.15 \cdot 10^{-2}$

Table B.11: Overview of the absorption of the samples that had not been in contact with Illite.

	Absorption				
Concentration [M]	Low salinity	Low salinity with $CaCl_2$	Medium salinity	Medium salinity with $CaCl_2$	High salinity
$5.00 \cdot 10^{-5}$	0.033	0.032	0.021	0.030	0.020
$7.50 \cdot 10^{-5}$	0.037	0.040	0.032	0.035	0.033
$1.00 \cdot 10^{-4}$	0.048	0.046	0.047	0.033	0.050
$2.50 \cdot 10^{-4}$	0.101	0.085	0.101	0.184	0.105
$5.00 \cdot 10^{-4}$	0.167	0.303	0.188	0.697	0.199
$7.50 \cdot 10^{-4}$	0.225	0.487	0.260	0.390	0.262
$1.00 \cdot 10^{-3}$	0.385	0.517	0.330	0.612	0.284
$2.50 \cdot 10^{-3}$	0.795	0.819	0.766	0.960	0.670

Appendix C Determination of CMC

The data obtained from the tensiometer measurements is shown in Table C.1 – C.5. The values of the interfacial tension are the averages of the three last values detected, thus well after equilibrium is reached. These values were used to create the CMC determining plots.

Table C.1: Overview of the surfactant concentrations and the measured interfacial tension values for the low salinity condition.

Surfactant concentration [M]	**IFT [mN/m]**
$5.00 \cdot 10^{-6}$	66.155
$1.00 \cdot 10^{-5}$	60.489
$5.00 \cdot 10^{-5}$	50.918
$1.00 \cdot 10^{-4}$	44.849
$5.00 \cdot 10^{-4}$	33.799
$1.00 \cdot 10^{-3}$	31.184
$5.00 \cdot 10^{-3}$	30.647
$1.00 \cdot 10^{-2}$	30.375

Table C.2: Overview of the surfactant concentrations and the measured interfacial tension values for the low salinity condition with $CaCl_2$.

Surfactant concentration [M]	**IFT [mN/m]**
$5.00 \cdot 10^{-6}$	65.043
$1.00 \cdot 10^{-5}$	57.954
$5.00 \cdot 10^{-5}$	41.109
$1.00 \cdot 10^{-4}$	35.096
$5.00 \cdot 10^{-4}$	27.385
$1.00 \cdot 10^{-3}$	27.214
$5.00 \cdot 10^{-3}$	29.101
$1.00 \cdot 10^{-2}$	29.423

Table C.3: Overview of the surfactant concentrations and the measured interfacial tension values for the medium salinity condition.

Surfactant concentration [M]	**IFT [mN/m]**
$5.00 \cdot 10^{-6}$	57.916
$1.00 \cdot 10^{-5}$	54.815
$5.00 \cdot 10^{-5}$	40.557
$1.00 \cdot 10^{-4}$	34.398
$5.00 \cdot 10^{-4}$	28.980
$1.00 \cdot 10^{-3}$	28.802
$5.00 \cdot 10^{-3}$	28.485
$1.00 \cdot 10^{-2}$	28.089

Table C.4: Overview of the surfactant concentrations and the measured interfacial tension values for the medium salinity condition with $CaCl_2$.

Surfactant concentration [M]	**IFT [mN/m]**
$5.00 \cdot 10^{-6}$	57.271
$1.00 \cdot 10^{-5}$	53.454
$5.00 \cdot 10^{-5}$	34.829
$1.00 \cdot 10^{-4}$	29.797
$5.00 \cdot 10^{-4}$	27.506
$1.00 \cdot 10^{-3}$	27.525
$5.00 \cdot 10^{-3}$	27.157
$1.00 \cdot 10^{-2}$	27.511

Table C.5: Overview of the surfactant concentrations and the measured interfacial tension values for the high salinity condition.

Surfactant concentration [M]	**IFT [mN/m]**
$5.00 \cdot 10^{-6}$	71.167
$1.00 \cdot 10^{-5}$	71.997
$5.00 \cdot 10^{-5}$	36.216
$1.00 \cdot 10^{-4}$	29.863
$5.00 \cdot 10^{-4}$	27.546
$1.00 \cdot 10^{-3}$	27.546
$5.00 \cdot 10^{-3}$	27.571
$1.00 \cdot 10^{-2}$	27.650

The calibration curves and the calculation of the CMC values are shown in the following sections (the plot for the low salinity condition without calcium is not included here, since it is displayed in the report).

Low Salinity with $CaCl_2$

The plot used for determination of CMC for the low salinity condition with $CaCl_2$ was obtained using the same procedure as for low salinity without $CaCl_2$, and is shown in Figure C.1.

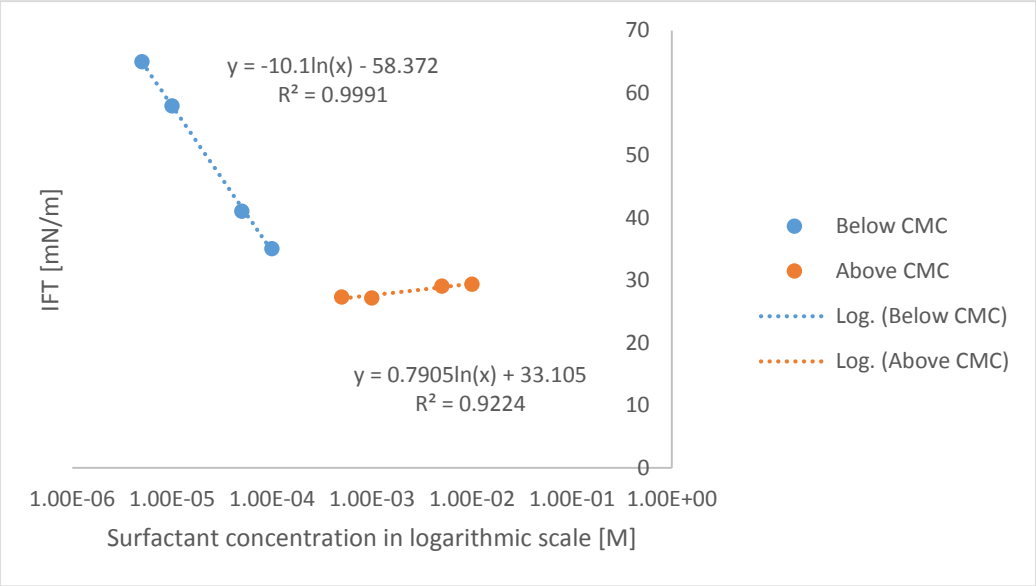

Figure C.1: A plot of various surfactant concentrations versus the corresponding interfacial tension values in a low salinity solution with $CaCl_2$. The trend line equations are included.

The CMC was obtained by putting the two equations for the low salinity condition with calcium equal to each other:

$$-10.1\ln(x) - 58.372 = 0.7905\ln(x) + 33.105$$

and solving for x:

$$x = \frac{1}{e^{\frac{182954}{21781}}} = 2.249 \cdot 10^{-4}$$

This resulted in a CMC of $2.249 \cdot 10^{-4}$ M.

Medium Salinity

The plot used for determination of CMC for the medium salinity condition was obtained using the same procedure as for low salinity without $CaCl_2$, and is shown in Figure C.2.

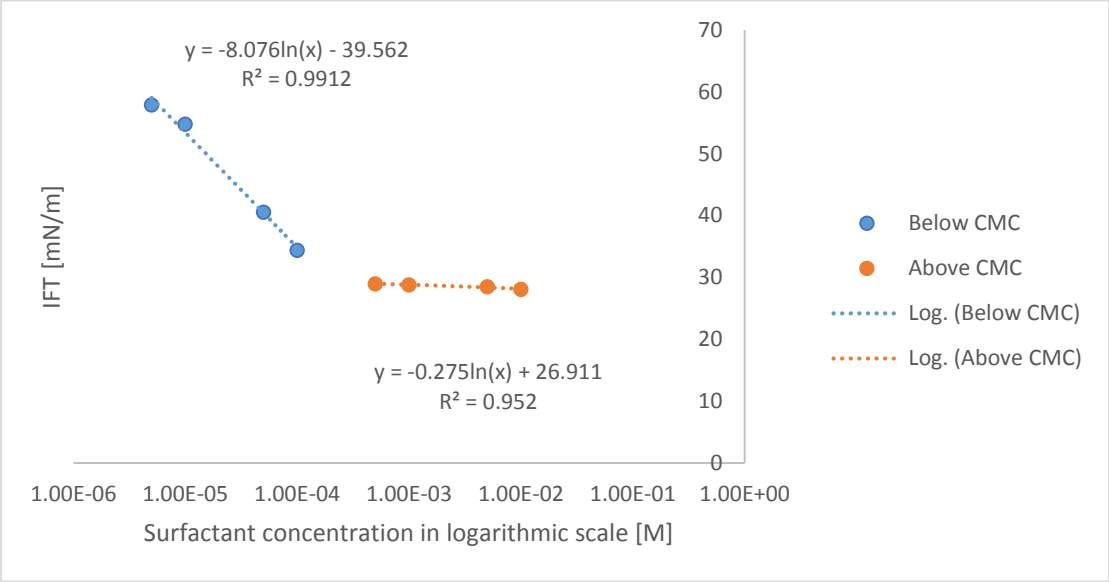

Figure C.2: A plot of various surfactant concentrations versus the corresponding interfacial tension values in a medium salinity solution. The trend line equations are included.

The CMC was obtained by putting the two equations for the medium salinity condition equal to each other:

$$-8.076\ln(x) - 39.562 = -0.275\ln(x) + 26.911$$

and solving for x:

$$x = \frac{1}{e^{\frac{66473}{7801}}} = 1.992 \cdot 10^{-4}$$

This resulted in a CMC of $1.992 \cdot 10^{-4}$ M.

Medium Salinity with $CaCl_2$

The plot used for determination of CMC for the medium salinity condition with $CaCl_2$ was obtained using the same procedure as for low salinity without $CaCl_2$, and is shown in Figure C.3.

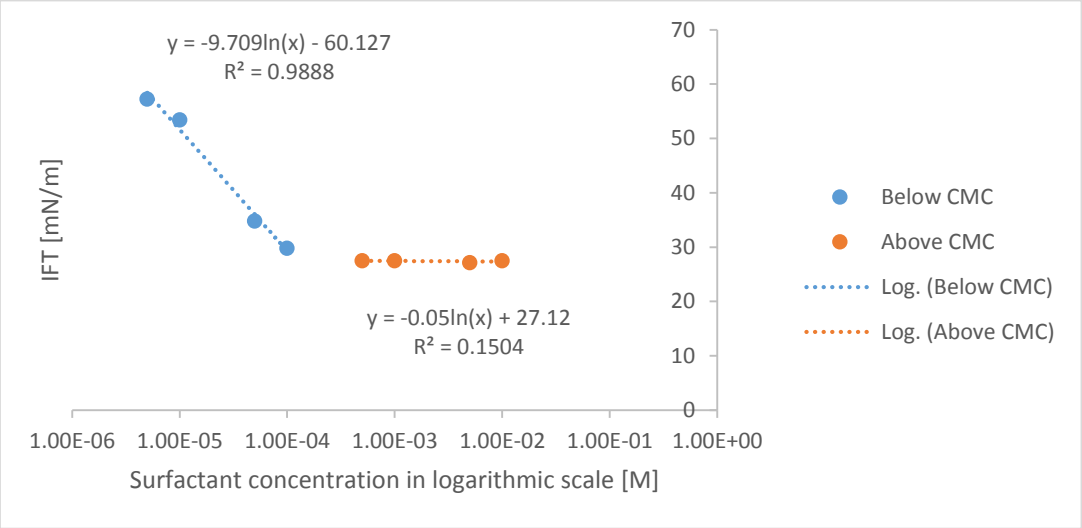

Figure C.3: A plot of various surfactant concentrations versus the corresponding interfacial tension values in a medium salinity solution with $CaCl_2$. The trend line equations are included.

The CMC was obtained by putting the two equations for the medium salinity condition with calcium equal to each other:

$$-9.709\ln(x) - 60.127 = -0.05\ln(x) + 27.12$$

and solving for x:

$$x = \frac{1}{e^{\frac{87247}{9659}}} = 1.194 \cdot 10^{-4}$$

This resulted in a CMC of $1.194 \cdot 10^{-4}$ M.

High Salinity

The plot used for determination of CMC for the high salinity condition was obtained using the same procedure as for low salinity without $CaCl_2$, and is shown in Figure C.4.

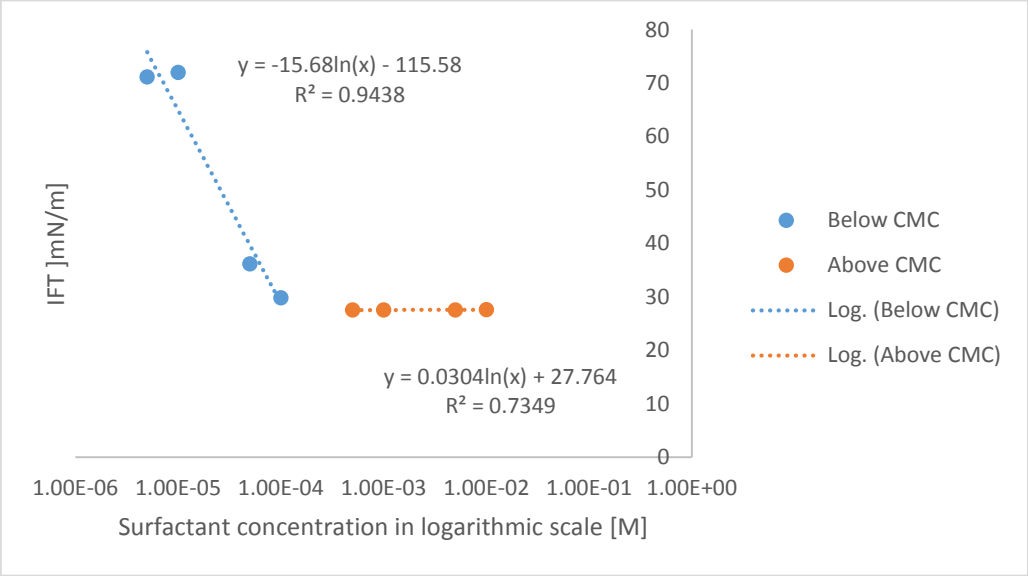

Figure C.4: A plot of various surfactant concentrations versus the corresponding interfacial tension values in a high salinity solution. The trend line equations are included.

The CMC is obtained by putting the two equations for the high salinity condition equal to each other:

$$-15.68\ln(x) - 115.58 = 0.0304\ln(x) + 27.764$$

and solving for x:

$$x = \frac{1}{e^{\frac{89590}{9819}}} = 1.09 \cdot 10^{-4}$$

This resulted in a CMC of $1.09 \cdot 10^{-4}$ M.

Appendix D Calibration Curves

Table D.1-D.5 shows the calibration curve data from the UV measurements. The absorption values originates from three different parallels for each concentration and they are obtained at 260 nm. The average values from the tables are the values used in the calibration curves in the report.

Table D.1: Overview of the surfactant concentrations and absorption at the low salinity condition.

Surfactant concentration [M]	Parallel	Absorption	Average
$5.0 \cdot 10^{-5}$	1	0.012	0.012
	2	0.010	
	3	0.014	
$1.0 \cdot 10^{-4}$	1	0.030	0.03
	2	0.040	
	3	0.020	
$2.0 \cdot 10^{-4}$	1	0.058	0.059
	2	0.060	
	3	0.059	
$4.0 \cdot 10^{-4}$	1	0.116	0.116
	2	0.116	
	3	0.116	
$6.0 \cdot 10^{-4}$	1	0.172	0.173
	2	0.174	
	3	0.173	
$8.0 \cdot 10^{-4}$	1	0.223	0.223
	2	0.223	
	3	0.223	
$1.0 \cdot 10^{-3}$	1	0.276	0.277
	2	0.277	
	3	0.277	
$1.2 \cdot 10^{-3}$	1	0.335	0.335
	2	0.335	
	3	0.334	

Table D.2: Overview of the surfactant concentrations and the absorption at low salinity condition with $CaCl_2$

Surfactant concentration [M]	Parallel	Absorption	Average
$1.0 \cdot 10^{-5}$	1	0.006	0.006
	2	0.008	
	3	0.004	
$5.0 \cdot 10^{-5}$	1	0.011	0.013
	2	0.013	
	3	0.014	
$1.0 \cdot 10^{-4}$	1	0.036	0.034
	2	0.033	
	3	0.033	
$2.0 \cdot 10^{-4}$	1	0.067	0.067
	2	0.066	
	3	0.068	
$4.0 \cdot 10^{-4}$	1	0.156	0.156
	2	0.157	
	3	0.156	
$6.0 \cdot 10^{-4}$	1	0.250	0.250
	2	0.250	
	3	0.250	
$8.0 \cdot 10^{-4}$	1	0.299	0.300
	2	0.300	
	3	0.300	
$1.0 \cdot 10^{-3}$	1	0.373	0.373
	2	0.373	
	3	0.373	
$1.2 \cdot 10^{-3}$	1	0.418	0.417
	2	0.417	
	3	0.417	

Table D.3: Overview of the surfactant concentrations and the absorption at medium salinity condition.

Surfactant concentration [M]	Parallel	Absorption	Average
$1.0 \cdot 10^{-5}$	1	0.001	0.001
	2	0.002	
	3	0.001	
$5.0 \cdot 10^{-5}$	1	0.011	0.013
	2	0.013	
	3	0.015	
$1.0 \cdot 10^{-4}$	1	0.030	0.031
	2	0.030	
	3	0.032	
$2.0 \cdot 10^{-4}$	1	0.055	0.054
	2	0.054	
	3	0.054	
$4.0 \cdot 10^{-4}$	1	0.107	0.107
	2	0.106	
	3	0.107	
$6.0 \cdot 10^{-4}$	1	0.157	0.156
	2	0.157	
	3	0.156	
$8.0 \cdot 10^{-4}$	1	0.207	0.207
	2	0.207	
	3	0.207	
$1.0 \cdot 10^{-3}$	1	0.257	0.257
	2	0.257	
	3	0.259	
$1.2 \cdot 10^{-3}$	1	0.375	0.375
	2	0.375	
	3	0.375	

Table D.4: Overview of the surfactant concentrations and the absorption at medium salinity condition with $CaCl_2$

Surfactant concentration [M]	Parallel	Absorption	Average
$1.0 \cdot 10^{-5}$	1	0.003	0.005
	2	0.007	
	3	0.005	
$5.0 \cdot 10^{-5}$	1	0.017	0.018
	2	0.017	
	3	0.019	
$1.0 \cdot 10^{-4}$	1	0.033	0.032
	2	0.032	
	3	0.032	
$2.0 \cdot 10^{-4}$	1	0.057	0.057
	2	0.057	
	3	0.058	
$4.0 \cdot 10^{-4}$	1	0.177	0.177
	2	0.176	
	3	0.177	
$6.0 \cdot 10^{-4}$	1	0.346	0.346
	2	0.346	
	3	0.346	
$8.0 \cdot 10^{-4}$	1	0.490	0.491
	2	0.491	
	3	0.491	
$1.0 \cdot 10^{-3}$	1	0.581	0.581
	2	0.581	
	3	0.581	
$1.2 \cdot 10^{-3}$	1	0.609	0.608
	2	0.608	
	3	0.608	

Table D.5: Overview of the surfactant concentrations and the absorption at high salinity condition.

Surfactant concentration [M]	Parallel	Absorption	Average
$5.0 \cdot 10^{-5}$	1	0.008	0.010
	2	0.009	
	3	0.012	
$1.0 \cdot 10^{-4}$	1	0.030	0.028
	2	0.027	
	3	0.027	
$2.0 \cdot 10^{-4}$	1	0.059	0.061
	2	0.063	
	3	0.060	
$4.0 \cdot 10^{-4}$	1	0.128	0.128
	2	0.128	
	3	0.127	
$6.0 \cdot 10^{-4}$	1	0.190	0.190
	2	0.190	
	3	0.190	
$8.0 \cdot 10^{-4}$	1	0.248	0.249
	2	0.249	
	3	0.249	
$1.0 \cdot 10^{-3}$	1	0.314	0.314
	2	0.314	
	3	0.313	
$1.2 \cdot 10^{-3}$	1	0.373	0.373
	2	0.373	
	3	0.373	

The calibration curves obtained from the UV-measurements are displayed in the following sections (the plot for the low salinity condition without calcium is not included here, since it is displayed in the main report).

Low Salinity with $CaCl_2$

The UV calibration curve for the low salinity condition with $CaCl_2$ was obtained using the same procedure as for low salinity without $CaCl_2$, and is shown in Figure D.1.

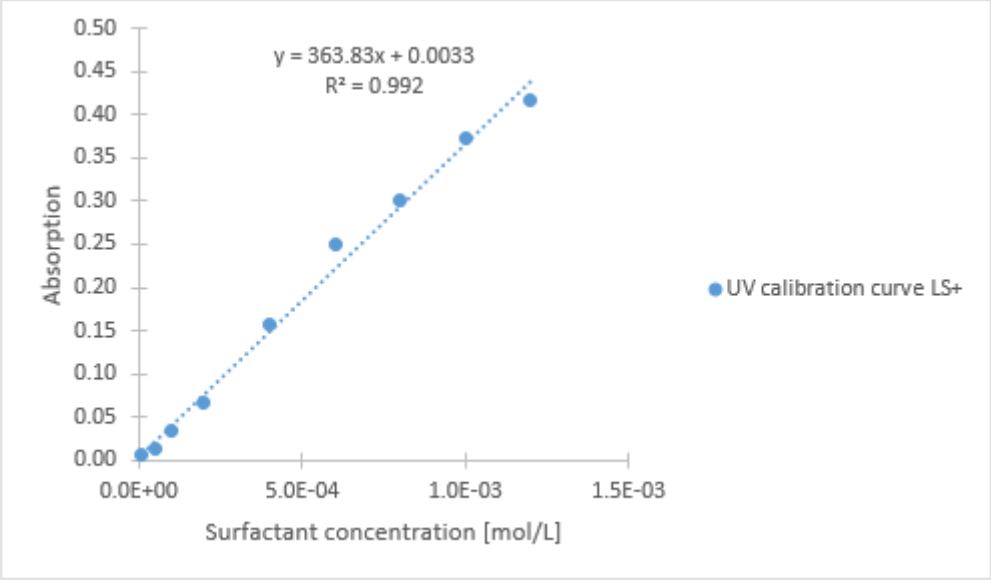

Figure D.1: The UV calibration curve for the low salinity solution with $CaCl_2$ obtained at 260nm. The trend line equation is included.

The graph has a R^2 value of 0.992. The deviation from the straight line is slightly S-shaped.

Medium Salinity

The UV calibration curve for the medium salinity condition was obtained using the same procedure as for low salinity without $CaCl_2$, and is shown in Figure D.2.

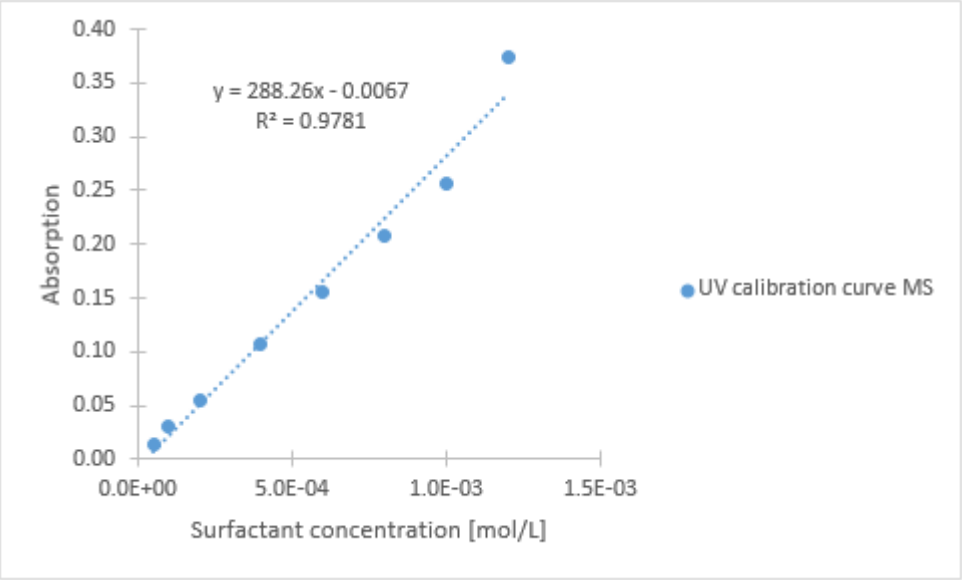

Figure D.2: The UV calibration curve for the medium salinity solution obtained at 260nm. The trend line equation is included.

The graph has a R^2 value of 0.9781, which correspond to a small deviation from a straight line. However, it is not S-shaped like the low salinity with calcium.

Medium Salinity with $CaCl_2$

The UV calibration curve for the medium salinity condition with $CaCl_2$ was obtained using the same procedure as for low salinity without $CaCl_2$, and is shown in Figure D.3.

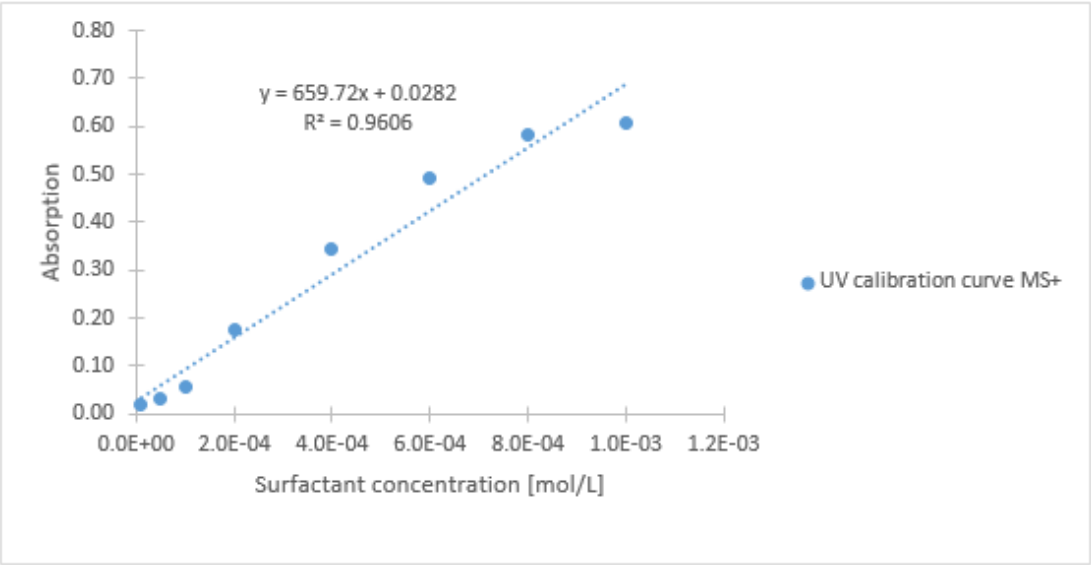

Figure D.3: The UV calibration curve for the medium salinity solution with $CaCl_2$ obtained at 260nm. The trend line equation is included.

The graph has a R^2 value of 0.9606 and similar to the other salinity condition with calcium, it is slightly S-shaped.

High Salinity

The UV calibration curve for the high salinity condition was obtained using the same procedure as for low salinity without $CaCl_2$, and is shown in Figure D.4.

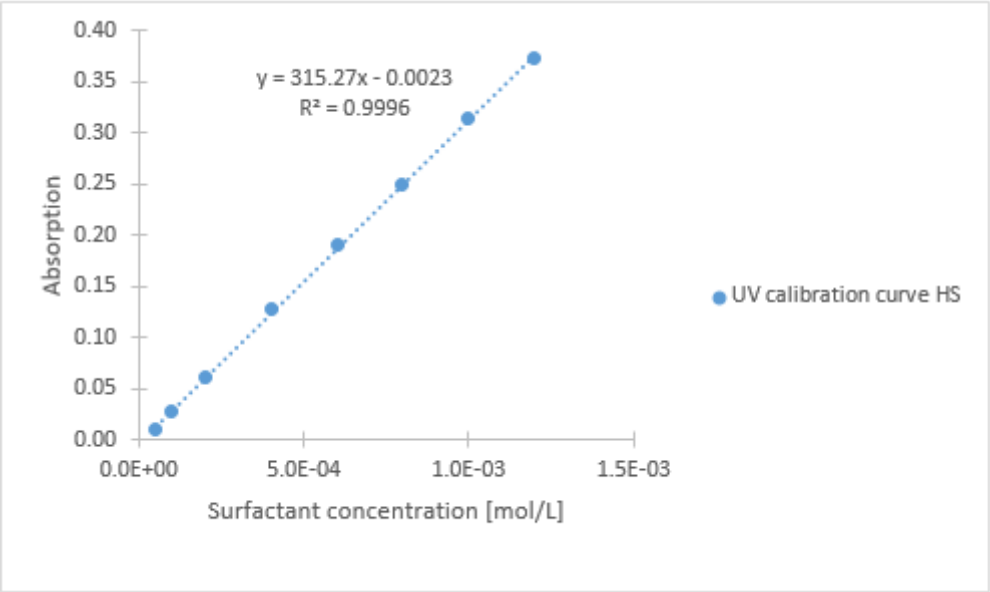

Figure D.4: The UV calibration curve for the high salinity solution obtained at 260nm. The trend line equation is included.

The graph has a R^2 value of 0.9996, which correspond to a good straight-line approximation.

Appendix E Calculation of the Debye Length

The Debye length was calculated for low salinity, medium salinity and high salinity using Equation E.1:

$$k_D^{-1} = \sqrt{\frac{\varepsilon_r \cdot \varepsilon_0 \cdot k_B \cdot T}{2 \cdot N_A \cdot e^2 \cdot I}} \quad \text{(E.1)}$$

where I is the ionic strength of the electrolyte, ε_0 is the permittivity of free space, ε_r is the dielectric constant, k_B is the Boltzmann's constant, T is the absolute temperature, e is the elementary charge and N_A is the Avogadro number. All the parameters in this equation are constant, except the ionic strength that changes for each salinity:

ε_r = 80.1 at 20°C

ε_0 = $8.854 \cdot 10^{-12}$ F/m

k_B = $1.381 \cdot 10^{-23}$ J/K

T = 20°C

N_A = $6.022 \cdot 10^{23}$ mol^{-1}

e = $1.602 \cdot 10^{-19}$ A·s

Low Salinity

The low salinity solution had an ionic strength, I, of 0.02 M. By insertion into Equation 1, the Debye length, k^{-1}, was obtained:

k_D^{-1} = $2.16 \cdot 10^{-9}$ m = 2.16 nm

Medium Salinity

The low salinity solution had an ionic strength, I, of 0.08. By insertion into Equation 1, the Debye length, k^{-1}, was obtained:

k_D^{-1} = 1.08·10^{-9} m = 1.08 nm

High Salinity

The low salinity solution had an ionic strength, I, of 0.02. By insertion into Equation E.1, the Debye length, k^{-1}, was obtained:

k_D^{-1} = 6.81^{-10} m = 0.68 nm

Appendix F Mathematical Fitting

Table F.1-F.5 displays the values used for the mathematical fitting of the Langmuir isotherms. For the Freundlich isotherms the plots were simply changed to a log-log scale.

Table F.1: The values used for the Langmuir isotherm fitting of the low salinity condition.

q_e	$1/q_e$	C_e	$1/C_e$
$3.14 \cdot 10^{-3}$	$3.18 \cdot 10^{2}$	$2.02 \cdot 10^{-5}$	$4.95 \cdot 10^{4}$
$1.42 \cdot 10^{-3}$	$7.02 \cdot 10^{2}$	$8.39 \cdot 10^{-5}$	$1.19 \cdot 10^{4}$
$4.31 \cdot 10^{-3}$	$2.32 \cdot 10^{2}$	$4.06 \cdot 10^{-5}$	$2.46 \cdot 10^{4}$
$3.06 \cdot 10^{-3}$	$3.27 \cdot 10^{2}$	$2.68 \cdot 10^{-4}$	$3.73 \cdot 10^{3}$
$2.93 \cdot 10^{-4}$	$3.41 \cdot 10^{3}$	$5.85 \cdot 10^{-4}$	$1.71 \cdot 10^{3}$
$6.70 \cdot 10^{-4}$	$1.49 \cdot 10^{3}$	$7.84 \cdot 10^{-4}$	$1.28 \cdot 10^{3}$
$2.35 \cdot 10^{-3}$	$4.26 \cdot 10^{2}$	$1.16 \cdot 10^{-3}$	$8.64 \cdot 10^{2}$
$7.37 \cdot 10^{-3}$	$1.36 \cdot 10^{2}$	$2.65 \cdot 10^{-3}$	$3.78 \cdot 10^{2}$

Table F.2: The values used for Langmuir isotherm fitting of the low salinity condition with $CaCl_2$.

q_e	$1/q_e$	C_e	$1/C_e$
$2.20 \cdot 10^{-3}$	$4.54 \cdot 10^{2}$	$1.57 \cdot 10^{-5}$	$6.38 \cdot 10^{4}$
$1.85 \cdot 10^{-3}$	$5.40 \cdot 10^{2}$	$4.77 \cdot 10^{-5}$	$2.09 \cdot 10^{4}$
$1.69 \cdot 10^{-3}$	$5.91 \cdot 10^{2}$	$6.88 \cdot 10^{-5}$	$1.45 \cdot 10^{4}$
$1.66 \cdot 10^{-3}$	$6.02 \cdot 10^{2}$	$1.77 \cdot 10^{-4}$	$5.65 \cdot 10^{3}$
$1.62 \cdot 10^{-2}$	$6.18 \cdot 10^{1}$	$3.59 \cdot 10^{-4}$	$2.78 \cdot 10^{3}$
$2.25 \cdot 10^{-2}$	$4.44 \cdot 10^{1}$	$6.84 \cdot 10^{-4}$	$1.46 \cdot 10^{3}$
$1.81 \cdot 10^{-2}$	$5.52 \cdot 10^{1}$	$8.92 \cdot 10^{-4}$	$1.12 \cdot 10^{3}$
$1.49 \cdot 10^{-2}$	$6.69 \cdot 10^{1}$	$1.81 \cdot 10^{-3}$	$5.52 \cdot 10^{2}$

Table F.3: The values used for Langmuir isotherm fitting of the medium salinity condition.

q_e	$1/q_e$	C_e	$1/C_e$
$1.81 \cdot 10^{-3}$	$5.51 \cdot 10^{2}$	$4.41 \cdot 10^{-5}$	$2.27 \cdot 10^{4}$
$2.62 \cdot 10^{-3}$	$3.82 \cdot 10^{2}$	$5.91 \cdot 10^{-5}$	$1.69 \cdot 10^{4}$
$3.18 \cdot 10^{-3}$	$3.14 \cdot 10^{2}$	$9.49 \cdot 10^{-5}$	$1.05 \cdot 10^{4}$
$4.47 \cdot 10^{-3}$	$2.24 \cdot 10^{2}$	$2.45 \cdot 10^{-4}$	$4.08 \cdot 10^{4}$
$1.69 \cdot 10^{-3}$	$5.91 \cdot 10^{2}$	$6.27 \cdot 10^{-4}$	$1.60 \cdot 10^{3}$
$1.49 \cdot 10^{-3}$	$6.71 \cdot 10^{2}$	$8.82 \cdot 10^{-4}$	$1.13 \cdot 10^{3}$
$1.77 \cdot 10^{-3}$	$5.64 \cdot 10^{2}$	$1.12 \cdot 10^{-3}$	$8.95 \cdot 10^{2}$
$7.33 \cdot 10^{-3}$	$1.36 \cdot 10^{2}$	$2.47 \cdot 10^{-3}$	$4.05 \cdot 10^{2}$

Table F.4: The values used for Langmuir isotherm fitting of the medium salinity condition with $CaCl_2$.

q_e	$1/q_e$	C_e	$1/C_e$
$8.80 \cdot 10^{-5}$	$1.14 \cdot 10^{4}$	$2.02 \cdot 10^{-7}$	$4.95 \cdot 10^{6}$
$3.17 \cdot 10^{-4}$	$3.16 \cdot 10^{3}$	$1.21 \cdot 10^{-6}$	$8.25 \cdot 10^{5}$
$1.58 \cdot 10^{-4}$	$6.31 \cdot 10^{3}$	$2.73 \cdot 10^{-6}$	$3.67 \cdot 10^{5}$
$6.20 \cdot 10^{-3}$	$1.61 \cdot 10^{2}$	$5.83 \cdot 10^{-5}$	$1.72 \cdot 10^{4}$
$2.96 \cdot 10^{-2}$	$3.38 \cdot 10^{1}$	$1.64 \cdot 10^{-4}$	$6.08 \cdot 10^{3}$
$9.95 \cdot 10^{-3}$	$1.01 \cdot 10^{1}$	$2.63 \cdot 10^{-4}$	$3.80 \cdot 10^{3}$
$1.86 \cdot 10^{-2}$	$5.37 \cdot 10^{1}$	$3.51 \cdot 10^{-4}$	$2.85 \cdot 10^{3}$
$1.57 \cdot 10^{-2}$	$6.37 \cdot 10^{1}$	$9.62 \cdot 10^{-4}$	$1.04 \cdot 10^{3}$

Table F.5: The values used for Langmuir isotherm fitting of the high salinity condition.

q_e	$1/q_e$	C_e	$1/C_e$
$1.11 \cdot 10^{-4}$	$9.05 \cdot 10^{3}$	$6.76 \cdot 10^{-5}$	$1.48 \cdot 10^{4}$
$1.60 \cdot 10^{-3}$	$6.24 \cdot 10^{2}$	$6.44 \cdot 10^{-5}$	$1.55 \cdot 10^{4}$
$3.04 \cdot 10^{-3}$	$3.29 \cdot 10^{2}$	$8.45 \cdot 10^{-5}$	$1.18 \cdot 10^{4}$
$7.67 \cdot 10^{-3}$	$1.30 \cdot 10^{2}$	$1.50 \cdot 10^{-4}$	$6.67 \cdot 10^{3}$
$1.31 \cdot 10^{-2}$	$7.65 \cdot 10^{1}$	$3.34 \cdot 10^{-4}$	$2.99 \cdot 10^{3}$
$1.06 \cdot 10^{-2}$	$9.44 \cdot 10^{1}$	$6.32 \cdot 10^{-4}$	$1.58 \cdot 10^{3}$
$6.03 \cdot 10^{-3}$	$1.66 \cdot 10^{1}$	$8.43 \cdot 10^{-4}$	$1.19 \cdot 10^{3}$
$5.15 \cdot 10^{-2}$	$1.94 \cdot 10^{1}$	$9.29 \cdot 10^{-4}$	$1.08 \cdot 10^{3}$

Appendix G Salinity Calculations

Calculations of the various ionic strengths for the different salinities are displayed in the following sections. The values were transformed into ppm by multiplying with the respective molar mass and a factor of 10^{-3}.

The ionic strength, I, is defined by Equation G.1:

$$I = \frac{1}{2}\sum_{i=1}^{n} C_i \cdot z_i \tag{G.1}$$

where z is the charge of the ion and C is the molar concentration of the ion.

Low salinity

An ionic strength of 0.02 gives Equation G.2:

$$0.02 = \frac{1}{2}[C_{NaCl} \cdot (+1)^2 + C_{NaCl} \cdot (-1)^2] \tag{G.2}$$

Solved for C_{NaCl} gives Equation G.3:

$$C_{NaCl} = 0.02 \text{ M} \tag{G.3}$$

Low salinity with $CaCl_2$

An ionic strength of 0.02 and a NaCl/$CaCl_2$ ratio of 1:45 gives Equation G.4:

$$0.02 = \frac{1}{2}[C_{NaCl} \cdot (+1)^2 + C_{NaCl} \cdot (-1)^2 + C_{CaCl2} \cdot (+2)^2 + 2 \cdot C_{CaCl2} \cdot (-1)^2]$$

$$0.02 = \frac{1}{2}[45 \cdot C_{CaCl2} + 45 \cdot C_{CaCl2} + 4 \cdot C_{CaCl2} + 2 \cdot C_{CaCl2}]$$

$$0.02 = \tfrac{1}{2}[96 \cdot C_{CaCl2}] \quad \text{(G.4)}$$

By solving for $CaCl_2$, Equation G.5 is obtained:

$$C_{CaCl2} = 4.17E - 04\ M \quad \text{(G.5)}$$

By solving for NaCl, Equation G.6 is obtained

$$C_{NaCl} = C_{CaCl2} \cdot 45 = 1.88E - 02\ M \quad \text{(G.6)}$$

Medium salinity

An ionic strength of 0.08 gives Equation G.7:

$$0.08 = \frac{1}{2}[C_{NaCl} \cdot (+1)^2 + C_{NaCl} \cdot (-1)^2] \quad \text{(G.7)}$$

By solving for NaCl, Equation G.8 is obtained:

$$C_{NaCl} = 0.08\ \text{M} \quad \text{(G.8)}$$

Medium salinity with $CaCl_2$

An ionic strength of 0.08 and a NaCl/$CaCl_2$ ratio of 1:45 gives Equation G.9:

$$0.08 = \frac{1}{2}[C_{NaCl} \cdot (+1)^2 + C_{NaCl} \cdot (-1)^2 + C_{CaCl2} \cdot (+2)^2 + 2 \cdot C_{CaCl2} \cdot (-1)^2]$$

$$0.08 = \tfrac{1}{2}[45 \cdot C_{CaCl2} + 45 \cdot C_{CaCl2} + 4 \cdot C_{CaCl2} + 2 \cdot C_{CaCl2}]$$

$$0.08 = \frac{1}{2}[96 \cdot C_{CaCl2}] \quad \text{(G.9)}$$

By solving for $CaCl_2$, Equation G.10 is obtained:

$$C_{CaCl2} = 1.7E-03\ M \quad \text{(G.10)}$$

By solving for NaCl, Equation G.11 is obtained:

$$C_{NaCl} = C_{CaCl2} \cdot 45 = 7.5E-02\ \text{M} \quad \text{(G.11)}$$

High salinity

An ionic strength of 0.2 gives Equation G.7:

$$0.2 = \frac{1}{2}[C_{NaCl} \cdot (+1)^2 + C_{NaCl} \cdot (-1)^2] \quad \text{(G.12)}$$

By solving for NaCl, Equation G.8 is obtained:

$$C_{NaCl} = 0.2 \text{ M} \quad \text{(G.13)}$$

Appendix H pH Measurements

The pH was measured using a pH-meter, and the determined values are shown in Table H.1.

Table H.1: Overview of the surfactant concentrations and the corresponding pH values.

Surfactant concentration [M]	**Average value of measured pH**
$5.0 \cdot 10^{-5}$	7.41
$7.5 \cdot 10^{-5}$	7.39
$1.0 \cdot 10^{-4}$	7.34
$2.5 \cdot 10^{-4}$	7.23
$5.0 \cdot 10^{-4}$	7.09
$7.5 \cdot 10^{-4}$	7.04
$1.0 \cdot 10^{-3}$	7.02
$2.5 \cdot 10^{-3}$	7.00

Appendix I Density Measurements

A densitymeter was used to determine the densities for the different surfactant concentrations. These densities were further used for the tensiometer measurements, and are shown in Table I.1-I.5.

Table I.1: Measured densities for low salinity.

Surfactant concentration [M]	**Density average [g/cm^3]**
$5 \cdot 10^{-6}$	0.997842
$1 \cdot 10^{-5}$	0.997842
$5 \cdot 10^{-5}$	0.997841
$1 \cdot 10^{-4}$	0.997844
$5 \cdot 10^{-4}$	0.997858
$1 \cdot 10^{-3}$	0.997925
$5 \cdot 10^{-3}$	0.998266
$1 \cdot 10^{-2}$	0.998791

Table I.2: Measured densities for medium salinity.

Surfactant concentration [M]	**Density average [g/cm^3]**
$5 \cdot 10^{-6}$	1.001078
$1 \cdot 10^{-5}$	1.001079
$5 \cdot 10^{-5}$	1.001087
$1 \cdot 10^{-4}$	1.001113
$5 \cdot 10^{-4}$	1.003350
$1 \cdot 10^{-3}$	1.003390
$5 \cdot 10^{-3}$	1.003730
$1 \cdot 10^{-2}$	1.001187

Table I.3: Measured densities for high salinity.

Surfactant concentration [M]		**Density average [g/cm^3]**
$5 \cdot 10^{-6}$		1.006226
$1 \cdot 10^{-5}$		1.006144
$5 \cdot 10^{-5}$		1.006182
$1 \cdot 10^{-4}$		1.006320
$5 \cdot 10^{-4}$		1.006122
$1 \cdot 10^{-3}$		1.006210
$5 \cdot 10^{-3}$		1.006574
$1 \cdot 10^{-2}$		1.006861

Table I.4: Measured densities for low salinity with $CaCl_2$.

Surfactant concentration [M]	**Density average [g/cm^3]**
$1 \cdot 10^{-6}$	0.998565
$5 \cdot 10^{-6}$	0.998566
$1 \cdot 10^{-5}$	0.998580
$5 \cdot 10^{-5}$	0.998587
$1 \cdot 10^{-4}$	0.998621
$5 \cdot 10^{-4}$	0.998680
$1 \cdot 10^{-3}$	0.999088
$5 \cdot 10^{-3}$	0.999478

Table I.5: Measured densities for medium salinity with $CaCl_2$.

Surfactant concentration [M]	**Density average [g/cm^3]**
$1 \cdot 10^{-6}$	1.000306
$5 \cdot 10^{-6}$	1.000312
$1 \cdot 10^{-5}$	1.000317
$5 \cdot 10^{-5}$	1.000320
$1 \cdot 10^{-4}$	1.000346
$5 \cdot 10^{-4}$	1.000368
$1 \cdot 10^{-3}$	1.000386
$5 \cdot 10^{-3}$	1.000675
$1 \cdot 10^{-2}$	1.001133